LEABHARLANN CHOLÁISTE NA TRÍONÓIDE, BAILE ÁTHA CLIATH | TRINITY COLLEGE LIBRARY DUBLIN
Ollscoil Átha Cliath | The University of Dublin

Terms and Conditions of Use of Digitised Theses from Trinity College Library Dublin

Copyright statement

All material supplied by Trinity College Library is protected by copyright (under the Copyright and Related Rights Act, 2000 as amended) and other relevant Intellectual Property Rights. By accessing and using a Digitised Thesis from Trinity College Library you acknowledge that all Intellectual Property Rights in any Works supplied are the sole and exclusive property of the copyright and/or other IPR holder. Specific copyright holders may not be explicitly identified. Use of materials from other sources within a thesis should not be construed as a claim over them.

A non-exclusive, non-transferable licence is hereby granted to those using or reproducing, in whole or in part, the material for valid purposes, providing the copyright owners are acknowledged using the normal conventions. Where specific permission to use material is required, this is identified and such permission must be sought from the copyright holder or agency cited.

Liability statement

By using a Digitised Thesis, I accept that Trinity College Dublin bears no legal responsibility for the accuracy, legality or comprehensiveness of materials contained within the thesis, and that Trinity College Dublin accepts no liability for indirect, consequential, or incidental, damages or losses arising from use of the thesis for whatever reason. Information located in a thesis may be subject to specific use constraints, details of which may not be explicitly described. It is the responsibility of potential and actual users to be aware of such constraints and to abide by them. By making use of material from a digitised thesis, you accept these copyright and disclaimer provisions. Where it is brought to the attention of Trinity College Library that there may be a breach of copyright or other restraint, it is the policy to withdraw or take down access to a thesis while the issue is being resolved.

Access Agreement

By using a Digitised Thesis from Trinity College Library you are bound by the following Terms & Conditions. Please read them carefully.

I have read and I understand the following statement: All material supplied via a Digitised Thesis from Trinity College Library is protected by copyright and other intellectual property rights, and duplication or sale of all or part of any of a thesis is not permitted, except that material may be duplicated by you for your research use or for educational purposes in electronic or print form providing the copyright owners are acknowledged using the normal conventions. You must obtain permission for any other use. Electronic or print copies may not be offered, whether for sale or otherwise to anyone. This copy has been supplied on the understanding that it is copyright material and that no quotation from the thesis may be published without proper acknowledgement.

"The Pharmacological and Toxicological Effects of Polystyrene and Silica Nanoparticles on Human Airway Epithelial Cells"

by

Johannah McCarthy

being a thesis submitted for the degree of

Doctor of Philosophy

at

UNIVERSITY OF DUBLIN
TRINITY COLLEGE

2010

DECLARATION

This thesis is submitted by the undersigned to the University of Dublin, Trinity College, for examination for the degree of Doctor of Philosophy. It has not been submitted as an exercise for a degree at this or any other University. I have carried out all the practical work except where duly acknowledged. I agree that the library may lend or copy this thesis upon request.

TRINITY COLLEGE
2 8 MAR 2011
LIBRARY DUBLIN
THESIS
8977

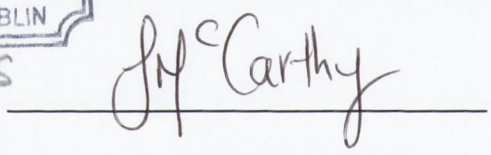

Johannah McCarthy

TABLE OF CONTENTS

SUMMARY i

ACKNOWLEDGEMENTS iii

LIST OF ABBREVATIONS v

INTRODUCTION.....1

CYSTIC FIBROSIS, A HISTORICAL OVER.....1

THE CF GENE.....2

CFTR: STRUCTURE AND FUNCTION.....3

CLINICAL SYMPTOMS OF CYSTIC FIBROSIS.....9

CFTR, AIRWAY INFECTION AND INFLAMMATION.....11

MATRIX METALLOPROTEINASES.....11

INTERLEUKINS.....14

NITRIC OXIDE, CF AND CFTR.....18

CYSTIC FIBROSIS, TREATMENT, CURE.....22

CYSTIC FIBROSIS IN IRELAND.....25

NANOPARTICLES.....26

ENVIRONMENTAL NANOPARTICLES.....26

ENGINEERED NANOPARTICLES.....28

AMORPHOUS SILICA.....30

NANOPARTICLE EXPOSURE AND ADVERSE EFFECTS.....31

AMBIENT NANOPARTICLES.....31

ENGINEERED NANOPARTICLES.....32

EXTRAPULMONARY RESPONSES.....35

NANOTECHNOLOGY AND NANOMEDICINE.....36

AIMS OF PROJECT.....37

MATERIALS AND METHODS.....39

REAGENTS.....39

NANOPARTICLES.....**40**

NANOPARTICLE CHARACTERSIATION.....**41**

CELL LINES FOR TEM STUDIES.....**42**

TEM ACUTE EXPOSURE.....**43**

a) APICAL MEMBRANE Cl^- CURRENT AND NPS.....44

(i) APICAL MEMBRANE TEM STUDIES AND POLYSTYRENE NPS.....44

(ii) BICARBONATE FREE APICAL TEM STUDIES AND POLYSTYRENE NPS...45

b) BASOLATERAL MEMBRANE K^+ CURRENT AND NPS.....45

c) ANION SUBSITUTION TEM STUDIES AND POLYSTRENE NPS.....46

(i) BICARBONATE FREE TEM STUDIES AND POLYSTYRENE NPS.....46

(ii) LOW CHLORIDE TEM STUDIES AND POLYSTYRENE NPS.....46

d) SILICA NPS AND STUDIES IN CYTOKINE-TREATED CELLS.....46

CHRONIC EXPOSURE.....**47**

PATCH CLAMP STUDIES.....**48**

***IN VITRO* TRANSLOCATION ASSAY**.....**49**

POLYSTYRENE NANOPARTICLES.....49

SILICA NANOPARTICLES.....50

MICROSCOPY.....**51**

a) PHASE CONTRAST MICROSCOPY.....51

b) CONFOCAL MICROSCOPY.....51

CYTOTOXICITY.....**53**

a) LDH ASSAY.....53

b) MTT ASSAY.....54

FLOW CYTOMETRY.....**56**

REAL TIME POLYMERASE CHAIN REACTION.....**57**

DATA ANALYSIS.....**59**

BUFFER COMPOSITION.....**60**

RESULTS.....63

1.0 NANOPARTICLE CHARACTERISATION.....63

1.1 POLYSTYRENE NANOPARTICLES.....63

1.1.2 SILICA NANOPARTICLES.....64

1.2 TRANSEPITHELIAL MEASUREMENTS: ACUTE EFFECTS.....65

1.2.1 POLYSTYRENE NANOPARTICLES ACTIVATE ANION SCRETION IN CALU-3 CELLS.....65

1.2.2 PHARMACOLOGICAL CHARACTERISATION OF POLYSTYRENE - ACTIVATED ISC.....67

1.2.3 NP AND APICAL MEMBRANE Cl^- CURRENTS.....74

1.2.4 NP EFFECTS ON Ca^{2+} -MEDIATED ANION SECRETION.....77

1.2.5 NP ACTIVATE CATION CHANNELS IN CALU-3 CELLS.....84

1.2.6 ANION SUBSITUTION TEM STUDIES AND NP.....88

1.2.7 NO/sGC/cGMP PATHWAY AND NP.....91

1.2.8 SILICA NPS AND CALU-3 CELLS.....96

1.2.9 NP AND NHBE CELLS.....98

1.2.10 SILICA NPS, TEM STUDIES IN THE PRESENCE OF CYTOKINES...101

1.3 TRANSEPITHELIAL MEASUREMENTS: CHRONIC EFFECTS.....105

1.4 PATCH CLAMP STUDIES.....108

1.4.1 EXCISED, INSIDE–OUT PATCH CLAMP RECORDINGS OF NP – STIMULATED CFTR ACTIVITY.....108

1.5 *IN VITRO* TRANSLOCATION ASSAY.....112

1.6 MICROSCOPY.....117

1.6.1 CONFOCAL MICROSCOPY.....117

1.7 CYTOTOXICITY.....118

1.7.1 LDH ASSAY.....118

1.7.1.1 POLYSTYRENE NANOPARTICLES.....118

1.7.1.2 SILICA NANOPARTICLES.....120

1.7.2 MTT ASSAY.....121

1.7.2.1 SILICA NANOPARTICLES.....121

2.0. CYTOKINES RELEASE FROM SILICA NP-TREATED CELLS.....123

2.1 FLOW CYTOMETRY AND SILICA NANOPARTICLES.....123

2.1.2 RT-PCR AND SILICA NANOPARTICLES.....127

DISCUSSION.....130

ACUTE EFFECTS OF NANOPARTICLES ON EPITHELIAL ION CHANNELS....130

NPS, CFTR Cl^- CHANNELS AND INTRACELLULAR SIGNALING.....135

INTERACTIONS OF NPS WITH OTHER ION CHANNEL TARGETS.....142

TRANSDUCTION MECHANISMS INVOLVED IN EFFECTS OF NPS ON EPITHELIAL ION FLUXES: A HOLISTIC HYPOTHESIS.....143

EFFECTS OF SILICA NPS IN THE PRESENCE OF CYTOKINES.....146

NANOPARTICLES, ANION SECRETION, CHRONIC EXPOSURE.....147

NANOPARTICLE TRANSLOCATION.....147

POLYSTYRENE NANOPARTICLES.....150

AMORPHOUS SILICA NANOPARTICLES.....152

TREATMENT OF CF WITH NANOPARTICLES.....156

CONCLUSIONS AND FUTURE DIRECTIONS.....159

REFERENCES.....164

SUMMARY

Background and purpose: A number of lung pathologies are associated with the dysfunction of ion flux through pulmonary epithelium. Cystic fibrosis (CF) is a chronic and life-threatening genetic disease that directly affects both the respiratory and gastrointestinal systems and is caused by a defective chloride (Cl^-) ion channel, the cystic fibrosis transmembrane conductance regulator, CFTR. Nanotechnology is providing researchers with new materials in the nanometer range which have the potential to provide new therapies for conditions such as CF. However, there is also much scientific data to suggest that nanoparticles (NPs)(small materials with sizes <100-nm) can induce pro-inflammatory responses in the respiratory system. Here I investigated the pharmacological and toxicological effects of polystyrene and silica nanoparticles on airway epithelial cells.

Experimental approach: Human submucosal Calu-3 cells that express CFTR and baby hamster kidney (BHK) cells engineered to express wild type CFTR were used to investigate the actions of polystyrene NPs on (1) short-circuit current (Isc) in Calu-3 cells using the Ussing chamber technique (2) single CFTR Cl^- channels alone and in the presence of known CFTR channel activators by using BHK cell patches. The effects of silica NPs were only measured using the Ussing chamber technique. Confocal microscopy was carried out using polystyrene NPs to examine cell-nanoparticle interactions. Cytotoxicity and pro-inflammatory responses to particles was measured using standard LDH, MTT assay procedures and flow cytometry.

Key results: Small (<100-nm) Polystyrene NPs caused (1) sustained, repeatable and concentration-dependent increases in Isc,

an effect inhibited by diphenylamine-2-carboxylate, a CFTR Cl^- channel blocker (2) activated basolateral K^+ channels and (3) affected Cl^- and HCO_3^- secretion. The results indicate that the mechanism of Isc activation by NPs is likely to be largely dependent on calcium- and cyclic nucleotide-dependent phosphorylation of CFTR Cl^- channels. Polystyrene NPs of 100-nm as well as silica NPs displayed no acute effects on Isc. Chronic exposure of Calu-3 cells to polystyrene NPs showed that NP-charge affected cytotoxicty whereas NP-size was involved in reducing Isc responses of Calu-3 cells to known agonists of anion secretion. Recordings from isolated inside-out patches using BHK cells confirmed the direct activation of CFTR Cl^- channels by small polystyrene NPs. Confocal microscopy showed the acute accumulation of NPs in close proximity to cellular membrane. Silica nanomaterials were found to affect cellular cytotoxicity and pro-inflammatory responses related to IL-8 and IL-6 production in both size- and concentration-dependent manner.

Conclusions and implications: This is the first study to identify the activation of ion channels after exposure to nanomaterials. I found that overall polystyrene NPs are capable of stimulating transepithelial anion secretion in airway epithelial cells dependent on both apical located CFTR Cl^- and basolateral K^+ ion channels. I conclude that NPs, specifically polystyrene NPs, may be a new therapeutic class of CFTR channel openers and that NPs in the future may be used in combination with traditional CF therapies. However, as the data points to potential nanotoxicological effects of long-term exposure of epithelial cells to NP, the potential nanopharmaceutical usefulness of NPs needs to be carefully assessed.

ACKNOWLEGEMENTS

I would like to express my sincere gratitude to both my supervisors **Prof. Marek Radomski** and **Prof. Marek Duszyk** for their willingness to teach me everything they know to make me a better scientist.

To **Prof. Marek Radomski** I would like to say a big thank you for taking me on as a Ph.D candidate under the suggestion of Dr. Murad in Houston, Texas. I was always reluctant to undergo the Ph.D program for many reasons however in your lab I found the ability to challenge myself and I am very lucky to have had a supervisor who strives to do the best for his Ph.D students.

To **Prof. Marek Duszyk**, thank you so much for all your help with the electro-physiology component of my Ph.D which was a major part of my studies. I really enjoyed my time at the University of Alberta, your lab had a lovely atmosphere and you always had time to answer my questions and guide my experiments in the right direction.

A big thank you to **Dr. Alex Gong** for carrying out the technically difficult Patch Clamp experiments at the University of Alberta, which helped to validate most of my Ussing chamber work.

To **Juan-Jose** and **Drew Nahirney** I would like to thank you guys so much for all your help for much needed chats and tea breaks where we brainstormed new experiments you guys were great fun to be around. To **Aneta**, **Carlos Medina**, **Maria-Jose** and **Alan** thank you for you assistance in the lab, ordering materials for my experiments, colourful conversations, pick-me ups when I was down and all-round support, thanks.

To all my friends in the School of Pharmacy, the guys from Dr Walsh's lab especially **Orla Woods** and **Deirdre Finn, Brian** our technician, a huge thank you. To my friend **Dr. Rhona Duane** I would like to say many thanks for all her words of wisdom about the Ph.D process and her kindness and support.

Finally to my Fiancé **David**, my parents **Abina** and **Timothy** as well as my friends in Cork thank you from the bottom of my heart, I am so lucky and also proud to be surrounded by such great people who support every new challenge I undertake including my Ph.D.

LIST OF ABBREVATIONS:

Adenosine triphosphate	ATP
AP-1	Activator protein-1
APM	Apical plasma membrane
BHK	Baby hamster kidney
CaCC	Calcium activated Cl^- channels
CEE	Capacitative Ca^{2+} entry
CNTs	Carbon nanotubes
DPC	Diphenylamine-2-carboxylate
CF	Cystic Fibrosis
CFTR	Cystic Fibrosis transmembrane conductance regulator
Cl^-	Chloride ion
DPBS	Dulbecco's Phosphate Buffered Saline
ER	Endoplasmic reticulum
GC	guanylate cyclase
HCO_3^-	Bicarbonate ion
HNE	Human neutrophil elastase
IL-	Interleukin
Isc	Short-circuit current
K^+	Potassium ion
KHS	Krebs Henseleit Solution
MDA	Malondialdehyde
MMP	Matrix metalloproteinase
Na^+	Sodium ion
NBD	Nucleotide binding domain
NF-κB	Transcription nuclear Factor-κB
NO	Nitric oxide
NBHE	Normal-derived human bronchial epithelial cells
iNOS	Inducible nitric oxide synthase
NOS	Nitric oxide synthase
NOS1	Neuronal nitric oxide synthase
NOS2	Inducible nitric oxide synthase
NOS3	Endothelial nitric oxide synthase
PCL	Periciliary layer
PD	Potential difference
PGLA	$_{D,L}$–lactide–co–gylcolide
PK	Protein kinase
PM	Particulate matter
NP	Nanoparticle
R-domain	Regulatory domain
RAECM	Rat alveolar epithelial cell monolayers

SF	Serum free
sGC	Soluble guanylyl cyclase
SiO_2	Silicon dioxide
SWCNT	Single walled carbon nanotube
TEER	Transepithelial electrical resistance
TiO_2	Titanium dioxide
tmAC	Transmembrane adenylyl cyclases
TMD	Transmembrane domain
TNF-α	Tumour Necrosis Factor-alpha
UAPs	Ultrafine ambient particulate suspensions
UFPs	Ultra-fine particles
WT	Wild-type

INTRODUCTION

CYSTIC FIBROSIS, A HISTORICAL OVERVIEW

In the 1930s physicians began to distinguish the condition of Cystic Fibrosis (CF) from coeliac disease [1-2]. The clinical symptoms of the disease included growth failure and pulmonary infections [2]. Nearly all infants with CF born at this time did not live longer than early childhood. It wasn't until 1948 that a diagnostic marker for CF was identified. During the summer of 1948 a heat wave gripped New York City. A young and perceptive paediatrician Paul di Saint'Agnese noticed that most infant children with CF during this time were also suffering from heat prostration. He went on to postulate correctly that the sweat of patients with CF was abnormal [3].

This initial observation made by Dr Paul di Saint'Agnese, lead to the development of a convenient diagnostic test for CF based on measuring sweat chloride concentrations. The diagnosis of CF was made on the basis of a sweat chloride concentration of 60 mEQ/L or greater but the patient also needed to fulfil one of the following criteria either display symptoms of lung disease or pancreatic insufficiency or have a close relative with CF [4].

Fig. 1 illustrates the use of the "sweat chloride test" as a diagnostic marker for CF. Borderline false negatives (40-60 mEQ/L) for this test can include patients with; edema, malnutrition or certain CF mutations [2]. However, some CF borderline false positives (60-80 mEQ/L) can result if patients suffer from hypothyroidism, Addison disease or fucosidosis to name a few [2]. It wasn't until the 1980s that significant milestones in physiology, biochemistry and genetics were made which enlightened our understanding of CF.

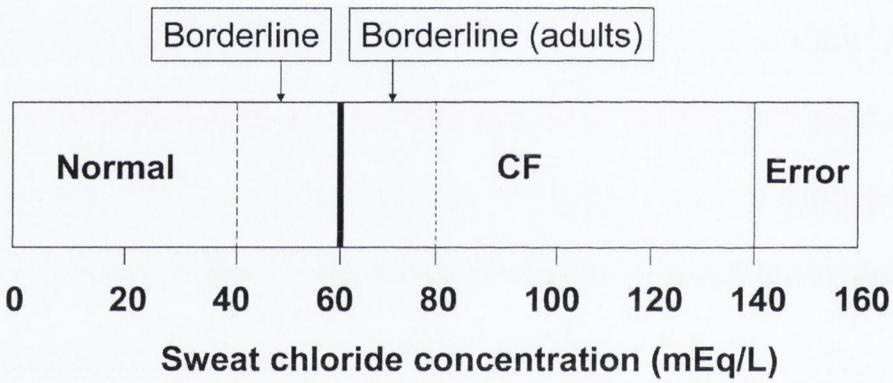

FIGURE 1. Sweat chloride concentrations related to Cystic Fibrosis diagnosis. The sweat of CF patients is greatly elevated (3-5 times normal) [5]. From Davis PB, 2006 [2].

THE CF GENE

In 1983 Paul Quinton used sweat ducts to identified chloride transport as the basic in CF [6]. The next major breakthrough came in 1989 when the gene mutated in CF patients was discovered by positional cloning due to the diligent work of three research groups; Lap-Chee Tsui and Jack Riordan at the Hospital for sick children in Toronto and Francis Collins at the University of Michigan. They identified the CF

gene as the cystic fibrosis transmembrane conductance regulator (*cftr*) gene located on chromosome 7 [7-9].

It was soon revealed that the *cftr* gene encoded a 1,480 amino acid protein product which functioned as a cAMP-regulated Cl^- channel, CFTR, located on the apical membrane of epithelial cells lining the lungs, pancreas, bile ducts of the gall bladder, sweat ducts and reproductive organs [10-11]. The identification of the CF gene also helped to improve diagnosis of the condition as genotyping could now be done on suspected CF sufferers. A definitive diagnosis of CF now depends on sweat testing and if necessary identification of mutant *cftr* alleles in the patient. However, other tests which examine CFTR function such as nasal potential difference (PD) measurements can be diagnostic too for CF as respiratory-epithelial PD are abnormally higher in CF patients [12].

CFTR: STRUCTURE AND FUNCTION

The CFTR Cl^- channel is unique among ion channels due to the fact that it is a member of the Adenosine triphosphate (ATP)-binding cassette transporter superfamily, whose members do not function normally as ion channels [13]. The CFTR Cl^- channel is composed of 2 nucleotide-binding domains (NBDs), 12 transmembrane domains (TMDs) and a unique regulatory domain (R-domain). The overall

organisation of CFTR is TMD1-NBD1-R-TMD2-NBD2 with 2 homologous halves brought together by the R domain [13].

The activation of the CFTR Cl^- channels involves ATP binding and hydrolysis at its NBDs and cAMP-dependent phosphorylation by protein kinase A (PKA) at multiple regulatory sites on the R-domain (Fig. 2) [14]. ATP-induced dimerization of NBDs plays also an important role in this process [15]. More importantly the gating of CFTR channels for Cl^- ions is strictly dependent on the phosphorylation of the R-domain by PKA as a prerequisite for channel opening [16]. CFTR channel activity is known to increase ~100 fold upon phosphorylation [17]. Other kinases outside of PKA can phosphorylate the R-domain of CFTR Cl^- channels including both Ca^{2+}-dependent and independent isoforms of protein kinase C (PKC) [18-20].

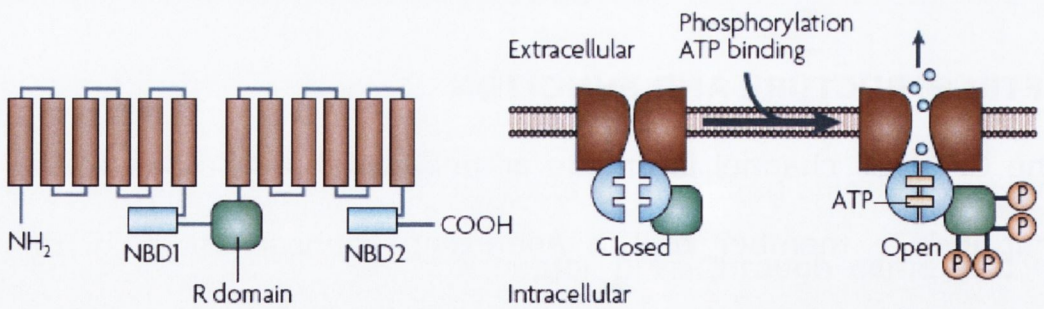

FIGURE 2. CFTR Cl^- channel structure and activation. Binding of ATP to nucleotide binding domains (NBDs) following phosphorylation of the R-domain by Protein Kinase A, leads to CFTR Cl^- channel activity. From Verkman and Galietta, 2009 [21].

There are just over 1,600 recognised mutations of the *cftr* gene which give rise to the disease [22]. CF mutations are sub-divided into 5 classes depending on the mechanism by which they affect CFTR function either due to impaired gating, channel conductance and/or improper CFTR protein trafficking [23]. The most common CF gene mutation which affects over two-thirds of CF patients, results from the deletion of 3 base pairs on CF alleles (position 1652-55) that leads to the loss of a phenylalanine residue at position 508, known as ΔF508, from NBD1 on the CFTR protein [23-24]. As a result of this class II mutation, a defective ΔF508-CFTR protein is produced which is held back in the endoplasmic reticulum of the cell due to mis-folding and is subsequently targeted for degradation by the ubiquitin–proteasome pathway [25-26]. Any ΔF508-CFTR which is expressed at the apical membrane exhibits defective gating and ion transport.

Another CF mutation, G55ID, results from a base substitution (G > A) at nucleotide position 1784 that causes a missense mutation with aspartic acid being substituted for glycine at position 551 [24]. The US cystic fibrosis foundation states that overall missense mutations of CF alleles have a frequency of 41.6 % [22]. Other CF mutations, for example R117H, affect only the channel activity and gating of CFTR. Although these CFTR Cl^- channels are expressed at the apical membrane their underlying defect produces CFTR Cl^- channels which

remain in a closed state, compared to wild-type CFTR even when maximally stimulated by cAMP [27].

In the airways CFTR Cl^- channels are expressed at higher levels on the apical membrane of serous cells associated with submucosal glands [28]. Hence, submucosal gland dysfunction has been proposed as the primary defect in CF [29]. CFTR expressed in the airways is involved in the regulation of a number of physiological processes including cell volume and transepithelial fluid transport (see table 1 for summary).

TABLE 1: Cell functions modulated by CFTR

- Transport of Na^+, K^+, Cl^- and H_2O
- Na^+/H^+ and Cl^-/HCO_3^- antiporters
- Intravesicular acidification
- Endocytic cycling
- Apoptosis
- *Pseudomonas* binding and internalization
- Gap junction communication
- Altered Ca^{2+} regulation
- Activation of NF-kB
- Chemokine production
- Activation of lysozymal enzymes

Table from McAuley and Elborn, 2000 [23].

Furthermore, CFTR also modulates the function of many other ion channels (see Fig. 3) such as the epithelial sodium channel (ENaC), outwardly rectifying chloride channel (ORCC) and potassium channels (K^+ channels) [21, 23].

The regulation of ENaC by CFTR is probably the most extensively studied relationship in CF research. Like CFTR, ENaC is also a major player in determining salt and water transport in the lungs [30]. In normal airways the activity of ENaC to re-absorb Na^+ is down-regulated by the presence of a functional CFTR protein. In CF, a dysfunctional CFTR protein results in the increased activity of ENaC, thus increasing salt and water re-absorption across the epithelium lining the airways [31].

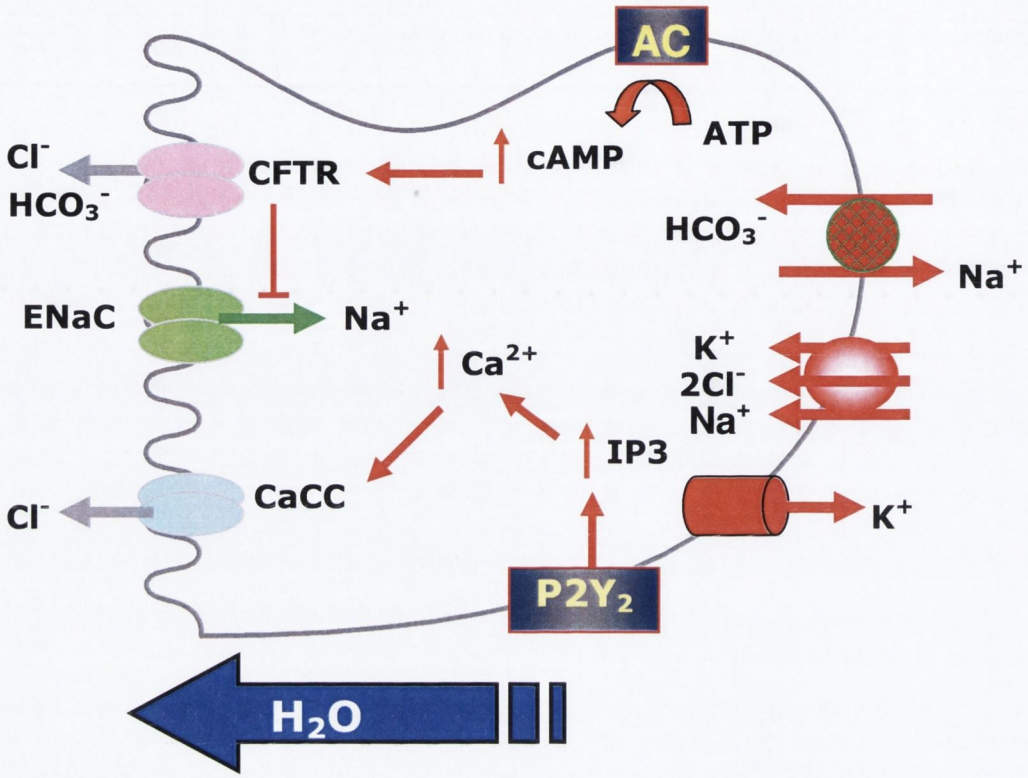

FIGURE 3. Schematic representation of ion transport in the human airways. Ion channels on the apical and basolateral membrane of airway epithelial cells regulate transepithelial fluid transport. Cl^- secretion is through CFTR Cl^- channels (CFTR) and/or calcium activated Cl^- channels (CaCC). Both types of Cl^- channels work to increase airway surface hydration. The epithelial Na^+ channel (ENaC) mediates Na^+ entry into the cell this results in the movement of Cl^- and H_2O through trans and/or paracellular pathways and causes a reduction in airway surface hydration. Active CFTR Cl^- channels inhibit ENaC. ATP and its metabolites at the cell surface activate mucosal $P2Y_2$ purinergic receptors which results in a decrease in PIP_2 this inhibits ENaC and the subsequent increase in IP_3 stimulates the release of intracellular Ca^{2+} which in turn activates CaCC. Adenylate cyclase (AC) produces cAMP from ATP. An increase in cAMP levels leads to PKA phosphorylation of the R-domain of CFTR and the activation of CFTR Cl^- channels [32].

CLINICAL SYMPTOMS OF CYSTIC FIBROSIS

Although CF patients experience a wide range of clinical symptoms (see table 2 for summary), lung disease in CF patients is the principal cause of morbidity and mortality associated with the condition [33]. CF lung disease is characterised by impaired mucus clearance due to altered ion transport by airway epithelial cells and submucosal glands [33].

A lack of Cl^- ion secretion by defective CFTR Cl^- channels and the re-adsorption of Na^+ by ENaC at the apical membrane of lung epithelial cells results in a reduction in the hydration and depth of the peri-ciliary layer (PCL). Briefly, the PCL lines airway surfaces where it provides a low viscosity environment that allows the beating of cilia, which is required for effective mucociliary clearance of bacterial pathogens and foreign bodies from the lungs. A normal PCL has a thickness of around 7 μm [33-34]. In CF patients due to defective glandular secretions, the PCL becomes reduced and highly viscosity, cilia are unable to beat and thick sticky mucus forms which block the airways [33].

TABLE 2: Clinical signs of Cystic Fibrosis
➢ **Chronic airway disease**
➢ Airway infections
➢ Airway obstruction
➢ Nasal polyps
➢ **Gastrointestinal disease**
➢ Abnormal liver and gall bladder function
➢ Biliary cirrhosis
➢ Pancreatic insufficiency & Diabetes
➢ Pancreatitis
➢ Deficiency of fat soluble vitamins
➢ **Pseudo-Bartter's syndrome**
➢ **Infertility due to obstructive azoospermia**

Modified from Ratjen and Doring, 2003 [11].

Eventually the lungs of CF patients become overwhelmed with opportunistic bacterial pathogens like *Pseudomonas aeruginosa, Staphylococcus aureus* and viral ones such as *Haemophilus influenzae*. CF patients develop these bacterial and viral infections early in life [33]. Bacteria take advantage of this build up in static CF mucus within the lungs to cause chronic recurring infections mediated most notably by neutrophilic inflammation. *P. aeruginosa* thrives in the lungs of CF patients where it acquires a mucoid phenotype, forming biofilm colonies that are highly resistant to antibiotic treatment. Thus, bacterial infections are a major factor in the acceleration and decline of pulmonary function in CF patients [33].

CFTR, AIRWAY INFECTION AND INFLAMMATION

There is a much evidence to suggest that inflammatory responses in CF patients are exaggerated. Bronchoalveolar lavage (BAL) samples of clinically stable and infant CF patients show evidence of inflammation including increased numbers of airway neutrophils as well as free elastase activity compared to normal samples [35-36]. Furthermore, stimulated neutrophils harvested from CF patients release more of the protease elastase and oxidants than those from normal subjects [37]. Human neutrophil elastase (HNE) is a potent secretagogue and serine protease which causes lung injury and structural damage by digesting its target elastin and other airway wall proteins [38]. Secreted HNE also promotes the generation of neutrophil chemoattractants, particularly interleukin (IL)-8, leukotriene (LT)B4 and C5a-like peptides from complement [39-40]. It is believed that this process worsens airway obstruction by impairing processes such as ciliary beating.

Another group of proteases expressed in the lungs are **matrix metalloproteinases** (MMPs). In humans, these proteins are members of a family of enzymes consisting of 24 zinc-dependent endopeptidases that have the capacity to remodel the extracellular matrix. MMPs exert numerous biologic functions by facilitating cellular interactions such as the modulation of cell mobility and migration as well as the degradation of matrix components and remodeling of

tissues [41]. MMPs promote tissue turnover and are regulated at the level of transcription and post-translational modification as well as by secretion and MMP inhibitors [41-42].

MMPs are formed as zymogens and activated following secretion into the extracellular matrix either by cleavages in the hydrophobic propeptide domain (pro-domain) that is located in the NH_2 terminus or in the *trans*-Golgi network by furin-like protein convertases [41, 43]. Specific serine proteases such as trypsin have been well-characterized as MMP activators [44]. Pro-MMP-8, 9 and 25 are packaged into peroxidase-negative granules within neutrophils where they are to be released upon leukocyte activation [45]. Cell culture experiments have shown that the pro-inflammatory cytokines IL-1, IL-6, and TNF-α can up-regulate MMPs [46-47]. More recently, Gaggar *et al*, 2007 showed that that the sputum of CF individuals undergoing acute pulmonary exacerbation exhibited a specific MMP isoform profile containing MMP-8, MMP-9, MMP-11, and MMP-12 [48]. Taken together inflammation-induced dysregulation of proteases such as NHE and MMPs in the CF airways can worsen airway obstruction by impairing normal physiological processes such as ciliary beating, mucus secretions, epithelial repair and airway remodelling.

Furthermore, the reaction of CF cell lines to infection by *P. aeruginosa* is excessive with high levels of pro-inflammatory cytokines being

produced compared to those of normal cell lines [49]. Moreover, other researchers showed that defective CFTR function in CF cells was associated with increased cytokine responses to pro-inflammatory cytokines such as TNF-α and interleukin (IL) 1-β [50]. Furthermore, a study carried out by Verhaeghe *et al*, 2007 using various CF cell models, demonstrated that CF cells in comparison with control cells over-expressed a number of transcription Nuclear Factor-κB (NF-κB) and Activator Protein-1 (AP-1)-dependent pro-inflammatory genes. This study suggested that the absence of functional CFTR at the plasma membrane leads to intrinsic AP-1 and NF-κB activity. This promotes a pro-inflammatory state in CF cells that is sustained through autocrine factors such as IL-1β and bFGF [51].

In normal airways when infection occurs neutrophils migrate into the airways where they phagocytose and kill bacterial pathogens. These neutrophils then undergo apoptosis, and are cleared by macrophages with little residual lung damage. However in CF airways this process fails for a number of reasons; (1) persistence of bacterial infections provides a continuing pro-inflammatory stimulus (2) there is a failure to turn off pro-inflammatory cytokine and chemokine production after an area is cleared of infection and (3) many neutrophils undergo necrosis rather than apoptosis, and there is impaired macrophage clearance of those which do enter apoptosis [38]. Thus, a vicious cycle

is established with progressive inflammation becoming a significant pathologic factor.

As mentioned above activated neutrophils and white cells produce many pro-inflammatory stimuli including cytokines and inflammatory mediators in the CF lung which help to sustain and heighten inflammatory responses. The examination of BAL fluid secretions and macrophages from CF patients reveals excessively high levels of pro-inflammatory cytokines such as IL-8, IL-6, IL1-β and Tumour Necrosis Factor-αlpha (TNF-α) [52].

Interleukins are non-antigen specific proteins that are part of the innate immune response. These proteins are small and soluble, thus allowing them to be secreted by immune cells to influence the behaviour of other cells in close proximity.

IL-8, Gene ID: 3576, [53] is a member of the CXC chemokine family. This cytokine is one of the major mediators of the pro-inflammatory immune response. IL-8 is secreted by several cell types where it functions as a chemoattractant to recruit leukocytes into the site of infection by forming a chemical gradient at the inflammation site and thus enhancing the immune response.

IL-6, Gene ID: 3569, [53] functions in inflammation and the maturation of B-cell growth and function. It is a pleiotropic cytokine, which has both pro- and anti-inflammatory activities. Additionally, IL-6 plays a major role in inducing acute phase reactant production and is primarily produced at sites of acute and chronic inflammation where it is secreted into the serum and induces a transcriptional inflammatory response through IL-6 receptor, alpha. IL-6 has been shown to suppress TNF-α and IL-1β transcription in human peripheral basophils.

TNF-α, Gene ID: 7124, [53] is a multifunctional pro-inflammatory cytokine that belongs to the tumour necrosis factor (TNF) superfamily. This cytokine is mainly secreted by macrophages. It plays an important role in inflammation especially induced by lipopolysaccharide expressing gram-negative bacteria. The cytokine functions through its receptor, TNF-Receptor. Like IL-8 this cytokine can too act as a chemoattractant for white cells. The production of other cytokines IL-2, IL-6 and IL-8 are also stimulated by released TNF-α through the activation of the transcription factor, NF-κB. TNF-α is involved in the regulation of a wide spectrum of biological processes including cell proliferation, differentiation, apoptosis, lipid metabolism and coagulation.

IL-1β, Gene ID: 3553, [53] is produced by activated macrophages as a pro-protein, which is proteolytically processed into its active form by caspase-1. This cytokine is an important mediator of the inflammatory response, and is involved in a variety of cellular activities, including cell proliferation, differentiation and apoptosis.

IL-10, Gene ID: 3586, [53] is a cytokine produced by monocytes, macrophages, epithelial cells and lymphocytes. This cytokine has pleiotropic effects in immuno-regulation and inflammation. It down-regulates the expression of Th1 cytokines, MHC class II Antigens, and co-stimulatory molecules on macrophages. It also enhances B cell survival, proliferation, and antibody production. IL-10 is constitutively expressed in normal airways [54]. More importantly, IL-10 can block NF-κB activity and thus the production of NF-κB-dependent cytokines and other genes by several mechanisms, including increasing I-κB, the inhibitor of NF-κB. Airway secretions from CF patients appear to be deficient in IL-10 compared to airway secretions from normal individuals [55]. Finally, stimulated peripheral blood T cells from CF patients produce less IL-10 than those from healthy subjects [56]. Altogether this data supports the idea that decreased IL-10 production along with an imbalance of pro- and anti-inflammatory process is associated with the basic CF defect in the airways. See Fig. 4 for overview of CFTR dysfunction and links to infection and inflammation.

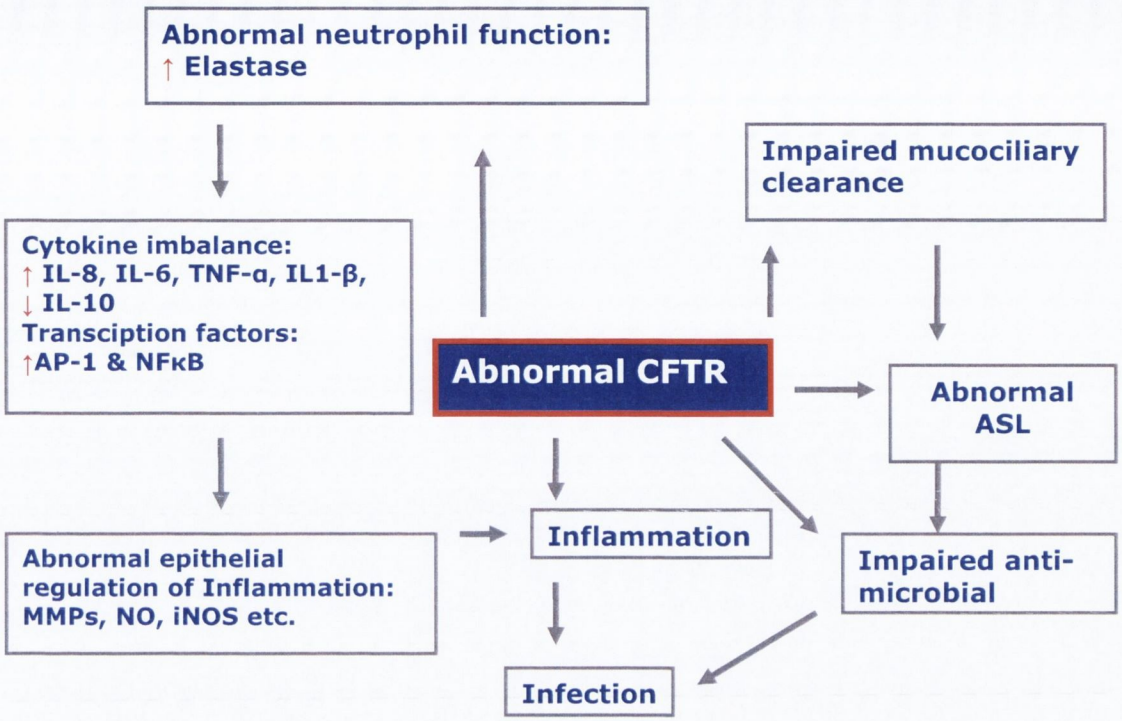

FIGURE 4. Flow chart outlining the consequences of CFTR dysfunction on airway inflammation and infection in CF patients. Modified from McAuley and Elborn, 2000 [23].

NITRIC OXIDE, CF AND CFTR

In the human airways **nitric oxide (NO)** is produced by many different cell types where it acts overall as an important signalling molecule. In airways, it plays a crucial role in processes such as bronchodilation, smooth muscle relaxation, anion secretion and immune responses against infection. NO is produced by the enzyme NO synthase (NOS) which converts L-arginine via an oxidative reaction to L-citrulline and NO. Three isoforms of NOS are present in the respiratory tract [57]; Ca^{2+}-dependent neuronal (NOS1) and endothelial NOS (NOS3), these enzymes are constitutively expressed and produce small amounts of NO, finally inducible NOS (iNOS or NOS2) a Ca^{2+} -independent enzyme that produces large amounts of NO upon stimulation.

NO is an important regulator of epithelial ion channels in human airway epithelial cells. It is a known activator of apical CFTR Cl^- channels as well as basolateral Cl^- channels in airway epithelial cells [58-59]. NO has also been shown to act as an inhibitor of Na^+ absorption across *in vitro* cultured alveolar type II monolayers [60]. Studies using submucsocal glands show that endogenous NO production has a stimulatory action in airway submucosal gland secretion and exogenous NO can induced the expression of mucin proteins such as the MUC5AC mucin gene and protein through the PKC-α and PKCΔ-ERK pathways in airway epithelial cells [61-62].

NO mediates most of its effects through the production of cyclic GMP (cGMP) by soluble guanylyl cyclase (GC) (See Fig. 5). Two types of GC proteins exist; transmembrane particulate GC and soluble GC (sGC). The latter enzyme sGC is typically found as a heterodimer, consisting of a larger α-subunit and a smaller heme (Fe^{2+})-binding β-subunit [63]. Altogether Four human sGC subunits exist: α1, α2, β1 and β2 of which the α1/β2 and α2/β1 heterodimers are the best studied and thus characterized [64]. NO-induced activation of sGC in response to various cellular stimuli, results in the conversion of GTP into the second messenger cGMP. The biological effects of cGMP are mediated by the activation of three major types of intracellular effectors; cGMP-dependent protein kinases I and II, cGMP-gated ion channels and cGMP-regulated phosphodiesterases [65-66].

In most inflammatory lung diseases such as asthma [67] NO production is typically increased as a result of cytokine-mediated activation of iNOS, however for CF patients with severe lung infections the amount of exhaled NO is considerably less compared to controls [68]. Furthermore, iNOS expression is regulated and dependent on the presence of a functional CFTR Cl^- channel [69] with both cystic fibrosis murine and human airway epithelial cells shown to express less iNOS compared with cell lines expressing wild-type CFTR Cl^- channels [70]. In addition, mice models for CF show that this deficiency in NO may compromise airway relaxation and it has been

suggested that this in turn may contribute to the bronchial obstruction seen in the disease [71]. Furthermore, the reactivity of lung epithelium to endogenous NO is reduced by cytokine-dependent generation of nitrogen-derived reactive species [72].

Interestingly, it has been shown that CF patients have a deficiency of L-arginine because it acts as a substrate for not only iNOS but also for arginase. Systemic arginase levels were found to be significantly increased in CF patients with pulmonary exacerbations compared to controls and arginase activity has shown to be increased in the sputum of CF patients [73-74]. Overall it has been proposed that this deficiency may too contribute to low NO levels in the airways of CF patients.

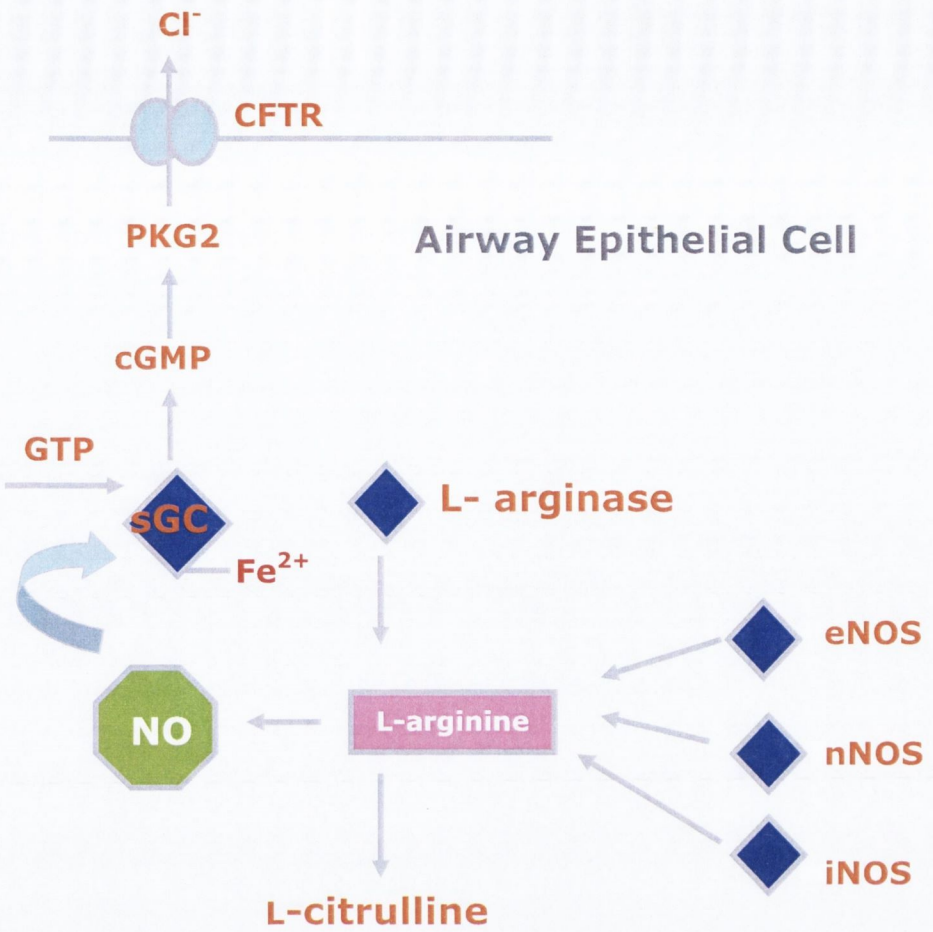

FIGURE 5. Nitric oxide dependent activation of CFTR Cl^- channels. Nitric oxide (NO) is produced by one of 3 NO synthases (eNOS, nNOS and iNOS) by the conversion of L-arginine to L-citrulline and NO. In turn NO binds to the Fe^{2+} (heme) group of the enzyme soluble guanylyl cyclase (sGC) which converts GTP to cGMP. Increased levels of cGMP activated Protein kinase G (PKG2) which phosphorylates CFTR and activates Cl^- secretion. In CF, arginase activity is increased and there is a lack of L-arginine substrate.

CYSTIC FIBROSIS, TREATMENT, CURE

Presently, the management of CF disease is based on 4 pillars of treatment; nutritional repletion, relief of airway obstruction, treatment of airway infection and suppression of inflammation [(2)].

Nutritional repletion: 85 % or greater of CF patients suffer from pancreatic insufficiency from birth. Poor fat adsorption by CF patients means that fat-soluble vitamins A, D, E must be specifically supplemented for [(2)].

Relief of airway obstruction: Postural drainage and clapping allows for the active clearance of thick, sticky airway secretions from CF patients [(75)]. Recombinant DNA technology has developed drugs which improve sputum clearance such as human DNase that cleaves free DNA into smaller parts thus reducing the viscosity of mucus found within CF lungs [(76)]. Bronchodilators such as β-adrenergic agonists are used to relax airway smooth muscle.

Treatment of airway infection: Antibiotic management is the cornerstone of CF therapy. Tobramycin is the most the most commonly used nebulized antibiotic in the USA [(77)]. Inhaled antibiotics have the advantage of reaching high drug concentrations at the site of infection without systemic absorption, therefore significantly reducing the potential for adverse effects. However,

aggressive oral and intravenous antibiotic treatments are still necessary. For milder cases of CF lung infection oral antibiotics such as the quinolone family for *Pseudomonas* and linezoid for *S. aureus* have an efficacy comparable to that of intravenous antibiotics [78-79].

Suppression of inflammation: As explained previously inflammation in the CF airways is vigorous and uncontrolled. It is now known that pharmacological suppression of inflammatory responses in CF patients by use of steroids and high-dose ibuprofen can reduce the rate of decline of pulmonary function in young healthy patients with CF [80]. Its been established that corticosteroids and non-steroidal anti-inflammatory drugs among other actions increase I-κB concentrations and decrease NF-κB-dependent production of pro-inflammatory cytokines [81-82].

Final treatment: Life can be extended by lung transplantation. Survival is 80 % after 1 year post-transplantation and 50 % by 4 years [2].

Future treatments: It has been proposed that for ΔF508-CFTR rescue to occur 2 classes of compounds or drugs are needed if the genetic defect itself cannot be corrected by gene-therapy; (1) a corrector drug to rescue mutant CFTR proteins from the ER and

locate them in the plasma membrane of the cell and (2) a potentiator to restore CFTR gating activity [21].

In CF research, modulators of CFTR Cl^- channels are considered crucially important for improving CFTR channel function, activity and gating. Several classes of small molecules and compounds have been shown pharmacologically to act as potentiators of CFTR in human bronchial cell lines, including the flavonoids; genistein, apigenin, curcumin, as well as xanthines and benzimidazolones [83-84].

The isoflavone genistein has been shown to be highly successful at stimulating WT-CFTR and mutant subtypes such as G551D-CFTR *in vitro*, and in CF patients with the G551D mutation genistein was found to stimulate chloride-dependent nasal PD measurements to levels found in healthy subjects [85]. However, there are limitations for the use of flavonoids as potentiators of CFTR *in vivo* due to the fact that these small compounds undergo quick metabolic degradation [86], this has lead to more research being carried out to investigate the efficacy of poorly metabolised methylether derives of apigenin as activators of CFTR [87]. At present this area of research is on-going.

CYSTIC FIBROSIS IN IRELAND

Ireland has now one of the highest incidence levels of CF in the world. There are over 1,100 individuals suffering from the condition in this country and it is now our most common life-threatening inherited disease with 1 in every 1,600 births. In Ireland, approximately 1 in 19 people are carriers of the defective CFTR gene [88]. An Irish population study carried out by Devaney *et al.* 2003, using PCR and DNA sequencing showed that the top 3 most common CF mutations in Ireland by % frequency were; ΔF508 (71 %), G551D (7.55 %) and R117H (2.7 %) [89].

More recently a review of CF services performed by Dr R.M Pollock MPA, Health strategy and planning concluded that staffing services related to CF patient care were dangerously inadequate and that facilities were seriously unsatisfactory. In total 11 recommendations were made in the report by Dr Pollock including a neonatal screening programme for newborn infants in Ireland [90]. The estimated cost of health care per annum in 2004 for a mild CF patient was 5,500 euro compared to 225,000 euro for a patient awaiting lung transplantation. Sadly, Ireland has a much higher death rate for CF sufferers than Wales, England and Northern Ireland [90].

NANOPARTICLES

ENVIRONMENTAL NANOPARTICLES: Ambient airborne particulate matter (PM) is a complex mixture of different particle types. Particles with an aerodynamic diameter of less than <10 μm can be classified into 3 main categories; coarse particles with aerodynamic diameters of between 2.5 and 10 μm, fine particles <2.5 μm, and ultra-fine particles (UFPs) <0.1 μm [91]. It has been stated that a typical urban atmosphere can contain in the region of 10^7 particles per cm^3 of air and that these particles in turn have a diameter of less then 300-nm [91]. Moreover, particles in the atmosphere are defined as either being (1) primary particles which are emitted directly from sources or processes which might be natural (fires, volcanoes, sea spray, erosion) or anthropogenic (traffic, industry) and (2) secondary particles that are formed in the atmosphere by gas-to-particle conversions [92].

UFPs consist predominantly of ambient nanoparticles* (NPs) 1-100-nm in size (Fig. 6) which have arisen from combustion processes such as hydrocarbons sourced from diesel exhausts and industrial emissions, wielding fumes and finally secondary particles made by reactions with gaseous compounds in the air e.g. SO_2 [93-94].

---

* The prefix 'nano' is derived from the Greek word for dwarf. One nanometre (nm) is equal to one-billionth of a metre, 10^{-9} m.

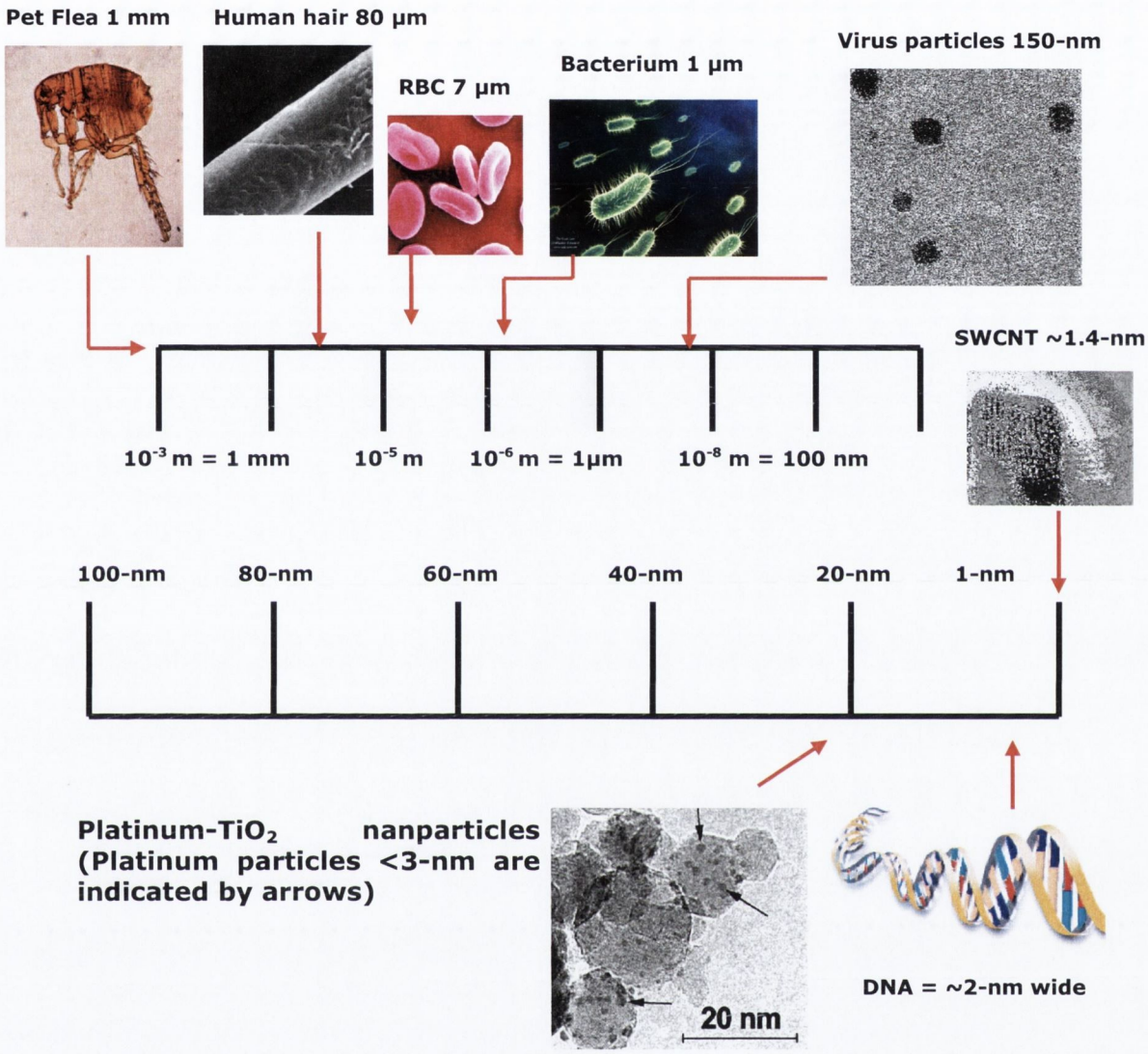

FIGURE 6. Length scale showing the nanometre in context against known biologicals. The length scale for nanoscience and nanotechnologists is from 100-nm to 1-nm. Adapted from the Royal Society and the Royal Academy of Engineering [95]. (TiO_2 = titanium dioxide)

Furthermore, ambient NPs compared to larger coarse particles of the same material exhibit extra toxicity due to their small size but increased surface area, shape, chemical composition and charge [93]. The combustion materials and the mode of combustion will ultimately determine the characteristics of the particles in the air pollution cloud including chemical composition, particle size and solubility [94]. The evaluation of inhaled fine and ambient NPs is of particular importance for toxicological studies related to pulmonary diseases due to the fact that only particles with an aerodynamic diameter of less then 2.5 μm are capable of depositing deep within lung tissue [91].

ENGINEERED NANOPARTICLES: Nanotechnology, is defined by the United States Nanotechnology Initiative as 'the understanding and control of matter at dimensionsns of roughly 1–100 nanometers, where unique phenomena enable novel applications" [96]. Nanotechnology provides a new platform in science which has the ability to integrate engineering with biology, chemistry and physics. It has the potential to supply disciplines and applications such as diagnostics, numerous industries, electronics and clinical medicine with new materials in the nanometer range that have far reaching applications. It has been predicted that nanotechnology in the future will provide environmentally friendly and cheap energy, clean water, reduce pollution and improve materials and new products [96].

The study of **nanoscience** is defined by the Royal Society and Royal Academy of Engineering as "the study of phenomena and manipulation of materials at atomic, molecular and macromolecular scales, where properties differ significantly from those at a larger scale" [95]. Nanomaterials comprise of nanoparticles, nanofibres and nanotubes, composite materials and nano-structured surfaces. The hallmark of nanotechnology lies in the fact that when the dimensions of a piece of solid material become very small i.e. in the nanometer range, its physical and chemical properties can become very different from those of the same material in larger mass form.

Over the last century carbon black nanoparticles have been used in the manufacture of rubber and pigments [92]. Fumed silica and titanium nanomaterials have continued to be used as thixotropic agents in pigments and cosmetics and more recently as the foundation for fine polishing powders [92]. Currently, the world wide growth of R&D in nanotechnology is leading to a vast increase in the production of engineered nanomaterials available for new technologies. Different classes of engineered nanoparticles exist including liposomes, emulsions, polymers, ceramic and metallic nanoparticles, gold shell nanoparticles, carbon nanomaterials and quantum dots [91].

Silica is the common name for silicon dioxide (SiO_2). It is one of the most abundant compounds found in nature. Silicas can be divided into crystalline (fibre-like structure) or non-crystalline (amorphous) silicas. Excessive exposure to crystalline silica has been linked to pulmonary diseases, such as silicosis a chronic lung disease characterised by granulomas and severe fibrosis in the lungs [97], chronic bronchitis and lung cancer [98].

Amorphous silicas can be further sub-divided into naturally occurring amorphous silicas (such as diatomaceous earth) and synthetic forms. Synthetic amorphous silica is intentionally manufactured to contain no measurable levels of crystalline silica [98]. The synthetic form of amorphous silica may be classified as either; (1) wet process manufactured silica (silica gel and precipitated silica) (2) pyrogenic (thermal or fumed) silica and (3) chemically or physically modified silica [98].

Due to its low cost and ease of production synthetic amorphous silica is widely used in pharmaceuticals, cosmetics, silicone rubber, fillers in the rubber industry, insulation material and biomedical and biotechnology products such as cancer therapy, DNA delivery and enzyme immobilization. Human exposure to nano-SiO_2 is ever increasing, according to the United States Nanotechnology Initiative the largest production volume in the year 2004 was for chemical-

mechanical polisher for semiconductor wafers, e.g. ammonia-stabilized 40-nm colloidal silica [92, 96]. At present the toxic effects of amorphous nano-SiO_2 on human remains unclear. However, there is a growing concern about the toxic effects of all intentionally and unintentionally engineered nanoparticles [91].

NANOPARTICLE EXPOSURE AND ADVERSE EFFECTS

Humans can be exposed to nanoparticles in an environmental, occupational and consumer setting.

AMBIENT NANOPARTICLES: It is well-known from epidemiological studies that long term exposure to airborne PM in susceptible populations contributes significantly to an increased risk of cardiovascular morbidity and mortality and respiratory disease [99-100]. Some specific pulmonary diseases such as CF have shown a direct negative relationship between airborne particulate matter exposure over time and an increased risk of pulmonary exacerbations and decline in lung function [101]. More recently, a study by Qu *et al.*, 2009 showed that the induction of cellular stress by ozone molecules can result in the down-regulation of CFTR protein and mRNA expression and CFTR chloride current in cultured human bronchial epithelial cells [102].

It is widely accepted from molecular toxicology studies that the inhalation of combustion-derived UFPs contained in PM increases oxidative stress and inflammation in susceptible individuals which eventually causes adverse health affects [94]. Two mechanisms have been proposed for UFP toxicity [103]. The first results from inflammation and oxidative stress. Indeed, the exposure of human volunteers to concentrated PM from diesel exhaust causes pulmonary inflammation [104-105]. More recently it has been shown that exposure to environmental pollutants increases oxidative stress as measured by markers such as malondialdehyde (MDA) in bronchial asthmatic sufferers [106].

The second mechanism results from the direct translocation of particles into the circulatory system. *In vivo* studies using genetically susceptible (apolipoprotein E–deficient) mice show that after exposure to UFPs mice display many proatherogenic effects including reduced plasma levels of high density lipoprotein as well as increased systemic oxidative stress as evidenced by elevated hepatic MDA levels and the up-regulation of Nrf2-regulated antioxidant genes [107].

ENGINEERED NANOPARTICLES: The same characteristics which make nanoparticles attractive for use in nanotechnology such as size, shape, chemical composition, surface modifications etc. can also influence the toxicity of engineered nanoparticles. In addition, it is

known that the increased surface area to mass ratio for nanoparticles means that a greater percentage of the atoms are present at the surface of the particle, thus increasing the number of potential reactive groups at the particle surface that may influence toxicity [108].

At present over 1,000 manufacturer-identified nanotechnology-based consumer products currently on the market are listed on the Woodrow Wilson database [109]. **Nanotoxicology** is an emerging discipline in nanoscience which is gaining much attention. It can be defined as the "science of engineered nanodevices and nanostructures that deals with their toxicity in living organisms". Nanotoxicology is an important aspect of nanoscience especially when we consider that our exposure to engineered NPs is increasing steadily, thus studies to assess NP-induced toxicity on biological systems and human health are essential.

The respiratory system is particularly susceptible to injury resulting from the inhalation of gases, aerosols, and particles, and also from systemic delivery of drugs, chemicals and other compounds to the lungs via blood [108] (see Fig. 7 for overview). Thus, the lung is a prime target for the possible toxic effects of engineered nanoparticles.

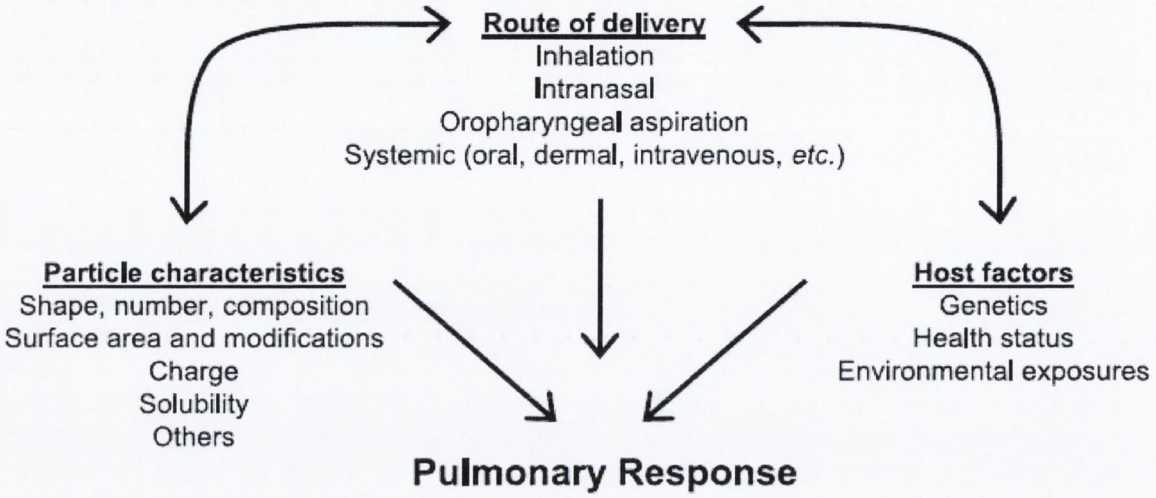

FIGURE 7. A flowchart depicting how engineered nanoparticles may enter and influence the respiratory system. From Card *et al.*, 2008 [108].

Chen *et al.*, 2006 showed that Nano-TiO_2 which is used as a photocatalyst in air and water cleaning induced emphysema-like lung injury in mice [110]. Cerium oxide nanoparticles are being developed for a wide range of applications involving solar and fuel cells acting as gas sensors and oxygen pumps [111]. Park *et al.*, 2007 showed that exposure of cultured human lung epithelial cells to these cerium oxide nanoparticles led to cell death, an increase in reactive oxygen species and the induction of oxidative stress-related genes such as heme oxygenase-1, catalase, glutathione (GSH), S-transferase and thioredoxin reductase [112]. Carbon nanotubes (CNTs) can be subdivided into single-walled and multi-walled types. Presently, CNTs are being developed for nanopharmacology purposes for the drug delivery of small interfering RNA, paclitaxel and for targeted and selective imaging [113]. However, CNTs have been shown in mice

studies to enhance acute pulmonary inflammation and injury in the presence of bacterial infection, thus suggesting that exposure to CNTs may lead to increased susceptibility to lung infection in exposed populations [114]. Lam *et al.*, 2004 showed that mice intratracheally instilled with 0, 0.1, or 0.5 mg of carbon nanotubes exhibited dose-dependent epithelioid granulomas and in some cases interstitial inflammation [115].

EXTRAPULMONARY RESPONSES: Inhaled NPs following deposition in the lungs have been shown to translocate into the circulatory system and deposit in secondary organs such as the central nervous system [116]. Translocated UFPs have been shown to promote inflammation in the central nervous system of mice. This inflammation was characterised by an increase in the nuclear translocation of pro-inflammatory transcription factors NF-κB and AP-1 as well as an increase in glial fibrillary acidic protein levels [117].

NPs are now known to interact with a wide range of cell types in the bloodstream. In 2005, Radomski *et al.* showed that carbon nanoparticulate matter as well as engineered carbon nanoparticles and nanotubes induced human platelet aggregation *in vitro* and increased the rate of thrombosis *in vivo* [118]. Furthermore, carbon black UFPs were found directly to cause endothelial cell damage such

as cytotoxicity and the induction of pro-inflammatory molecules e.g. monocyte chemoattractant protein-1 [119].

NANOTECHNOLOGY AND NANOMEDICINE

As already discussed NPs are currently under development for targeted delivery of nanosensors, nanoimaging agents, nanorobotic devices or drugs. When it comes to drug delivery, NPs provide numerous advantages over other delivery systems. The targeted delivery of drugs using nanocarriers for the treatment of respiratory diseases is an emerging area of interest [120]. Nanocarriers work to increase drug availability at the target site as well as minimising drug degradation and preventing harmful side effects [121]. Many approaches have been undertaken for the delivery of nanostructures such as micelles, liposomes and nanoparticles to the lungs via the use of nebulisation for suspensions and dry powder carriers [120].

AIMS OF PROJECT

As NPs have been shown to interact avidly with proteins [122], I was interested in studying the interactions of NPs with ion channels in human airway epithelial cells, with specific focus on the CFTR Cl^- channel. To study the effects of NPs on ion fluxes in lung epithelium I selected Calu-3 cells as a model of airway submucosal epithelial cells. These cells are widely used in epithelial research and have many special properties which make them useful for physiological/toxicological studies due to their ability to (1) mimic wild-type (WT) serous cells *in vivo*; (2) show polarity and tightness when grown as a monolayer on permeable supports (3) express high levels of WT CTFR protein and therefore can secrete the necessary Cl^- and HCO_3^- ions needed for transepithelial electrical measurements and (4) express and secrete many markers of inflammation.

For comparison with submucosal cells normal–derived human bronchial epithelial cells (NHBE cells) were used. Finally, baby hamster kidney (BHK) cells stably transfected with wild-type human CFTR were used in patch clamp studies.

Therefore, the **general objective** of my research was to study the pharmacological and toxicological response(s) of human lung

epithelial cells *in vitro* upon challenge with carbon (polystyrene) and silica nanoparticles.

Specific aims:

1) To investigate and characterise the acute (minute) and chronic (hour) effects of nanoparticles on transepithelial ion fluxes in normal and cytokine-stimulated bronchial epithelial cells.

2) To study the translocation of NPs across polarized human airway submucosal cells.

3) To test the cytotoxicity and inflammatory effects of polystyrene and silica nanoparticles on human airway submucosal cells.

MATERIALS AND METHODS

REAGENTS

Clotrimazole (30 mM, Sigma-Aldrich) and forskolin (10 mM, LC Laboratories, M.A.) were prepared as 1,000-fold stock solution in ethanol. Barium Chloride (500 mM), carbachol (100 mM) and *S*-nitrosoglutathione (GSNO, 100 mM) were purchased from Sigma–Aldrich and were dissolved in distilled H_2O. NG-nitro-$_L$-arginine methyl ester ($_L$-NAME, 100 mM) was purchased from Alexis Biochemicals (San Diego, CA). Diphenylamine-2-carboxylate (DPC, 1 M, Sigma-Aldrich) was dissolved in DMSO and was prepared fresh for each experiment. 1*H*-[1, 2, 4] oxadiazolol-[4, 3-*a*] quinoxalin-1-one (ODQ, 10 mM, Tocris Cookson, St. Louis, MO) and thapsigargin (1 mM, Sigma-Aldrich) were prepared as 1,000-fold stock solutions in DMSO. Furosemide (100 mM, Sigma-Aldrich) was dissolved in distilled H_2O with 1 drop of concentrated 5N NaOH. XE991 (10 mM) was a generous gift from Dr. B.S. Brown, DuPont, Wilmington, DE, USA) was dissolved in 0.1 N HCl. Nystatin was prepared as a 180 mg/ml stock solution in DMSO and sonicated for 30 seconds prior to use.

Transwell-Clear polyester membrane inserts were obtained from Corning Costar (The Netherlands). Snapwell™ inserts were obtained from Corning (Cambridge, MA, USA). FluorSave™ reagent was purchased from Calbiochem and CellMask™ Red plasma membrane

stain from Invitrogen. Cytokines Interleukin-1-beta (IL1-β), Tumour necrosis factor-alpha (TNF-α) and Interferon-gamma (IFN-γ) these were purchased from Sigma-Aldrich. All other items were purchased from Sigma-Aldrich.

NANOPARTICLES

POLYSTYRENE NANOPARTICLES. Polystyrene latex nanoparticles were purchased from Sigma (amine-modified 50-nm and 100-nm), Invitrogen (carboxyl-modified 20-nm) and Polysciences (unmodified, carboxyl-modified 50 and 100-nm). All particles are core–labelled with fluorophores according to manufacturer's specifications.

SILICA NANOPARTICLES. Unmodified 10-nm amorphous colloidal silica nanoparticles were purchased from Polysciences (Eppelheim, Germany). Amine and carboxyl–modified 50-nm core FITC-labelled ($\lambda_{Ex/Em}$: 485/520 nm) silica nanoparticles were purchased from G. Kisker (Steinfurt, Germany). Amine-modified (unlabelled) 50-nm silica nanoparticles were purchased from Corpuscular Inc. Cold Spring New York. For comparison I also used larger micro-sized particles, unmodified 150-nm and 500-nm, these were also purchased from Polysciences (Eppelheim, Germany).

NANOPARTICLE CHARACTERISATION

The size and zeta-potential for all nanoparticles tested was determined using a Zetasizer Nano ZS (Malvern Instruments, Malvern, UK). Zeta-potential and size were measured at either 25°C or 37°C, with three repeats per sample using a DTS 1060C clear disposable zeta-cell. Measurements were conducted using a concentration of 100 µg/ml for both polystyrene and silica nanoparticles.

POLYSTYRENE NANOPARTICLES were diluted in Krebs-Henseleit solution (KHS) (see table 3). All samples were measured at 37°C. The dielectric constant of the dispersant was set at 78.5, viscosity, at 0.8872 cP and refractive index (R.I) at 1.330.

SILICA NANOPARTICLES were diluted in distilled H2O with a R.I of 1.440 and viscosity, cP, of 0.6844. All samples were measured at 25°C.

CELL LINES FOR TRANSEPITHELIAL MEASUREMENT (TEM) STUDIES

A Calu-3 cell line was obtained from the American Type Culture Collection (ATCC-HBT-55) and maintained as a monolayer culture in plastic T–75 cm^2 tissue culture flasks. The cells were grown in Dulbecco's Modified Eagles Medium, a low glucose media 1 g/L containing also sodium pyruvate 110 mg/L and supplemented with 10 % fetal bovine serum, 5 µg/ml gentamicin sulphate, 6 µg/ml penicillin-G and 10 µg/ml streptomycin. Cells were maintained at 37°C in a humidified atmosphere of 95 % O_2-5 % CO_2. When confluent the cell line was detached enzymatically with trypsin-EDTA and sub-cultured into a new cell culture flask either T–75 or T-25 cm^2. The medium was replaced every 2 days. Cells were used for all experiments between the passages of 21–45.

Normal–derived human bronchial epithelial cells (NHBE cells) also known as EpiAirway "ready-to-use" tissues were purchased from MatTek Corporation (Ashland, MA, USA) and were prepared for experiments according to the manufacturer's instructions. Briefly, upon receipt cells were returned to culture at 37°C, 95 % O_2–5 % CO_2 in fresh EpiAirway media using sterile tissue culture techniques. The tissues were allowed to equilibrate overnight (16-18 hours). Finally the snapwell tissue inserts were once again feed with pre-

warmed EpiAirway media and were now ready to be used in TEM studies.

TEM ACUTE EXPOSURE

Standard methods were employed to measure transepithelial anion secretion. Ussing chamber studies were carried out using the apparatus and methods stated by Duszyk et al., [58-59, 123]. Calu-3 cells were seeded at a density of 2 x 10^5 cells/cm^2 onto Snapwell™ inserts, (0.45 µm, 1 cm^2). For the first 7 days cells were grown using 20% MEM–media using liquid covered culture techniques, with the basolateral and apical media being changed every 2 days (2 ml basolateral, 500 µl apical). Seven days after initial seeding on Snapwell™ inserts cells were grown using air interface culturing in which medium was added only to the basolateral side of the inserts (2 ml). Cells were used in TEM studies between the days of 12 to 22.

Prior to use in TEM studies all Calu-3 cell inserts were fed with 20% MEM-media as described for one hour and were washed for 30 minutes in KHS (2 ml basolateral, 500 µl apical). The cell monolayers were bathed at a temperature of 37°C in KHS. Chemicals were added from concentrated stocks and all chambers were continuously mixed by bubbling the KHS with 95 % O_2–5 % CO_2 unless otherwise stated to maintain a constant pH of 7.4.

In all TEM studies, cells were used for experiments between the days of 12 to 22. The transepithelial potential difference was clamped to zero using a DVC 1000 voltage/current amplifier (World Precision Instruments), and the resulting short-circuit current (Isc) was recorded through Ag–$AgCl_2$ electrodes, using 3 M KCl-agar bridges. The Isc was allowed to stabilize for approximately 10-15 minutes before the application of nanoparticles or other tested chemicals. Nanoparticles were always added apically unless stated. The transepithelial resistance was calculated using Ohm's law, by measuring current changes in response to 0.5 mV pulses.

(a) APICAL MEMBRANE Cl^- CURRENT AND NPS

(i) APICAL MEMBRANE STUDIES AND POLYSTYRENE NPS. The effects of nanoparticles on apical membrane Cl^- current (A_{Cl}) were measured after permeabilisation of the basolateral membrane with 180 µg/ml nystatin and establishment of a basolateral-to-apical Cl^- concentration gradient. The basolateral membrane was bathed in normal KHS. However, apical NaCl was equimolarly exchanged for sodium gluconate and the concentration of Ca gluconate was increased from 2.5 to 5.0 mM to compensate for the Ca^{2+}-buffering capacity of the gluconate (see table 4). Under these conditions, the contribution of basolateral ion co-transporters and Na^+-K^+-ATPase to the Isc are eliminated, and Isc represents A_{Cl} as these ions move down their concentration gradient through apical Cl_2 channels.

(ii) BICARBONATE FREE APICAL TEM STUDIES AND POLYSTYRENE NPS.

The effects of nanoparticles on A_{Cl} were assessed in the absence of bicarbonate ions (HCO_3^-) after permeabilisation of the basolateral membrane with 180 µg/ml nystatin and establishment of a basolateral-to-apical Cl^- concentration gradient. Apical HCO_3^- and NaCl were equimolarly exchanged for HEPES and sodium gluconate, respectively, and the concentration of Ca gluconate was increased from 2.5 to 5 mM (see table 5). Basolateral HCO_3^- was equimolarly exchanged for HEPES and mixing was carried out using an air pump.

(b) BASOLATERAL MEMBRANE K^+ CURRENT AND NPS

The effects of nanoparticles on basolateral membrane K^+ channels were assessed after permeabilisation of the apical membrane with 180 µg/ml of nystatin and establishment of an apical-to-basolateral K^+ concentration gradient. Apical NaCl was replaced by equimolar amounts of potassium gluconate and basolateral NaCl with sodium gluconate (see table 6 and 7 respectively). The concentration of Ca gluconate was increased from 2.5 mM to 5 mM. Under such conditions, the contribution of apical Cl^- channels to Isc is eliminated and the measured Isc represents K^+ currents as these ions move down the concentration gradient through basolateral K^+ channels.

(c) ANION SUBSITUTUION TEM STUDIES AND NPS

(i) BICARBONATE FREE TEM STUDIES AND POLYSTYRENE NPS. The effects of nanoparticles on Isc were assessed in the absence of bicarbonate ions. A bicarbonate–free KHS was used with apical and basolateral HCO_3^- ions being equimolarly exchanged for HEPES (100 mM). The overall pH was adjusted to 7.4 and the solutions were mixed with O_2 (see table 8).

(ii) LOW CHLORIDE TEM STUDIES AND POLYSTYRENE NPS. The effects of nanoparticles on Isc were assessed under low chloride conditions. A low chloride KHS was used with apical and basolateral NaCl being equimolarly exchanged for sodium gluconate. The concentration of Ca gluconate was increased from 2.5 mM to 5 mM to compensate for the Ca^{2+}-buffering capacity of the gluconate (see table 4).

(d) SILICA NPS AND STUDIES IN CYTOKINE-TREATED CELLS

Calu-3 cells were seeded at a density of 10^5 cells/ cm^2 onto Costar Transwell ™ inserts (0.45 µm, 1.12 cm^2). For the first 5-7 days cells were grown using 10 % MEM–media using liquid covered culture (LCC) techniques, the basolateral and apical media being changed every 2 days (1 ml media basolaterally, 500 µl apically). After day 7 from initial seeding on transwell inserts all cells were grown using air interface culturing (AIC) in which medium was added only to the basolateral side of the inserts (1 ml basolaterally).

In these experiments the effects of silica NP was examined in cytokine-treated cells. The cell inserts were incubated overnight in the presence or absence of the combination of cytokines IL1-β, TNF-α and IFN-γ (10-100 ng/ml), which was placed in the apical compartment. After incubation inserts were used for TEM studies.

CHRONIC EXPOSURE

Calu-3 cells were seeded at a density of 10^5 cells/cm^2 onto Costar Transwell ™ inserts (0.45 μm, 1.12 cm^2), and were grown using LCC and AIC culturing as previously described above. Cells were used these TEM studies from days 12 to 22.

Cells were treated for 24 hours with 200 μg/ml of various NPs (N20, P50 and P100) in serum free (SF) media before being mounted into modified Ussing chambers. Cell monolayers were bathed at a temperature of 37°C in KHS and Isc was allowed to stabilise. Chronic effects of NPs on ion fluxes were accessed by measuring the Peak or integral increase in Isc produced by a dose of 100 μM carbachol basolaterally, occurring within 5 min as compared to the control (no chronic exposure to NPs).

PATCH CLAMP

Experiments were carried using baby hamster kidney (BHK) cells stably transfected with wild-type human CFTR, as described previously [124]. The experiments were performed in the excised, inside-out configuration of the patch clamp technique. In all experiments the pipette solution contained (in mM) 150 Na gluconate, 2 $MgCl_2$ and 10 HEPES, and the bath solution 150 NaCl, 2 $MgCl_2$ and 10 HEPES. All solutions were adjusted to pH 7.4 with 5N NaOH. Membrane potential was held at 0 mV and the junction potential was compensated. Following patch excision channel activity was assessed by the addition of nanoparticles (50 µg/ml) to the bath solution. In the second set of experiments the patch excision was exposed to polystyrene latex nanoparticles as already discussed in the presence of 10 to 20 nM Protein kinase A (PKA) catalytic subunit and 0.2 to 1 mM MgATP in the bath. $Au(CN)_2^-$ (500 µM) was used as a blocker of the CFTR pore [124]. Patch clamp recordings were analysed by the clampfit program and open probability (P_o) was calculated using standard techniques.

IN VITRO TRANSLOCATION ASSAY

POLYSYTENE NANOPARTICLES. Calu-3 cells were seeded at a density of 10^5 cells/cm^2 onto Costar Transwell^{TM} inserts (0.45 μm, 1.12 cm^2), and were grown using LCC and AIC culturing as previously described above. Cell monolayers were used for *in vitro* translocation studies from days 12 to 22.

On the day of experiments the media in the basolateral compartment was removed and 600 μl of SF media was added to fill the compartment. To the apical surface of the cells (note the mucus secretions of the Calu-3 cells were not removed) 300 μl of SF media containing 195 μg/ml of nanoparticles was added. At the time points of 6 and 24 hr the basolateral media was sampled and transferred into a black 96-well plate. The samples were then tested for the presence of fluorescent-labelled nanoparticles using a 96-well plate reader (FLUOstar OPTIMA, BMG Labtech, Aylesbury, UK) set a λ_{ex} = 485 nm and λ_{em} = 520 nm. The concentration of nanoparticles in the samples was then extrapolated from a standard curve of known concentrations (0.13–26 μg/ml) of the same fluorescently-labelled nanoparticles diluted in SF media. Different types of fluorescently-labelled nanoparticles were used for the translocation assay including unmodified and carboxyl-modified polystyrene nanoparticles of 50-nm and 100-nm in diameter.

Larger polystyrene nanoparticles of 500-nm and 200-nm in diameter were used as controls. Prior to use all nanoparticle stock suspensions were visually inspected for aggregates and were vortexed before treatments to prevent non-specific aggregations. **SILICA NANOPARTICLES.** The experimental set up was repeated as stated above but in place of polystyrene nanoparticles, amine and carboxyl–modified 50-nm core FITC-labelled silica nanoparticles were used.

MICROSCOPY

(a) PHASE-CONTRAST MICROSCOPY. Calu-3 cells were cultured in T–75 and T-25 cm^2 flasks and were routinely viewed using an inverted Olympus light microscope (Model CKX41, Japan).

(b) CONFOCAL MICROSCOPY. Calu-3 cells were seeded at a density of 2 X 10^5 cells/cm^2 onto Costar Transwell™ inserts (0.45 µm, 1.12 cm^2), and were grown using LCC and AIC culturing as previously described above. After apically exposing Calu-3 cell monolayers to 50 µg/ml of unmodified 50-nm nanoparticles (FITC- core labelled) for 30 minutes in SF media monolayers were processed for confocal fluorescence microscopy. Briefly, exposed monolayers were washed twice with Dulbecco's Phosphate Buffered Saline (DPBS), pH 7.4 ± 0.1. A fresh solution of CellMask™ Red plasma membrane stain was diluted in warm DPBS at a final concentration of 7.5 µg/ml and cell monolayers were stained with CellMask™ Red for 5 minutes at 37°C. Cells were then washed twice with DPBS and then fixed with 3.75 % para-formaldehyde diluted in DPBS for an incubation period of 10 minutes at 37°C according to manufacturer's instructions.

Next, cells were washed three times with DPBS and mounted onto microscope slides using a FluorSave™ reagent and sealed with a coverslip. In some experiments cell inserts were mounted using both the FluorSave™ reagent and 15 µl of DAPI contained in a mounting

mixture before sealing the coverslip. Samples were allowed to dry overnight and were imaged within 24 hours. Microscopy was performed on an Olympus FV1000 laser scanning confocal microscope. Results are presented as 3-dimensional reconstructions (xyz-imaging). A PLAPON 60X/ 1.42 NA oil objective was used and the images were acquired with the accompanying software.

CYTOTOXICITY

(a) LACTATE DEHYDROGENASE (LDH) ASSAY. Extracellular LDH release was measured using a colorimetric CytoTox 96® Non-Radioactive Cytotoxicity Assay kit from Promega (Madison, WI, USA) following the manufacturer's instructions. This assay quantitatively measures LDH, a stable cytosolic enzyme that is released upon cell lysis. Released LDH in culture supernatants is measured with a 30-minute coupled enzymatic assay, which results in the conversion of a tetrazolium salt (INT) into a red formazan product. Absorbance is recorded at 492 nm. The amount of colour formed is proportional to the number of lysed (dead) cells.

The general chemical reaction of the LDH assay is as follows:

LDH

NAD^+ + Lactate -------→ Pyruvate + NADH

DIAPHORASE

NADH + INT -------→ NAD^+ + Formazan

Following the optimisation of Calu-3 cell numbers from the initial plate assay set-up stage, Calu-3 cells were seeded into a 96-well round–bottom plate for a final concentration of 10,000 cells per well in 100 µl medium. 24 hours later, cells were treated in triplicate with varying concentrations of either polystyrene or silica nanoparticles

diluted in SF media for 24 hours at 37°C. **POLYSTYRENE NANOPARTICLES.** Carboxyl–modified 20-nm and amine–modified 50-nm NPs at concentrations of 1-200 µg/ml. **SILICA NANOPARTICLES.** Unmodified 10-nm, 150-nm and 500-nm NPs were tested at concentrations of 1-50 µg/ml.

To determine the percentage cytotoxicity the average absorbance of the triplicate was calculated. As control, extracellular release of LDH was obtained from unexposed cells (low control) and maximum release of LDH was obtained by lysis of cells with the supplied lysis buffer (10X) (high control). To the experimental values obtained the following equation was applied:

EQUATION 1

% CYTOTOXICITY = (RELEASE OF LDH OF EXPOSED CELLS – RELEASE OF LDH (LOW CONTROL) / RELEASE OF LDH (HIGH CONTROL) – RELEASE OF LDH (LOW CONTROL) X 100.

(b) METHYLTHIAZOLYLDIPHENYL-TETRAZOLIUM BROMIDE (MTT) ASSAY. Cytotoxicity was measured using a CellTiter 96® Non-Radioactive Cell Proliferation Assay kit from Promega (Madison, WI, USA) following the manufacturer's instructions. This assay is also

based on the cellular conversion of a tetrazolium salt into a formazan product. The MTT assay evaluates mitochondrial activity (assesses cell growth and cell death) and is performed by adding a premixed optimised dye solution to culture wells. During a 4 hour incubation period, living cells convert the tetrazolium component of the dye solution into the formazan product. A solubilisation solution is then added to culture wells to solubilise the blue formazan product and the absorbance is recorded at 570 nm. This absorbance is directly proportional to the number of live cells.

Calu-3 cells were seeded into a 96-well round–bottom plate for a final concentration of 10,000 cells per well in 100 µl medium.

SILICA NANOPARTICLES. Cells were allowed to equilibrate for 24 hours and then treated in triplicate with varying concentrations of unmodified 10-nm silica nanoparticles (1-50 µg/ml) in SF media for 24 hours at 37°C.

To determine the percentage cytotoxicity the average of the triplicates was calculated for each concentration tested. Results are presented as a percentage of the control values (unexposed cells).

EQUATION 2

% CYTOTOXICITY = (EXPERIMENTAL ABS_{570nm} OF EXPOSED CELLS / ABS_{570nm} OF UNEXPOSED CELLS) x 100.

FLOW CYTOMETRY

Calu-3 cells were cultured in T–25 cm^2 flasks for between 5-7 days until confirmed to be 80 % confluent by phase-contrast microscopy. Cells were then treated in SF media with either: unmodified 10-nm, 150-nm and 500-nm silica particles at concentrations of 10, 25, 50 and 100 µg/ml for 24 hours at 37°C. After 24 hours, conditioned media was collected and samples were centrifuged for 5 minutes at 300 rpm to remove cellular debris. Next, the concentration of protein in the samples was quantified using a Bradford protein assay. Controls were cells unexposed to silica nanoparticles.

A BD CBA Human Inflammation kit (Oxford, United Kingdom) was then used to quantitatively measure interleukin-8 (IL-8), interleukin-1β (IL-1β), interleukin-6 (IL-6), interleukin-10 (IL-10), tumour necrosis factor (TNF), and interleukin-12p70 (IL-12p70) from the conditioned media collected from controls and nanoparticle-treated Calu-3 cells by BD FACSArray™ (BD, Biosciences, Oxford, UK). The measurements were performed according to the supplier's recommendations and data were analysed using the BD FACSArray™ system software version 1.0.3.

REAL TIME POLYMERASE CHAIN REACTION

Calu-3 cells were cultured in T–25 cm^2 flasks for 5-7 days until confirmed to be 80 % confluent by light microscopy. Cells were then treated in SF media with either: unmodified 10-nm, 150-nm and 500-nm silica NPs at concentrations of 10, 25, 50 and 100 µg/ml for 24 hours at 37°C. Controls were cells unexposed to silica nanoparticles.

Following incubation of cells with silica NPs, conditioned media was aspirated, and the cells were washed twice with phosphate saline buffer (PBS). DNA-free RNA was isolated using the Ambion® RiboPure™ kit (Huntingdon, United Kingdom) according to the supplier's recommendations. RNA quantity and purity was assessed spectrophotometrically (Nanodrop ND-1000, Labtech International, Ringmer, East Sussex, United Kingdom). Thereafter, RNA in each sample was reverse-transcribed by the Applied Biosystems High Capacity cDNA Reverse Transcription kit (Woolston, United Kingdom).

Real-time PCR was performed on duplicate, with pre-designed Applied Biosystems TaqMan® Gene Expression Assay for matrix metalloproteinase-9 (MMP-9, Hs00957562_m1) and Applied Biosystems TaqMan® Universal PCR Master Mix. 18S ribosomal ribonucleic acid (18S rRNA, Hs99999901_s1) was used as an internal control. Both reverse-transcription and real-time PCR reaction were performed using the Eppendorf Realplex^2 Mastercycler (Histon,

Cambridge, United Kingdom). The expression of each gene within each sample was normalized against 18S rRNA expression and expressed relative to the control sample using the formula $2^{-(\Delta\Delta Ct)}$, in which $\Delta\Delta Ct$ = (Ct mRNA – Ct 18S rRNA) sample – (Ct mRNA – Ct 18S rRNA) control sample.

DATA ANALYSIS

Nanoparticle concentration-responses (EC_{50}) were fitted with an equation: Y = Bottom + (Top-Bottom) / (1+10^ ((LogEC50-X) * Hill Slope)). The data points show the mean ± SEM. Isc is expressed as either (1) $\mu A/cm^2$ or (2) the integral value $\mu A/cm^2.s^{-1}$ x min^{-1} which represents an enclosed area between the sampled data and their minimum on the selected interval within 5 minutes.

For the assessment of cytotoxicity by polystyrene and silica nanoparticles concentration-responses (TC_{50}) for both LDH and MTT assays were fitted using a variable slope model, log(inhibitor) vs. responses curve, with an equation: Y = Bottom + (Top-Bottom) / (1+10^((LogIC50-X) * HillSlope)). The data points show the mean ± SEM. Cytotoxicity is expressed as a percentage of relative viability of treated cells when compared to controls.

All data are presented as group means ± SEM for n individual experiments. Statistical analysis of the mean difference between multiple groups was determined by one-way Anova followed by either Kramer-Tukey or Bonferroni post tests or between two groups by paired/unpaired t tests as appropriate. A P-value of < 0.05 is considered statistically significant and calculated P values are given throughout. All statistical analyses were performed using GraphPad Prism version 5.00 for Windows, GraphPad Software, San Diego, California, USA, www.graphpad.comData.

BUFFER COMPOSITION

Tables 3 through 8 show the composition of buffers used during TEM studies.

TABLE 3.

KREBS HENELEIT SOLUTION	
COMPONENTS	**Final concentration (mM)**
Inorganic salts	
NaCl	**116**
KCl	**4.7**
$CaCl_2.2H_2O$	**2.5**
$MgSO_4.7H_2O$	**1.2**
$NaHCO_3$	**24.8**
KH_2PO_4	**1.2**
Other components	
D-glucose	**11.1**
pH 7.4	**Gas with 95 % O_2/5 % CO_2**

TABLE 4.

LOW CHLORIDE BUFFER	
COMPONENTS	**Final concentration (mM)**
Inorganic salts	
Na gluconate	**116**
KCl	**4.7**
Ca gluconate	**5.0**
$MgSO_4.7H_2O$	**1.2**
$NaHCO_3$	**24.8**
KH_2PO_4	**1.2**
Other components	
D-glucose	**11.1**
pH 7.4	**Gas with 95 % O_2/5 % CO_2**

TABLE 5.

BICARBONATE FREE BUFFER	**APICAL MEMBRANE STUDIES**
COMPONENTS	**Final concentration (mM)**
Inorganic salts	
Na gluconate	**116**
KCl	**4.7**
Ca gluconate	**5.0**
$MgSO_4.7H_2O$	**1.2**
HEPES	**10**
KH_2PO_4	**1.2**
Other components	
D-glucose	**11.1**
pH 7.4	**Gas with O_2 only**

TABLE 6.

HIGH POTASSIUM BUFFER	
COMPONENTS	**Final concentration (mM)**
Inorganic salts	
K gluconate	**116**
KCl	**4.7**
Ca gluconate	**5.0**
$MgSO_4.7H_2O$	**1.2**
$NaHCO_3$	**24.8**
KH_2PO_4	**1.2**
Other components	
D-glucose	**11.1**
pH 7.4	**Gas with 95 % O_2/5 % CO_2**

TABLE 7.

HIGH SODIUM BUFFER	
COMPONENTS	**Final concentration (mM)**
Inorganic salts	
Na gluconate	**116**
KCl	**4.7**
Ca gluconate	**5.0**
$MgSO_4.7H_2O$	**1.2**
$NaHCO_3$	**24.8**
KH_2PO_4	**1.2**
Other components	
D-glucose	**11.1**
pH 7.4	**Gas with 95 % O_2/5 % CO_2**

TABLE 8.

BICARBONATE FREE BUFFER	
COMPONENTS	**Final concentration (mM)**
Inorganic salts	
NaCl	**116**
KCl	**4.7**
$CaCl_2.2H_2O$	**2.5**
$MgSO_4.7H_2O$	**1.2**
HEPES	**10**
KH_2PO_4	**1.2**
Other components	
D-glucose	**11.1**
pH 7.4	**Gas with O_2**

RESULTS

1.0 NANOPARTICLE CHARACTERISATION

1.1 POLYSTYRENE NANOPARTICLES. I selected a panel of polystyrene latex nanoparticles that according to manufacturer's specifications differed in size (20-100-nm) and surface charge (positively charged, amine-modified and negatively charged, carboxyl-modified). I found that the negatively charged 20-nm nanoparticles (**N20**) showed a larger particle size of 45.2-nm which deviated from the manufacturers specifications of 20-nm. Positively charged 50-nm nanoparticles (**P50**) were found to have a mean size of 58.9-nm which did not deviate largely from the manufacturers specifications.

Size and zeta-potential measurements of the positively charged 100-nm nanoparticles (**P100**) demonstrated that these particles have a propensity to aggregate giving a mean size measurement of 339.7-nm and a zeta-potential which was negative (-11.7 ± 0.7 mV) instead of a positive. Similar nanoparticle characteristics have been published for P100 underscoring the particles tendency to form aggregates and to exhibit a negative zeta-potential [122]. A summary of results is shown in table 9.

TABLE 9. PROPERTIES OF POLYSTYRENE NPS USED IN TEM STUDIES.

Charge, Size* nm	(-) 20	(+) 50	(+) 100
Size in buffer§, nm	45.2	58.9	339.7
PDI in buffer§	0.21	0.06	0.80
Surface modification	-COOH	$-NH_2$	$-NH_2$
zeta-potential in buffer§, mV	-15.1 ± 0.8	+23.6 ± 1.2	-11.7 ± 0.7
Fluorophore¶	Yellow-Green	Blue	Orange
Abbreviation	N20	P50	P100

*According to the manufacturer: (-) 20-nm carboxyl-modified, (+) 50-nm (amine modified) and (+) 100-nm (amine-modified).

§Krebs-Henseleit solution, pH 7.4 ± 0.1 (see methods).

¶Polystyrene nanoparticles were core-labelled with fluorophores.

1.1.2 SILICA NANOPARTICLES. The sizes and zeta-potentials of commercially available amorphous colloidal silica NPs were measured using a Zetasizer Nano ZS (Malvern Instruments, Malvern, UK). It was found that the 10-nm silica NPs (**Si-10**) differed from the manufacturers specifications considerably (37.4-nm). As expected all unmodified silica particles tested had a highly negative zeta–potential ranging from -23.4 to -48.8 mV. Amine-modified 50-nm silica showed less than optimal dispersion (PDI). A summary of these results is shown in table 10.

TABLE 10. PROPERTIES OF SILICA NPS USED IN THIS STUDY.

Charge, Size* nm	10	(+) 50	150	500
Size in H_2O, nm	37.4	45.2	166.4	506.9
PDI in H_2O	0.260	4.338	0.024	0.026
Surface modification	n/a	$-NH_2$	n/a	n/a
zeta-potential in H_2O, mV	-39.0 ± 0.1	+45.2 ± 0.8	-41.3 ± 0.2	-48.8 ± 0.4
Abbreviation	Si-10	Si-P50	Si-150	Si-500

*According to the manufacturer.

1.2 TRANSEPITHELIAL MEASUREMENTS: ACUTE EFFECTS

1.2.1 POLYSTYRENE NANOPARTICLES ACTIVATE ANION SECRETION IN CALU-3 CELLS. Acute apical exposure of Calu-3 cells to either **N20** or **P50** resulted in activation of Isc ($\mu A/cm^2$) that showed a biphasic response: initial peak followed by a plateau. In contrast, P100 did not affect either peak or plateau Isc. Plateau values were used to determine EC_{50} from the Isc vs. nanoparticle concentration curve (Fig. 8). The EC_{50} for N20 and P50 was 0.315 and 2.53 µg/ml, respectively (Fig. 8.**a** and **c**). When the data is plotted as function of Isc vs. particle number we observed that N20 again has a lower EC_{50} value than P50 (3.0 vs. 8.6 x 10^5 particles/ml respectively).

FIGURE 8. N20 and P50 induced activation of Isc in Calu-3 cells: concentration-response curves. The effect of N20 (a-b) and P50 nanoparticles (c-d) on Isc responses.

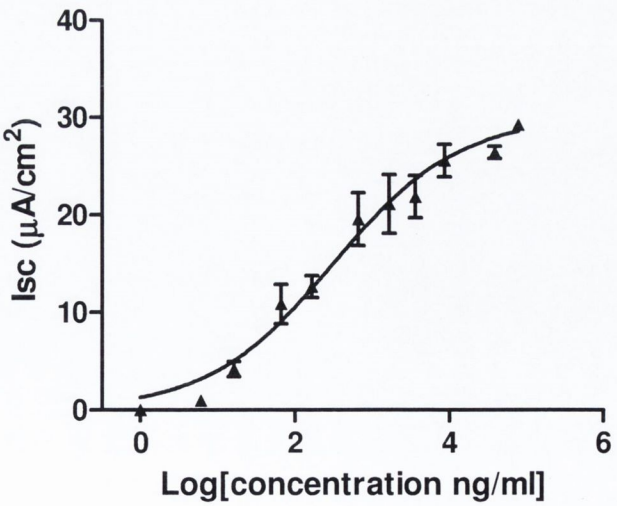

(a) N20 showed an EC_{50} = 0.315 µg/ml on Isc and a corresponding Hill co-efficient of 0.54 ± 0.045, n=4.

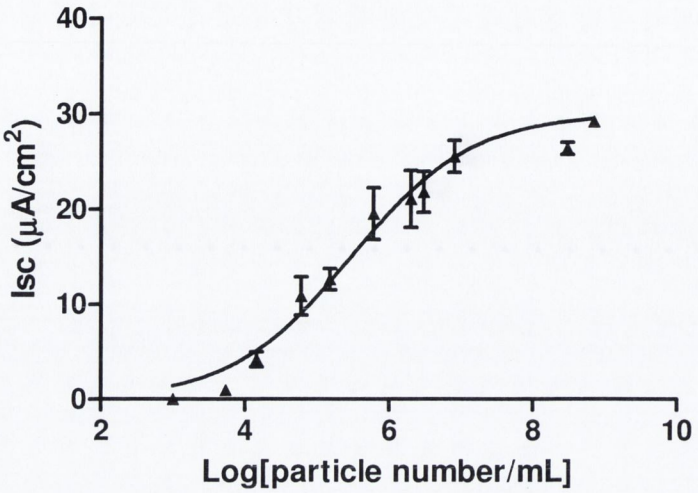

(b) N20 showed an EC_{50} = 3.0 x 10^5 particles/ml on Isc and a corresponding Hill co-efficient of 0.52 ± 0.087, n=4.

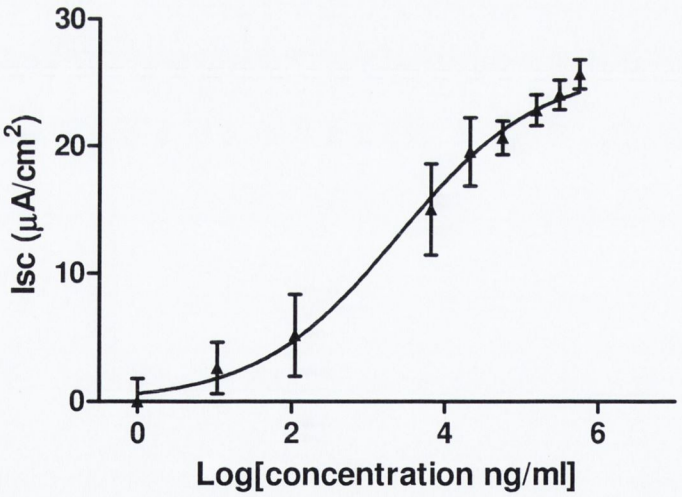

(c) P50 showed an EC_{50} = 2.53 µg/ml on Isc and a corresponding Hill co-efficient of 3.4 ± 0.031, n=4.

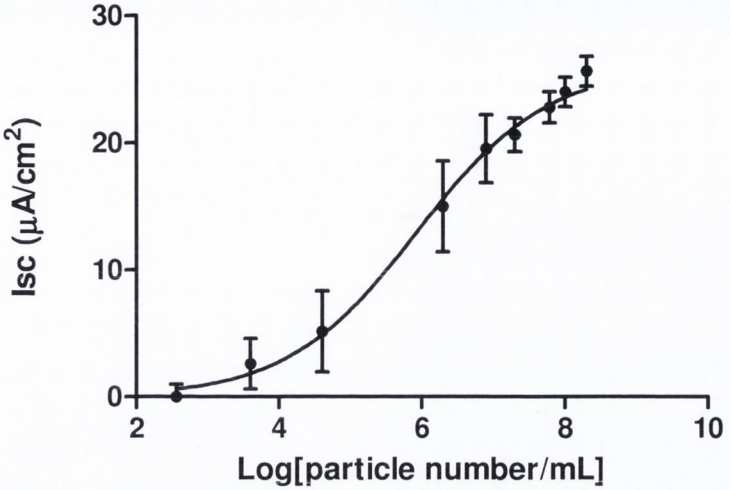

(d) P50 showed an EC_{50} = 8.6 x 10^5 particles/ml on Isc and a corresponding Hill co-efficient of 4.7 ± 0.03, n=4.

1.2.2 PHARMACOLOGICAL CHARACTERISATION OF POLYSTYRENE NANOPARTICLE-ACTIVATED ISC. Apically located CFTR Cl^- channels serve as the primary conductive pathway for anion secretion in Calu-3 cells and are the main contributors to Isc in transepithelial studies. To determine the mechanism(s) of action of nanoparticles on Isc activation a number of pharmacological agents were used to probe the actions of nanoparticles.

N20 (10 μg/ml) increased Isc by 12.4 ± 0.4 μA/cm^2 (plateau I_{sc}, Fig. 9.**a**). The subsequent addition of an activator of adenylyl cyclase, forskolin (10 μM), further increased Isc by 15.8 ± 2.9 μA/cm^2 (plateau I_{sc}, Fig. 9.**a**) and this effect was blocked by DPC (1 mM) a blocker of CFTR. In the absence of nanoparticles forskolin activated

Isc by 16.2 ± 1.0 μA/cm^2 (plateau I_{sc}, Fig. 9.**b**). However, the addition of N20 after forskolin resulted in a significantly lower Isc response (4.7 ± 2.4 μA/cm^2) when compared to control responses ($P < 0.05$, n=3) (Fig. 9.**b**) showing there is partial overlap between the mechanism of Isc activation by N20 and forskolin.

As expected DPC (1 mM) reduced basal Isc by 9.2 ± 1.56 μA/cm^2 prior to the addition of N20 (10 μg/ml) (Fig. 9.**c**). However, this pre-treatment with DPC only partially inhibited the activation of Isc by N20 when compared with control responses (Integral I_{sc}, 3.43 ± 1.43 μA/cm^2.s^{-1} x min^{-1}, $P < 0.023$, t test, n=3) (Fig. 9.**c**). Furosemide, a blocker of the NKCC co-transporter located on the basolateral membrane, exerted little effect on the inhibition of Isc induced by N20 in the presence of DPC (1 mM) (Fig. 9.**c**). A summary of these results is shown in Fig. 9.**d**.

FIGURE 9. The effects and mechanisms of action of N20 on transepithelial anion secretion. Representative recordings (a-c) of 3 experiments and the statistical analysis of data (d).

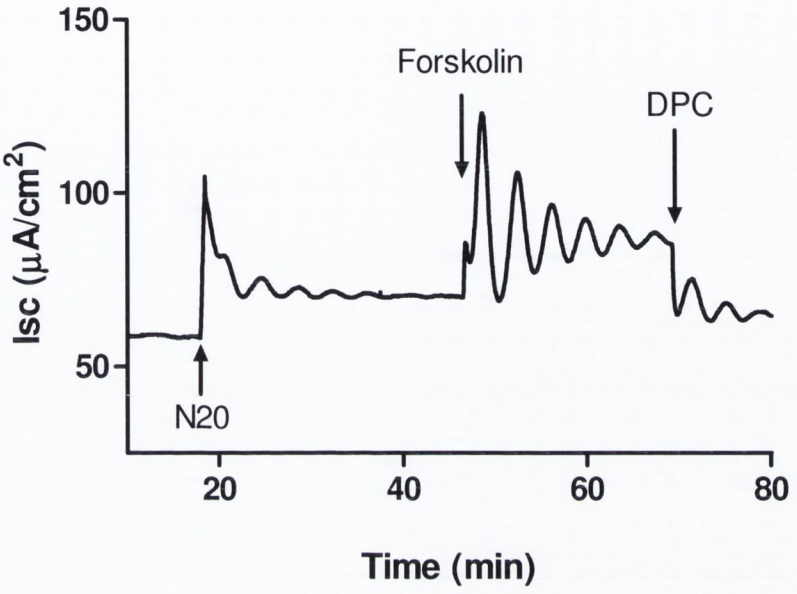

(a) The activation of Isc by N20 (10 μg/ml apical) in Calu-3 cells. Forskolin (10 μM both sides) further increased Isc in N20 pre-treated cells.

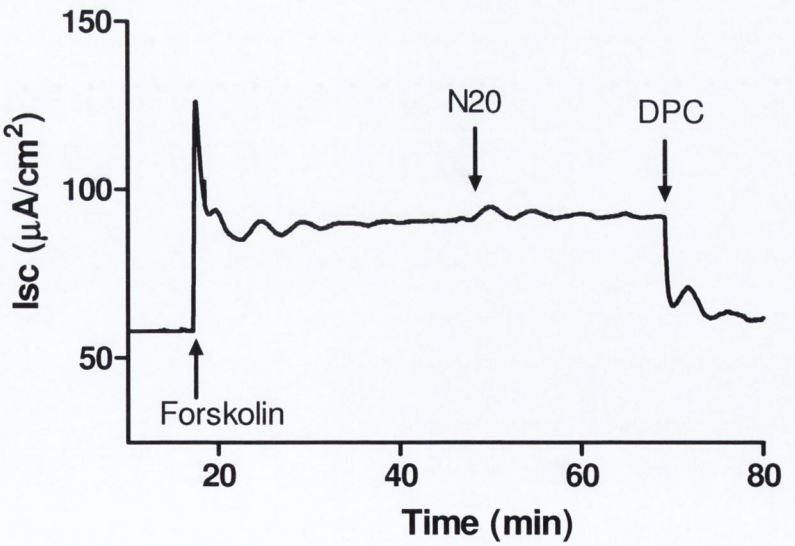

(b) The activation of Isc by N20 (10 μg/ml apical) was significantly reduced when cells had been pre-stimulated with forskolin (10 μM both sides).

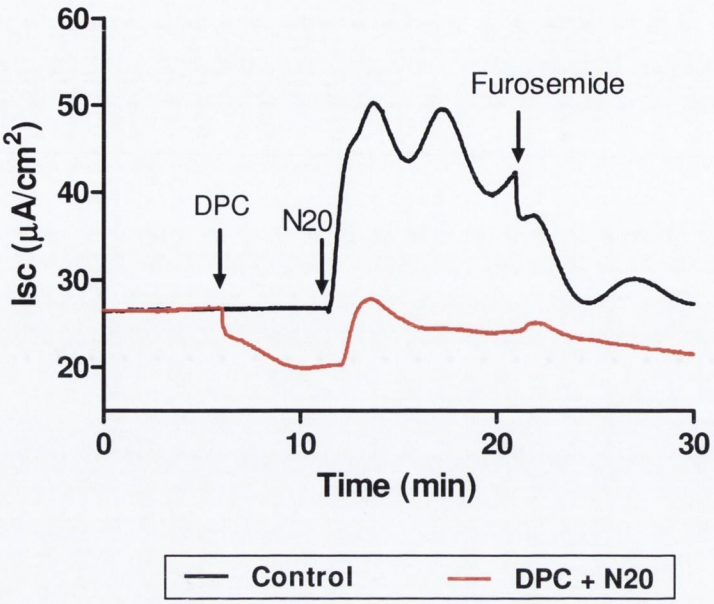

(c) The pre-treatment of cells with DPC (1 mM apical) reduced the effects of N20 (10 μg/ml apical). Furosemide (1 mM basolaterally) reversed the effect of N20 on Isc.

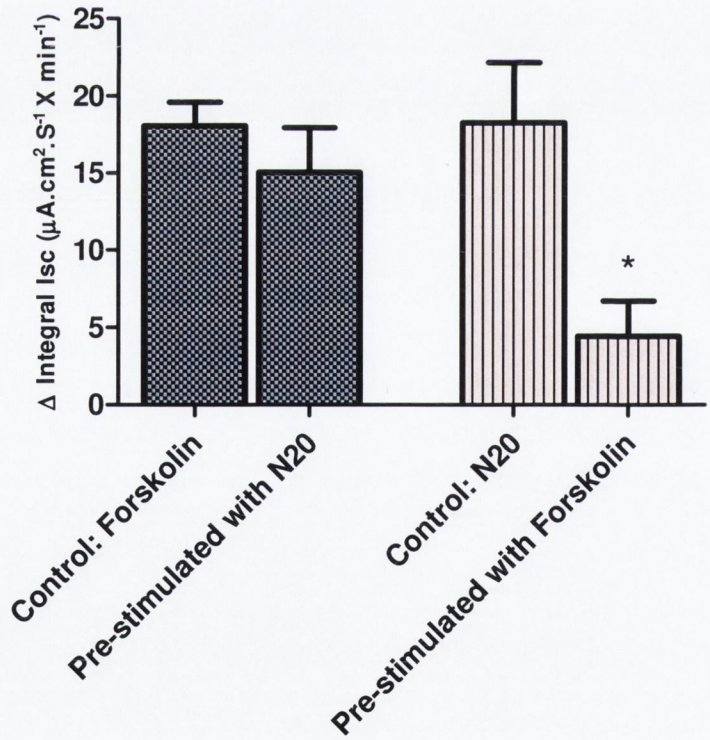

(d) Forskolin-induced Isc was not significantly altered ($P > 0.05$, n=3) by pre-stimulation with N20. In contrast, pre-stimulation of cells with forskolin resulted in a significant decrease in N20-induced responses; one-way ANOVA $P < 0.0236$, Bonferroni post-test *$P < 0.05$, n=3, control vs. pre-stimulated.

P50 (100 µg/ml) increased Isc by 20.7 ± 1.2 µA/cm^2 and the subsequent application of forskolin further increased the Isc by 14.1 ± 0.6 µA/cm^2 (plateau I_{sc}, Fig. 10.**a**). Similar effect was observed when the order of addition of forskolin and P50 was reversed. Forskolin activated Isc by 31.7 ± 2.3 µA/cm^2. The subsequent addition of P50 increased the Isc by only 5.0 ± 2.6 µA/cm^2 (plateau I_{sc}, Fig. 10.**b**). **P100** (100 µg/ml) exerted no significant effect on Isc activation in Calu-3 cells (Fig. 10.**c**). A summary of these results is shown in Fig. 10.**d**.

Furthermore, I also observed similarities between the mechanisms of action by P50 and N20 in the presence of forskolin with both nanoparticles showing reduced activation of Isc once cell monolayers had been pre-stimulated with Forkolin (10 µM) (Fig. 9.**d** and 10.**d**). In contrast, I observed that the pre-treatment of cell monolayers with P50 (100 µg/ml) blocked the effects of forskolin on Isc (Fig. 10.**d**).

FIGURE 10. Activation of Isc by P50 but not P100 in Calu-3 cells. Representative recordings (a-c) of 3 experiments and the statistical analysis of data (d).

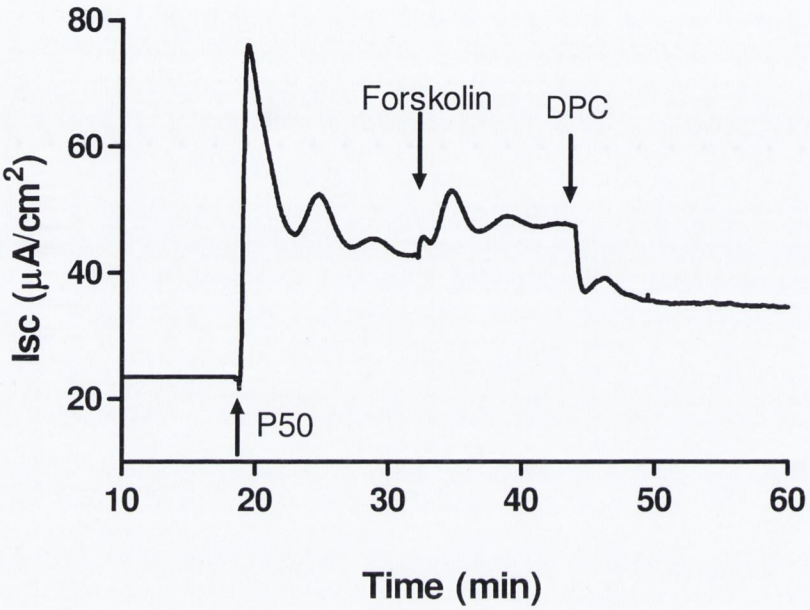

(a) Forskolin, (10 μM both sides) only minimally increased Isc following pre-stimulation by P50 (100 μg/ml apical) in Calu-3 monolayers.

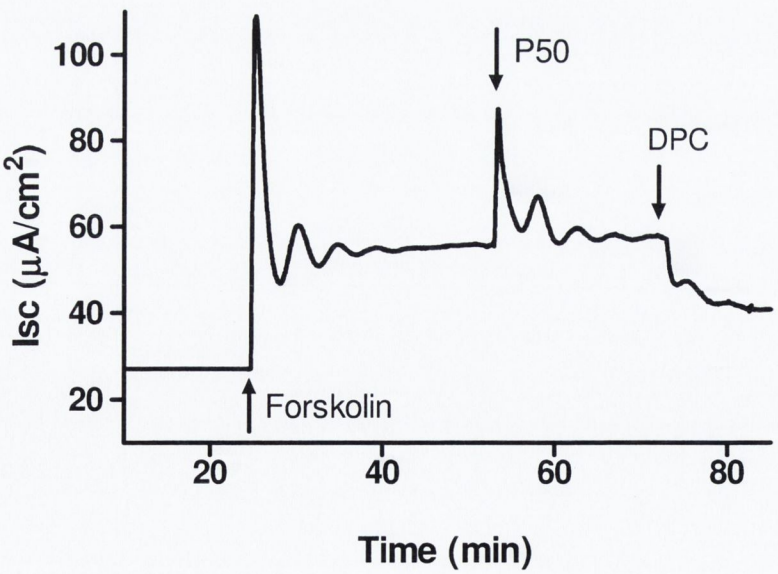

(b) Pre-stimulation with forskolin (10 μM both sides) decreased the effect of P50 (100 μg/ml apical).

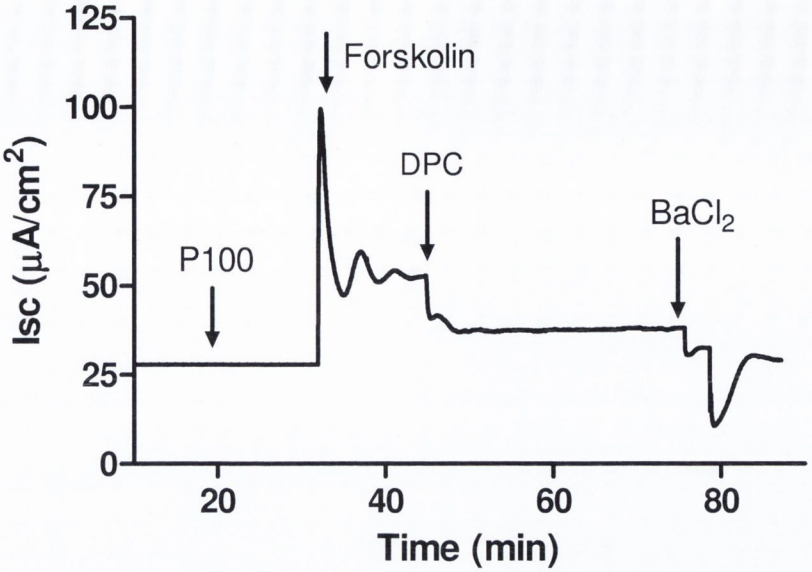

(c) P100 exerted no significant effect on Isc responses. All Isc currents were significantly reduced by the application of DPC (1 mM apical) as shown in **(a-c)** and $BaCl_2$ (5 mM basolateral) as in **(c).**

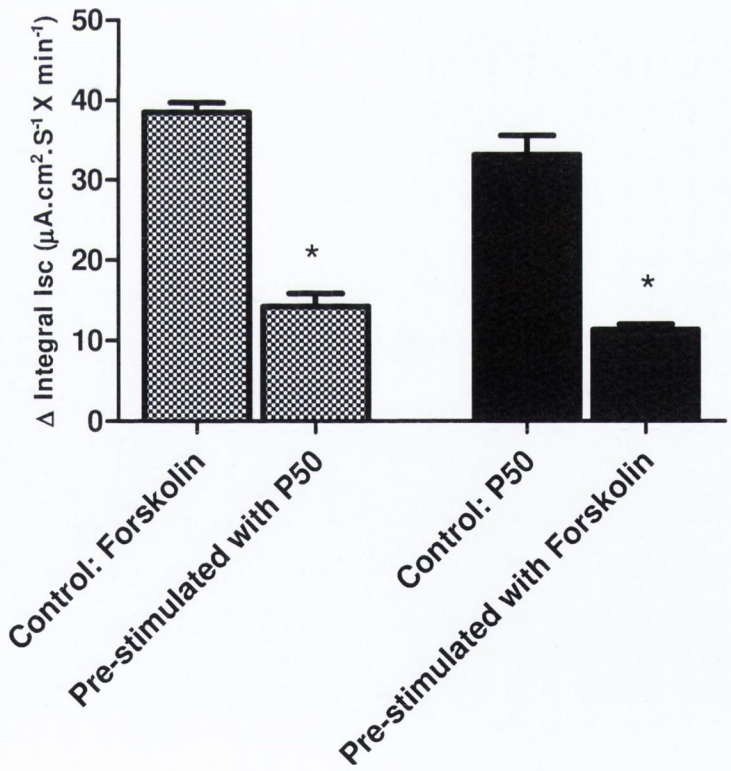

(d) Forskolin-induced Isc was significantly reduced by pre-stimulation with P50. Similarly, pre-stimulation of cells with forskolin resulted in a significant decrease in P50-induced responses. One-way ANOVA $P < 0.0001$, Bonferroni post-test $*P < 0.05$, n =3-4, control vs. pre-stimulated.

1.2.3 NANOPARTICLES AND APICAL MEMBRANE Cl^- CURRENT. To further investigate the conductance pathways activated by N20 and P50 nanoparticles, nystatin was used to permeabilize the basolateral membrane and the appropriate transepithelial ion gradient was established to measure apical membrane Cl^- currents (A_{Cl}).

First, I showed that **N20** nanoparticles (10 µg/ml apical) activated A_{Cl} in Calu-3 cell monolayers by 131.6 ± 32 µA/cm^2 (Fig. 11.**a**). Next, I examined if N20 and P50 nanoparticles could activate A_{Cl} in the absence of HCO_3^- ions. Fig. 11.**b** shows that N20 (10 µg/ml apical) can activate A_{Cl} in the absence of HCO_3^- ions, with an average increase in Isc of 85.8 ± 11.5 µA/cm^2. Likewise, **P50** (100 µg/ml apical) was also capable of increasing A_{Cl} in the absence of HCO_3^- ions by 129.8 ± 13.3 µA/cm^2 (Fig. 11.**c**). Finally in all experiments (Fig 11.**a-c**) DPC (1 mM apical) was able to block the nanoparticle-induced increases in A_{Cl} thus confirming that CFTR Cl^- channels are a target of polystyrene nanoparticles in TEM studies.

FIGURE 11. Effects of polystyrene nanoparticles on apical membrane Cl^- currents. Representative recordings (a-c) of 3 experiments.

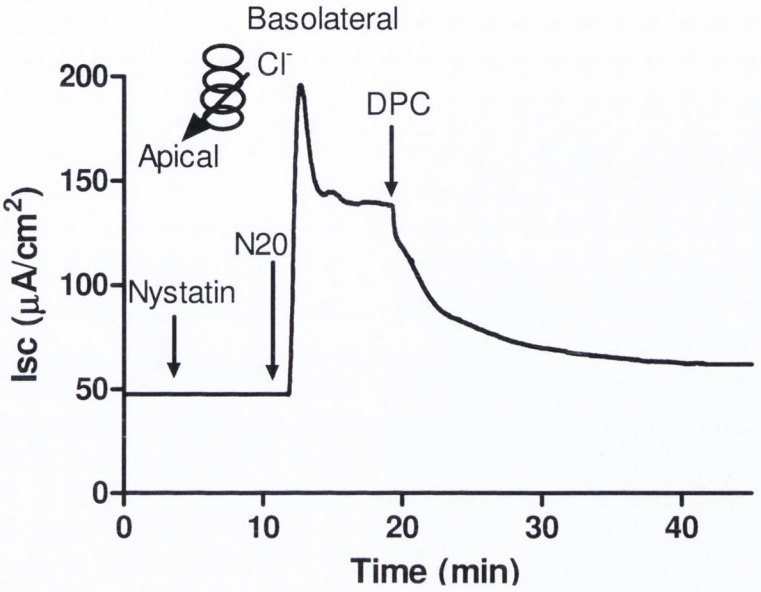

(a) N20 (10 μg/ml apical) activated Isc following the permeabilisation of the basolateral membrane with nystatin (180 μg/ml) and in the presence of a basolateral-to-apical Cl^- gradient. The effect of N20 was inhibited by DPC (1 mM).

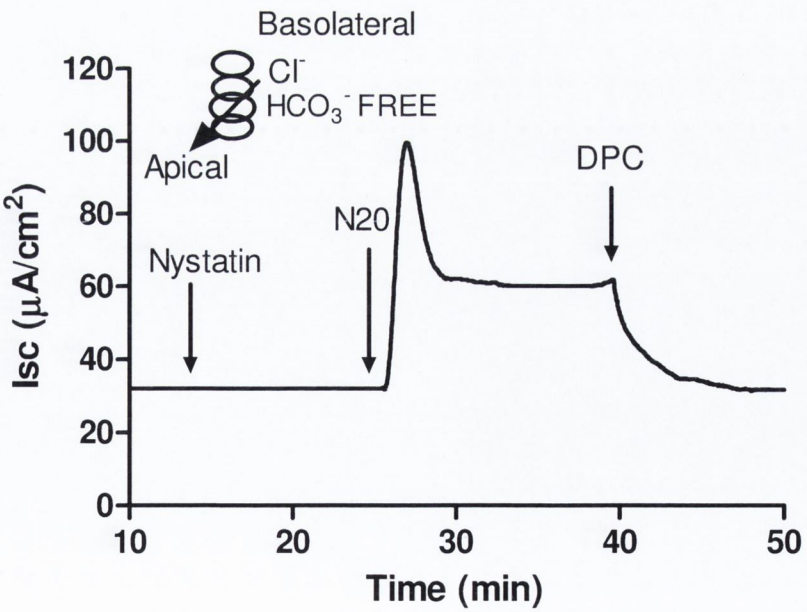

(b) N20 (10 μg/ml apical) activated Isc following the permeabilisation of the basolateral membrane with nystatin (180 μg/ml) and in the presence of a basolateral-to-apical Cl^- gradient but without HCO_3^-. The effect of N20 was inhibited by DPC (1 mM).

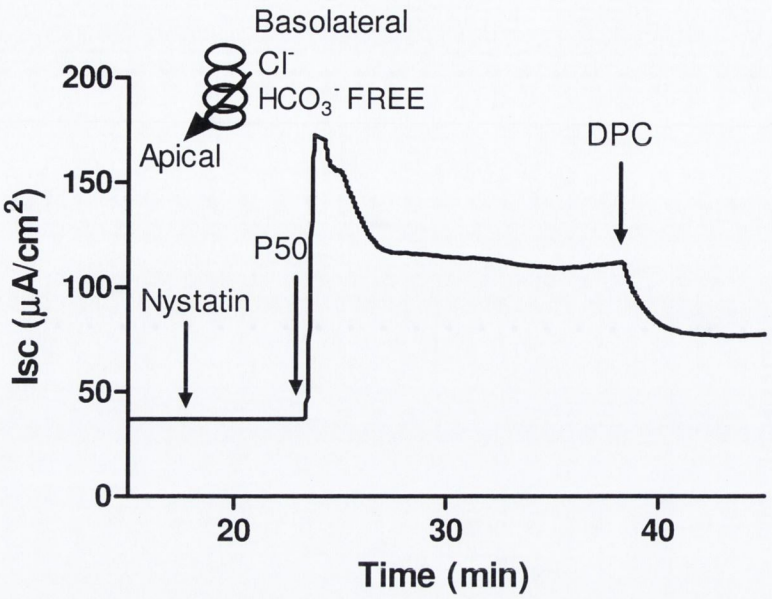

(c) P50 (100 µg/ml apical) activated Isc following the permeabilisation of the basolateral membrane with nystatin (180 µg/ml) and in the presence of a basolateral-to-apical Cl^- gradient but without HCO_3^-. The effect of P50 was inhibited by DPC (1 mM).

1.2.4 NANOPARTICLES EFFECT Ca^{2+}-MEDIATED ANION SECRETION. These experiments were performed in order to establish if other cell signalling pathways in addition to the cAMP-dependent pathway for anion secretion were activated by polystyrene nanoparticles. For this purpose, I used carbachol and thapsigargin, known agonists of Ca^{2+}-dependent signalling, to probe the actions of nanoparticles on Ca^{2+}-mediated Isc responses in Calu-3 cells monolayers.

Carbachol (100 μM basolateral), a cholinergic agonist which causes the release of Ca^{2+} ions from intracellular stores, increased Isc by 14.5 ± 2.1 μA/cm^2 (peak I_{sc}, data not shown). The subsequent addition of **N20** (10 μg/ml apical) further increased Isc by 44.1 ± 8.2 μA/cm^2 (peak I_{sc}) this effect was blocked by $BaCl_2$ (5 mM, basolateral) a blocker of K^+ channels (data not shown).

In the next set of experiments I found that in the absence of carbachol, N20 activated Isc by 37.9 ± 5.8 μA/cm^2 (peak I_{sc}, Fig. 12.**a**). Furthermore, the addition of carbachol after N20 significantly increased Isc by 123 ± 22 μA/cm^2 (peak I_{sc}, Fig. 12.**a**). As expected $BaCl_2$ (5 mM, basolateral) blocked all effects on Isc (peak I_{sc}, Fig. 12.**a**). A summary of these results is shown in Fig. 12.**b**.

I then investigated if **P50** nanoparticles also exhibited the same synergistic effects on Ca^{2+}-mediated Isc responses in Calu-3 cells monolayers. I observed that carbachol-induced Isc was significantly increased (*$P < 0.05$, n=3) by pre-stimulation of Calu-3 cell monolayers with P50 (100 µg/ml apical). However the magnitude of this stimulation was not significantly different to control Isc responses to P50 alone or when Calu-3 cells were pre-stimulated with carbachol ($P > 0.05$, n=3). A summary of this data is shown in Fig. 12.**c**.

To further elucidate the mechanisms by which N20 nanoparticles synergistically increase Isc responses in the presence of carbachol, I used the endoplasmic reticulum Ca^{2+}-ATPase inhibitor thapsigargin, to investigate if N20 nanoparticles were affecting Ca^{2+}-dependent cell signalling directly via the involvement of intracellular Ca^{2+} stores.

Thapsigargin (1 µM bilaterally) was found to increased Isc by 16.54 ± 3.6 µA/cm^2 in Calu-3 cells (peak I_{sc}, Fig. 12.**d**). The subsequent addition of N20 (10 µg/ml apical) further increased Isc by 53.46 ± 5.2 µA/cm^2 (peak I_{sc}, Fig.12.**d**) and this effect was blocked by furosemide (1 mM) a blocker of the NKCC co-transporter and $BaCl_2$ (5 mM basolateral).

In the absence of thapsigargin, N20 activated Isc by 49.42 ± 3.4 µA/cm^2 (peak I_{sc}, Fig.12.**e**). Furthermore, the addition of thapsigargin

after N20 increased Isc by 65.8 ± 3.6 μA/cm^2 (peak I_{sc}, Fig. 12.**e**). As expected furosemide (1 mM basolateral) and $BaCl_2$ (5 mM basolateral) blocked the effect on Isc (Fig. 12.**d** and **e**). The statistical analysis of these results is shown in Fig. 12.**f**.

Overall these results indicate that N20 nanoparticles can act synergistically with Ca^{2+}-dependent cell signalling to drive anion secretion and that intracellular calcium stores may be the source of this cation in Calu-3 cells.

FIGURE 12. Effects of N20 and P50 nanoparticles on Ca^{2+}-mediated anion secretion in Calu-3 cells. Representative recordings (a, d, e) of 3 experiments and the statistical analysis of data (b, c, f).

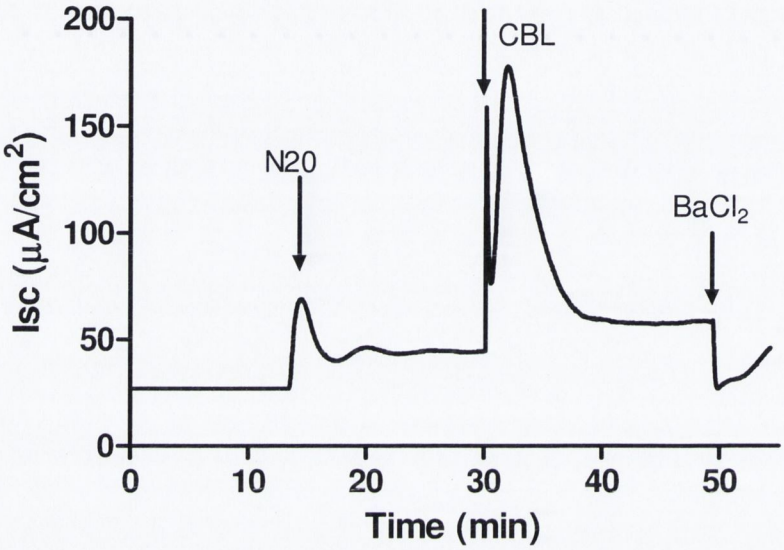

(a) Carbachol (CBL, 100 μM basolateral) significantly increased Isc following pre-stimulation by N20 (10 μg/ml apical), $BaCl_2$ (5 mM basolateral) as shown inhibited Isc.

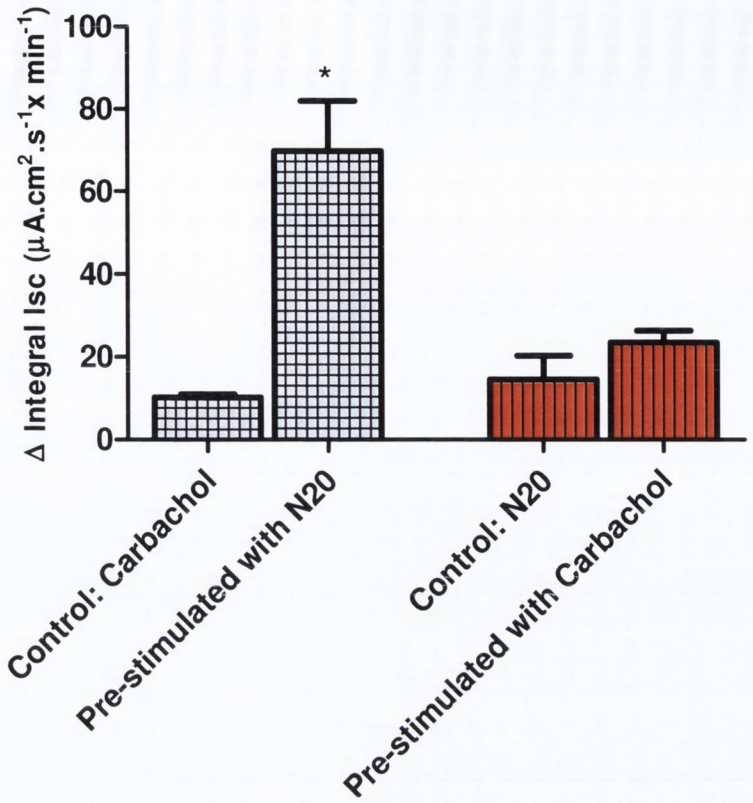

(b) Carbachol-induced Isc was significantly increased by pre-stimulation with N20. In contrast, pre-stimulation of cells with carbachol did not significantly affect N20-induced Isc. One-way ANOVA $P < 0.0001$, Bonferroni post-test $^*P < 0.05$, n=3-5, control vs. pre-stimulated.

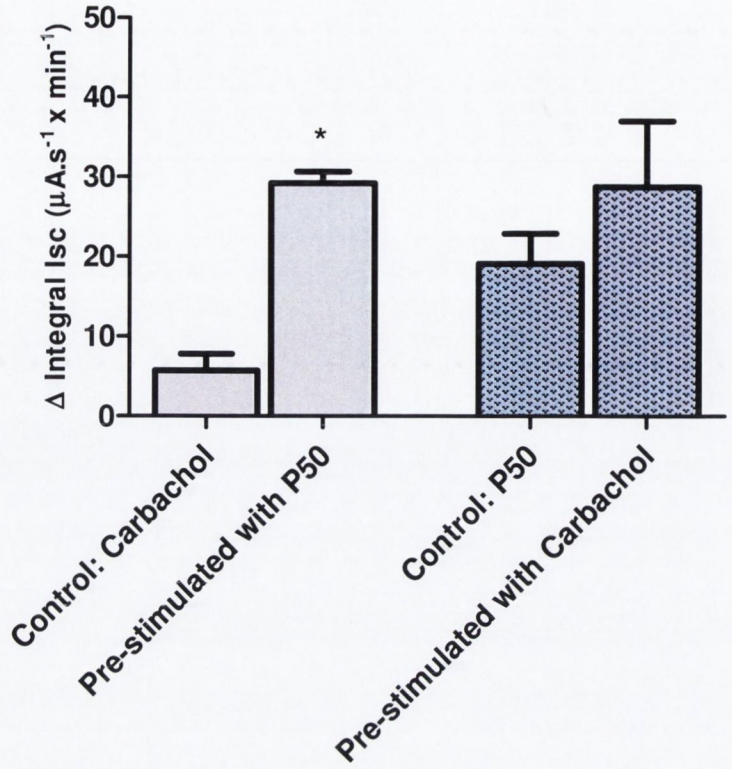

(c) Carbachol-induced Isc was significantly increased (by pre-stimulation with P50. In contrast, pre-stimulation of cells with carbachol did not result in a significant increase in P50-induced responses. One-way ANOVA $P < 0.0241$, Bonferroni post-test $^*P < 0.05$, n=3, control vs. pre-stimulated.

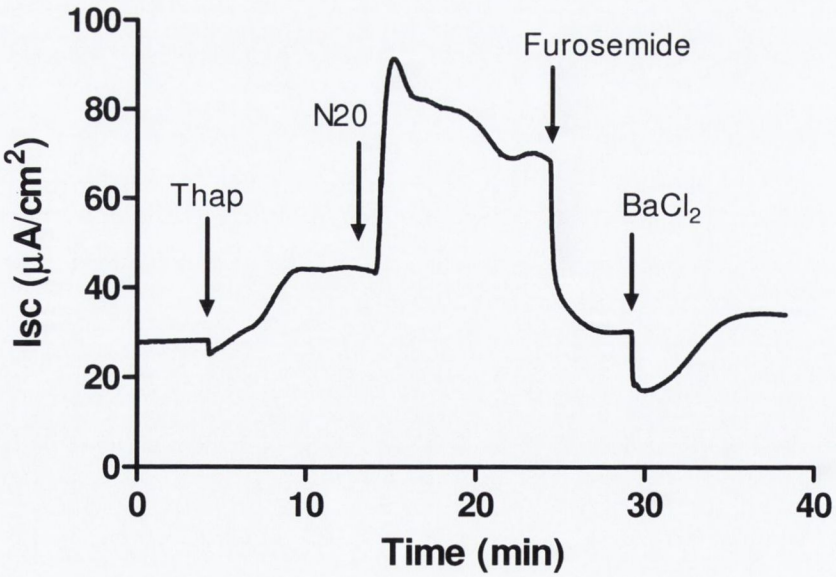

(d) The activation of Isc by thapsigargin (Thap) (1 μM both sides) in Calu-3 cells. N20 (10 μg/ml apical) further increased Isc in thapsigargin pre-treated cells. Furosemide (1 mM basolateral) and $BaCl_2$ (5 mM basolateral) inhibited Isc.

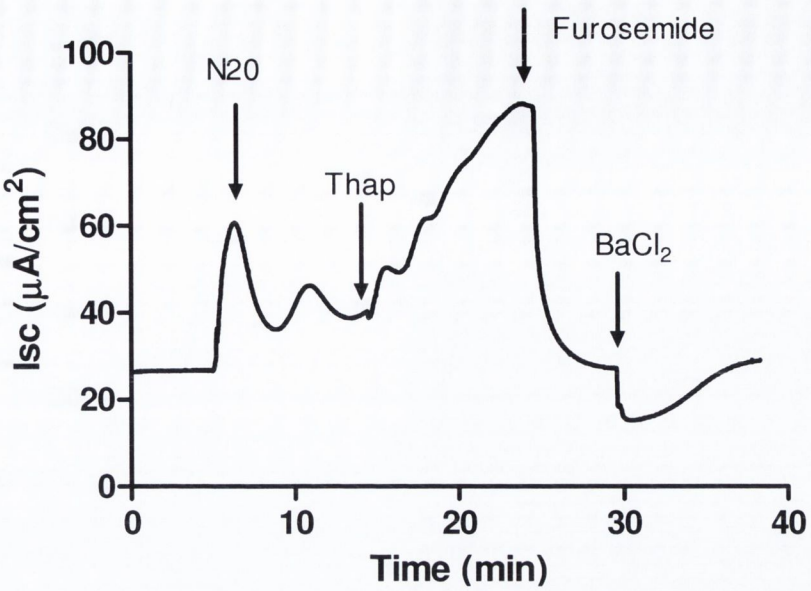

(e) Thapsigargin (Thap) (1 μM both sides) significantly increased Isc following pre-stimulation by N20 (10 μg/ml apical) in Calu-3 monolayers. Furosemide (1 mM basolateral) and $BaCl_2$ (5 mM basolateral) inhibited Isc.

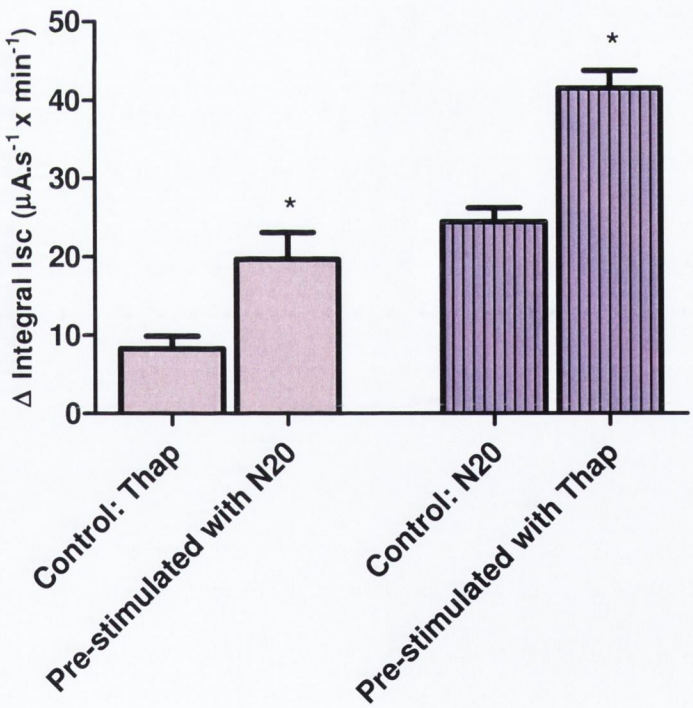

(f) Thapsigargin-induced Isc was significantly increased by pre-stimulation with N20. Furthermore, pre-stimulation of cells with thapsigargin resulted in a significant increase in N20-induced Isc responses. One-way ANOVA $P < 0.0001$, Bonferroni post-test *$P < 0.05$, n=4-5, control vs. pre-stimulated.

1.2.5 NANOPARTICLES ACTIVATE CATION CHANNELS IN CALU-3 CELLS.

I investigated the interactions between basolateral K^+ channels and nanoparticles, as these channels can also act as a driving force for anion secretion in Calu-3 cells.

Nystatin was used to permeabilise the apical membrane in the presence of an established transepithelial ion gradient to measure K^+ currents. **N20** (10 µg/ml apical), activated K^+ current in Calu-3 cells (Fig. 13.**a**), an effect inhibited by XE991, a potent and selective inhibitor of K^+ channels.

To investigate if this effect of nanoparticles was cAMP-dependent Calu-3 cells were pre-treated with forskolin (10 µM both sides). Fig. 13.**b** shows that forskolin abolished the affect of N20 (10 µg/ml) on K^+ currents. Moreover, forskolin-induced activation of K^+ channels was XE991-sensitive thus showing that N20-activated K^+ currents in a cAMP-dependent manner. Further affirmation that N20 nanoparticles act through the cAMP-pathway came from my data which showed that N20–activated K^+ currents in Calu-3 cells were not sensitive to clotrimazole, which is a known inhibitor of Ca^{2+}-regulated K^+ channels (Fig. 13.**c**). In contrast, **P50** nanoparticles (100 µg/ml) exerted no significant effect on basolateral K^+ currents (Fig. 13.**d**). As expected N20–activated K^+ currents were sensitive to $BaCl_2$ a non-specific blocker of all K^+ channels (Fig. 13.**e**).

FIGURE 13. Effects of polystyrene nanoparticles on basolateral membrane K^+ currents. Representative recordings (a-c) of 3 experiments.

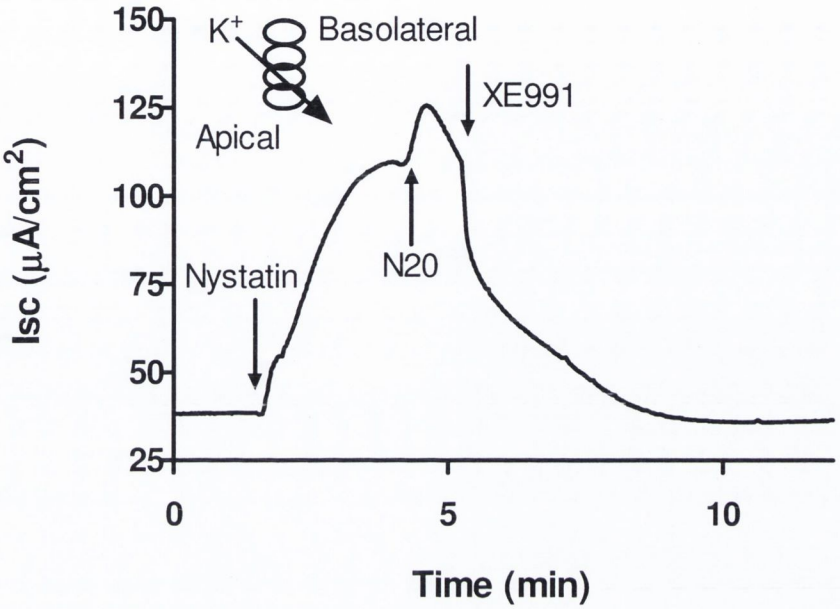

(a) N20 (10 μg/ml apical) activated K^+ currents following the permeabilisation of the apical membrane with nystatin (180 μg/ml) and in the presence of a apical-to-basolateral K^+ gradient. The effect of N20 was inhibited by XE991 (10 μM).

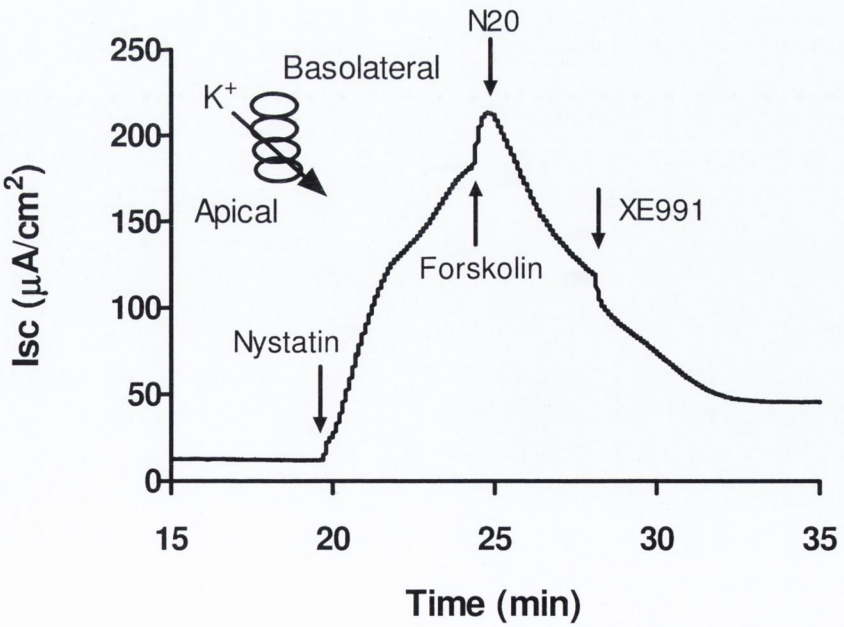

(b) Pre-stimulation of cell monolayers with Forskolin (10 μM both sides) abolished the effects of N20 on basolateral K^+ currents. The effect of forskolin was inhibited by XE991 (10 μM basolateral).

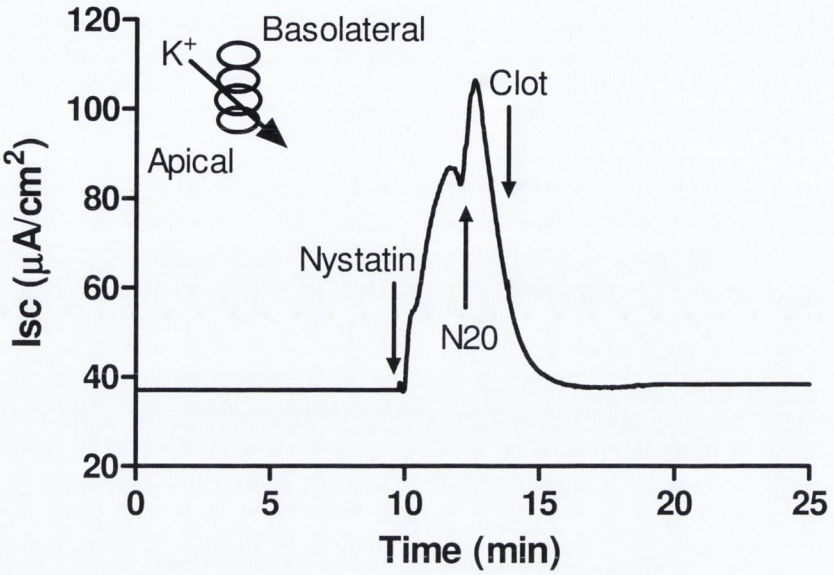

(c) Clotrimazole (30 μM basolateral) did not block the effects of N20 (10 μg/ml both sides) on basolateral K^+ currents.

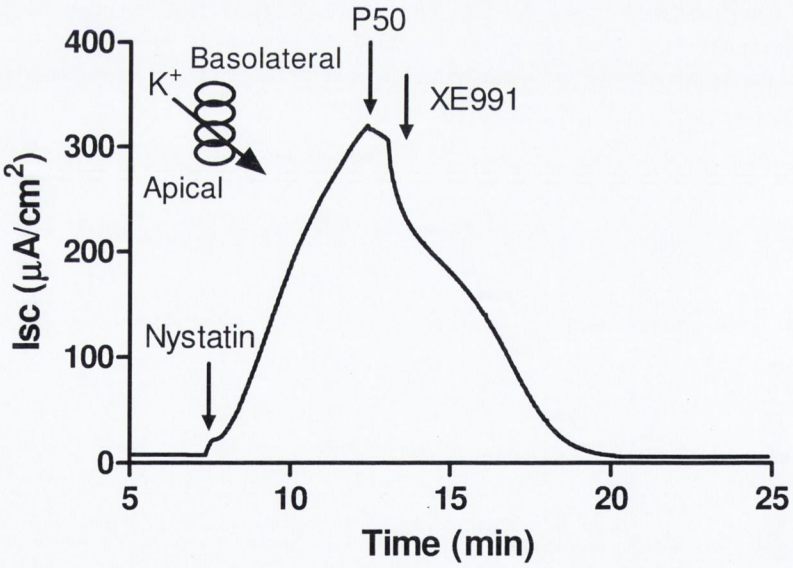

(d) P50 (100 μg/ml apical) did not activate basolateral K^+ currents following the permeabilisation of the apical membrane with nystatin (180 μg/ml) and in the presence of a apical-to-basolateral K^+ gradient. The effect of nystatin was inhibited by XE991 (10 μM basolateral).

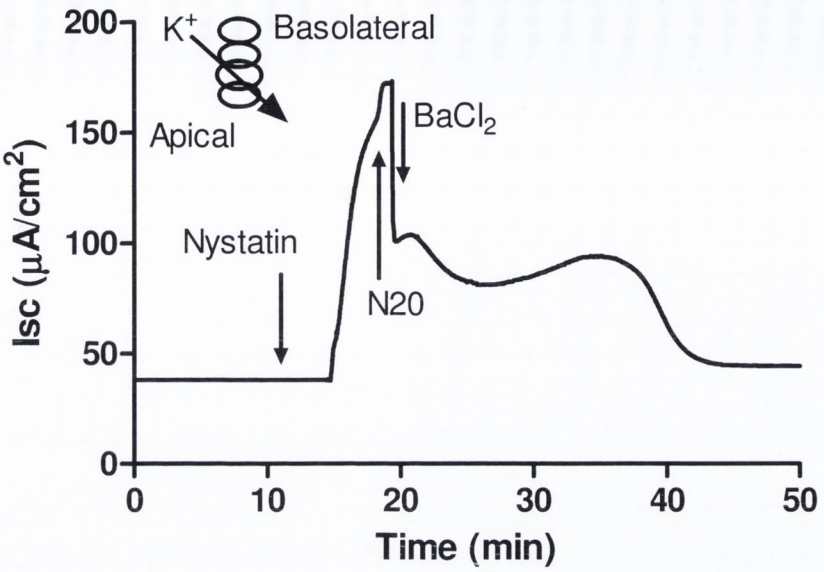

(e) $BaCl_2$ (5 mM basolateral) blocked the effects of N20 (10 μg/ml) on basolateral K^+ currents.

1.2.6 ANION SUBSITUTION TEM STUDIES AND NANOPARTICLES. The results of our previous TEM studies revealed that apically located CFTR Cl^- channels are targeted by N20 nanoparticles. In airway epithelial cells such as Calu-3, the primary basolateral entry pathways for Cl^- and HCO_3^- anions are through the NKCC and Na^+-HCO_3^- co-transporters, respectively. Both anions have been shown to exit the cell via CFTR Cl^- channels. Thus, I wanted to examine if either one of these two anions (Cl^- or HCO_3^-) was preferentially secreted by Calu-3 cells upon stimulation by N20 nanoparticles. In these experiments I decided to use forskolin Isc responses as a reference for comparison with N20-induced Isc responses.

The comparison of the the responses of forskolin and **N20** on Isc using normal KHS showed that there were no significant differences between their responses; 36.3 ± 1.5 vs. 29.8 ± 4.8 respectively $\mu A/cm^2$ (Peak $_{Isc}$, $P > 0.05$, n=3, Fig. 14). However, under HCO_3^- free conditions there was a significant decrease in N20-induced Isc; 11.7 ± 2.0 vs. forskolin 35.7 ± 8.8 $\mu A/cm^2$ we (Peak $_{Isc}$, $P < 0.05$, n=4, Fig. 14). Similarly, reduced N20-induced Isc response was observed under low Cl^- conditions 26.1 ± 3.5 vs. forskolin 58.8 ± 0.7 $\mu A/cm^2$ (Peak $_{Isc}$, $P < 0.05$, n=4, Fig. 14). In all these experiments addition of DPC (1 mM apical) decreased Isc to baseline levels.

For each set of experiments carried out using either normal KH, HCO_3^- free or low Cl^- solutions the ratio for N20 activated Isc as a factor of forskolin activated Isc was calculated (N20-induced Isc/Forskolin induced Isc). The ratio value under normal KHS conditions was found to be 0.82 ± 0.1. The ratio value we obtained under HCO_3^- free and low Cl^- conditions was 0.32 ± 0.06 and 0.42 ± 0.08, respectively. Therefore, each anion contributes ~ 50% of the N20-induced Isc responses we observed in TEM studies showing that NKCC and Na^+-HCO_3^- co-transporters located in the basolateral membrane are possible targets for N20 nanoparticles.

FIGURE 14. Effects of anion substitution on forskolin and N20 Isc responses in Calu-3 cell monolayers.

N20-induced Isc was significantly decreased under low Cl^- and HCO_3^- levels when compared with forskolin responses. One-way ANOVA $P < 0.0004$, Bonferroni post-test $^*P < 0.05$, n=4, as indicated.

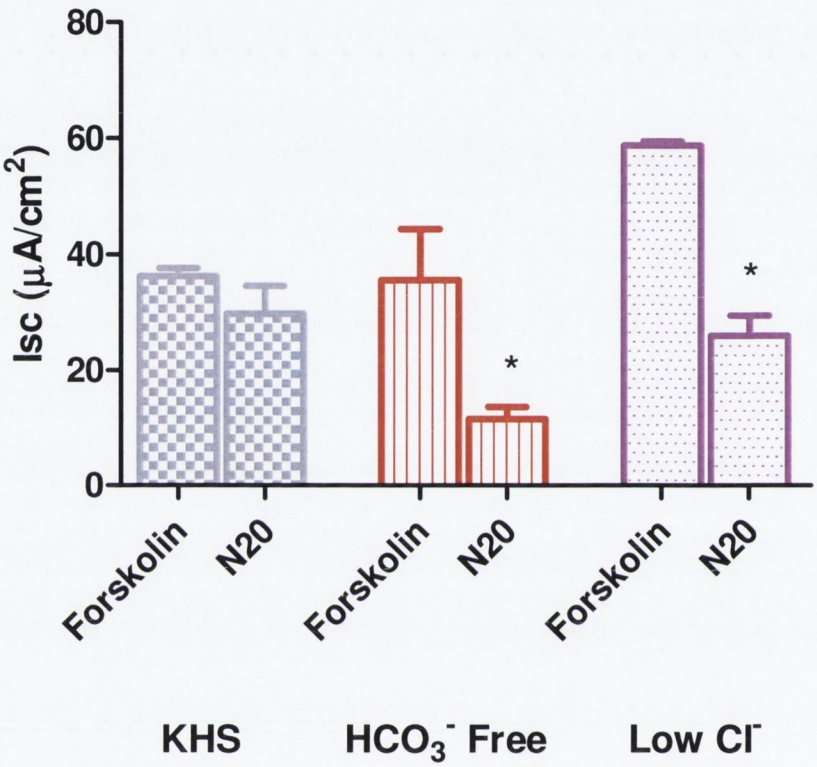

1.2.7 NO/sGC/cGMP PATHWAY AND NANOPARTICLES. It is known that the NO/cGMP pathway is an important pathway for anion secretion in respiratory cells [58]. Therefore, I designed the next set of experiments to investigate if polystyrene nanoparticles activate Isc in Calu-3 cells via the NO/cGMP pathway.

First, I examined the response of **N20** nanoparticles in the presence and absence of the NO donor, GSNO. N20 (10 µg/ml apical) was found to increased Isc by 12.0 ± 3.0 µA/cm^2 in Calu-3 cells (peak I_{sc}, Fig. 15.**a**). The subsequent addition of GSNO (100 µM both sides) further increased Isc by 26.1 ± 2.5 µA/cm^2 (peak I_{sc}, Fig. 15.**a**), this effect was blocked by DPC (1 mM apical) a blocker of CFTR Cl^- channels and $BaCl_2$ (5 mM basolateral).

In the absence of N20, GSNO (100 µM both sides) activated Isc by 39.1 ± 1.6 µA/cm^2 (peak I_{sc}, Fig. 15.**b**). The subsequent addition of N20 (10 µg/ml apical) increased Isc by 2.4 ± 0.7 µA/cm^2 (peak I_{sc}, Fig. 15.**b**). Again Isc was inhibited by the addition of DPC (1 mM apical) and $BaCl_2$ (5 mM basolateral). The statistical analysis of these results is shown in Fig. 15.**c**.

Next, I examined the response of **N20** nanoparticles in the presence of a NO synthase inhibitor, L-NAME that inhibits generation of endogenous NO. I found that application of L-NAME (1 mM both

sides) caused a transient reduction in basal Isc (Fig. 15.**d**). The subsequent addition of N20 (10 µg/ml apical) increased Isc by 9.4 ± 1.2 µA/cm^2. This increase was not significantly different from the effects detected in the absence of L-NAME ($P > 0.05$, n=3). Isc was inhibited by the addition of DPC (1 mM apical) and $BaCl_2$ (5 mM basolateral) (Fig. 15.**d**).

The effects of NO on Isc in Calu-3 cells are known to be mediated by activation of the enzyme soluble guanylyl cyclase (sGC) leading to an increase in the cGMP levels [58]. To determine whether this pathway was involved in Isc activation by **N20** nanoparticles, Calu-3 cell monolayers were pre-treated with a selective inhibitor of sGC, ODQ (10 µM both sides). ODQ caused a transient reduction in Isc and prevented the activation of Isc by N20 nanoparticles (10 µg/ml apical) (*$P < 0.05$, n=3) (Fig. 15.**e**). As expected, Isc was inhibited by the addition of DPC (1 mM apical) and $BaCl_2$ (5 mM basolateral). These results indicate that sGC and down-stream cGMP plays a crucial role in N20-mediated Isc activation in Calu-3 cells.

FIGURE 15. Effect of N20 on NO/cGMP–mediated transepithelial Cl^- secretion in Calu-3 cells. Representative recordings (a, b, d, e) of 4 experiments and the statistical analysis of data (c).

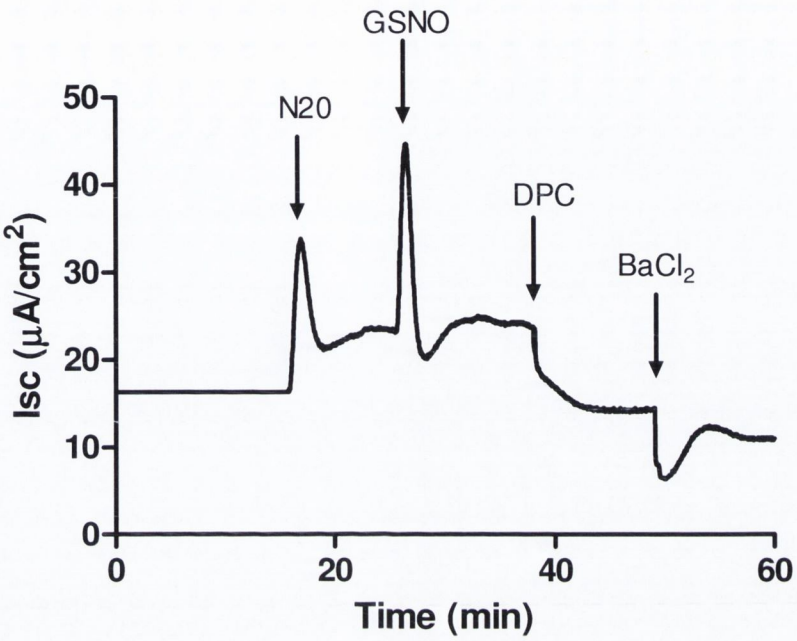

(a) The activation of Isc by N20 (10 μg/ml apical) in Calu-3 cells. GSNO (100 μM both sides) further increased Isc in N20 pre-treated cells.

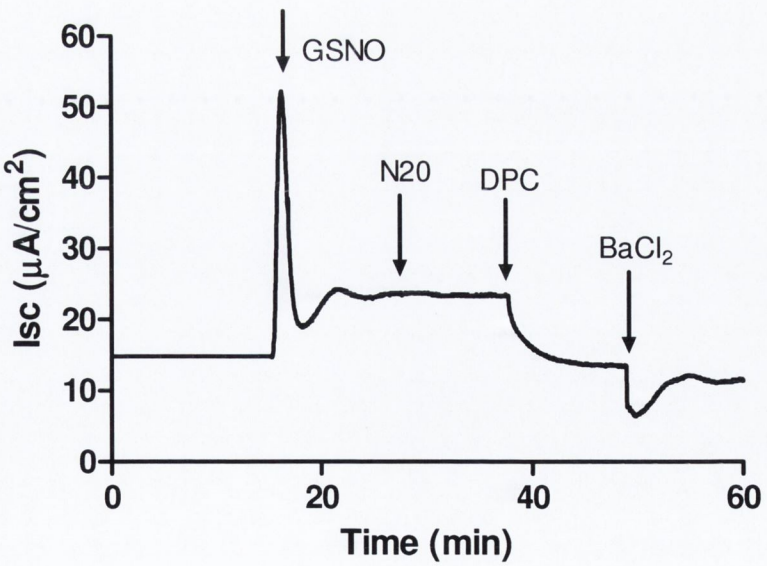

(b) The activation of Isc by N20 (10 μg/ml apical) was abolished when cells were pre-stimulated with GSNO (100 μM both sides). All Isc currents were significantly reduced by the application of DPC (1 mM apical) and barium chloride (5 mM basolaterally) as shown in **(a-b)**.

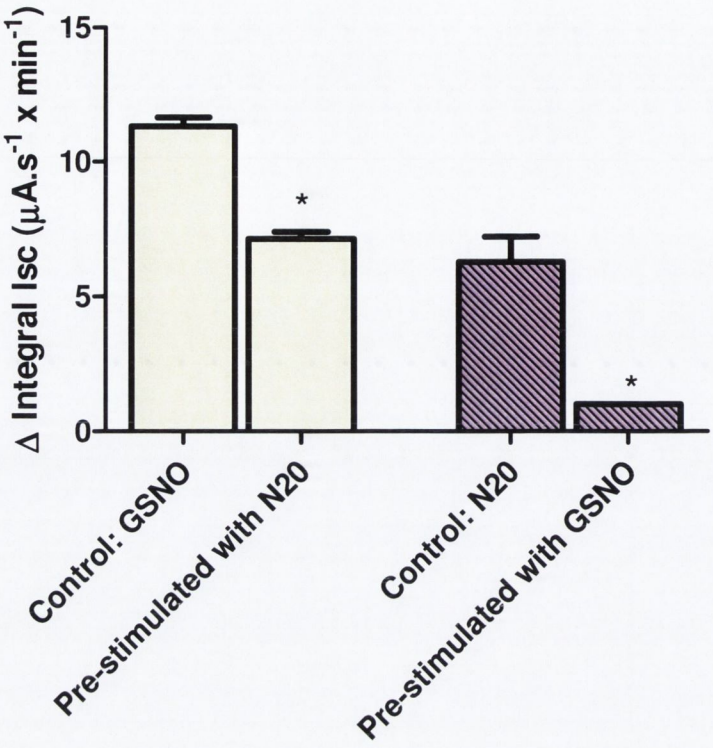

(c) GSNO-induced Isc was significantly altered by pre-stimulation with N20. Similarly, pre-stimulation of cells with GSNO resulted in a significant decrease in N20-induced responses. One-way ANOVA $P < 0.0001$, Bonferroni post-test $*P < 0.05$, n=4, control vs. pre-stimulated.

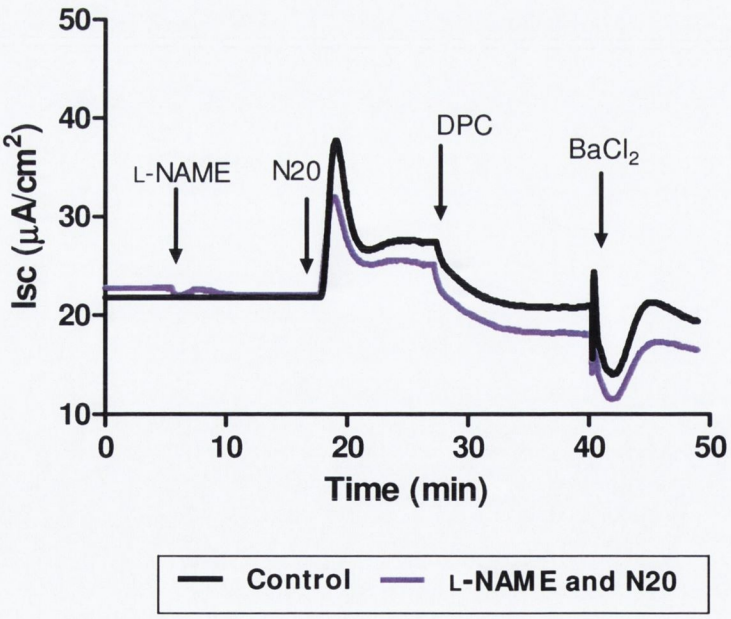

(d) The pre-treatment of cells with L-NAME (1 mM both sides) did not inhibit the effects of N20 (10 μg/ml apical) on Isc activation. Isc was significantly reduced by the application of DPC (1 mM apical) and barium chloride (5 mM basolaterally).

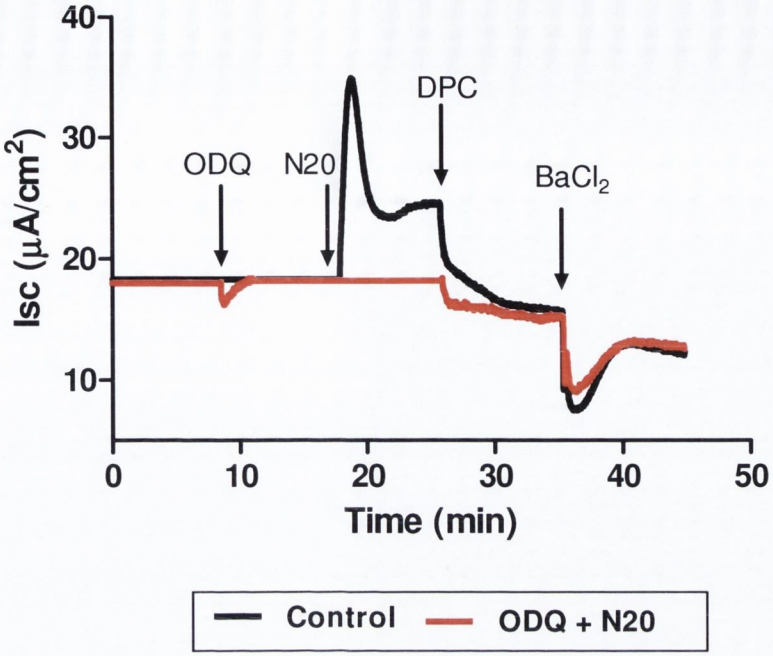

(e) The pre-treatment of cells with 1*H*-[1, 2, 4] oxadiazolol-[4, 3-*a*] quinoxalin-1-one (ODQ, 10 μM both sides) inhibited the effects of N20 (10 μg/ml apical) on Isc activation. Isc was significantly reduced by the application of DPC (1 mM apical) and barium chloride (5 mM basolaterally).

1.2.8 SILICA NANOPARTICLES AND CALU-3 CELLS. As synthetic amorphous silica is now being used widely in both diagnostics and biomedical research due to its low cost and ease of production I decided to investigate if silica nanoparticles could acutely affect transepithelial ion fluxes in Calu-3 cells.

I tested the effects of amine-modified 50-nm silica nanoparticles (**Si-P50**) on Isc in Calu-3 cell monolayers. Si-P50 at concentrations ranging from 10-150 µg/ml exerted no significant effects on Isc (Fig. 16). Furthermore, pre-treatment of cells with these nanoparticles did not affect increases in Isc induced by forskolin (Peak I_{sc} responses ranging from 38.2–112.8 µA/cm^2, $P > 0.05$) Thus, Si-P50 NPs do not acutely affect Isc in Calu-3 cell monolayers.

FIGURE 16. Acute effects of silica nanoparticles on transepithelial ion fluxes in Calu-3 cell monolayers.

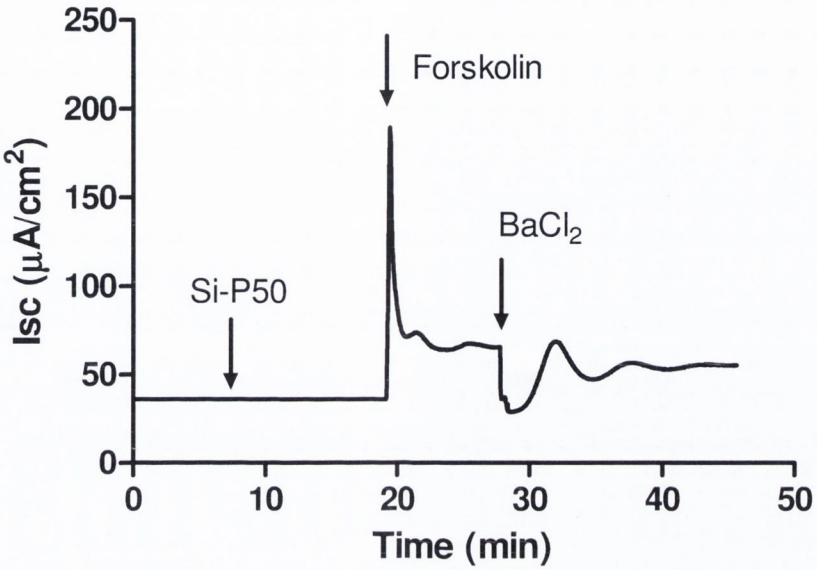

Si-P50 (100 μg/ml apical) exerted no significant effect on Isc responses in Calu-3 cells. All Isc currents were significantly reduced by the application of DPC (1 mM apical) of barium chloride (5 mM basolaterally).

1.2.9 NANOPARTICLES AND NHBE CELLS. In these experiments I have examined the effects of polystyrene and silica nanoparticles on Isc responses in NHBE cells. These cells were chosen specifically because they have been cultured commercially to form a pseudo-stratified highly differentiated respiratory cell model, which closely resembles the epithelial tissues of the tracheal/bronchial tract.

First, I tested the ability of **N20** polystyrene nanoparticles to increase Isc in NHBE cell monolayers. No significant effect was detected on Isc after apically exposing NHBE cells to N20 (10 µg/ml apical) (Fig. 17.**a**) either in the presence or absence of forskolin (10 µM both sides). Forskolin responses (10 µM both sides) in the absence of N20, increased Isc by 14.3 ± 1.24 µA/cm^2 (peak I_{sc}). In turn forskolin responses in the presence of N20 (10 µg/ml apical) were 14.08 ± 0.81 µA/cm^2, these were found not to be significantly different from control responses (Peak I_{sc}, P >0.05, unpaired t test, n=4). In NHBE Isc currents were found to be only minimally sensitive to DPC (1 mM apical) but were profoundly inhibited by the application of barium chloride (5 mM Basolateral).

Next, I tested the ability of **Si-P50** to increase Isc in NHBE cell monolayers. Again no significant effect was detected on Isc after apically exposing NHBE cells to Si-P50 (100 µg/ml apical) (Fig. 17.**b**). In the presence of Si-P50, Forskolin (10 µM both sides) increased Isc

by 13.75 ± 1.25 μA/cm^2 (Peak I_{sc}). Similar to experiments with **N20**, Isc currents were found to be only minimally sensitive to DPC (1 mM apical) but were rapidly inhibited by the application of barium chloride (5 mM basolateral).

FIGURE 17. Effects of nanoparticles on transepithelial Cl^- secretion in Normal Human Bronchial Epithelial Cells.

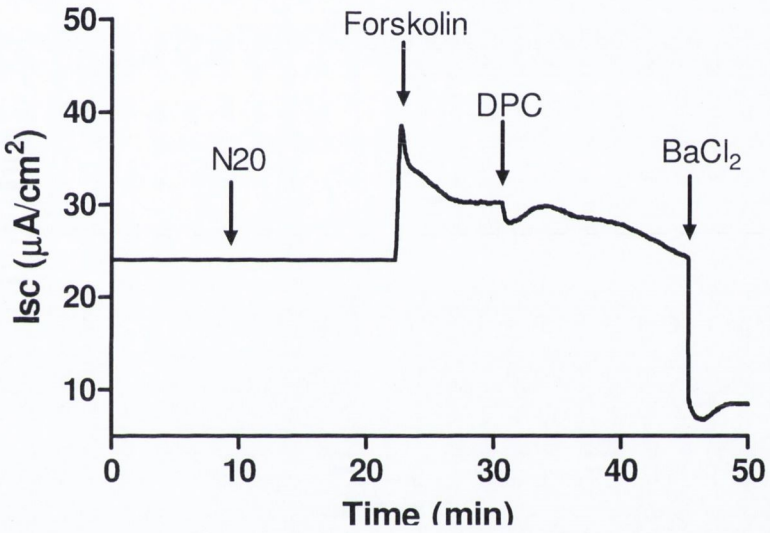

(a) N20 exerted no signficant effect on Isc responses in NHBE cells. Application of Forskolin (10 μM both sides) caused a significant increase in Isc.

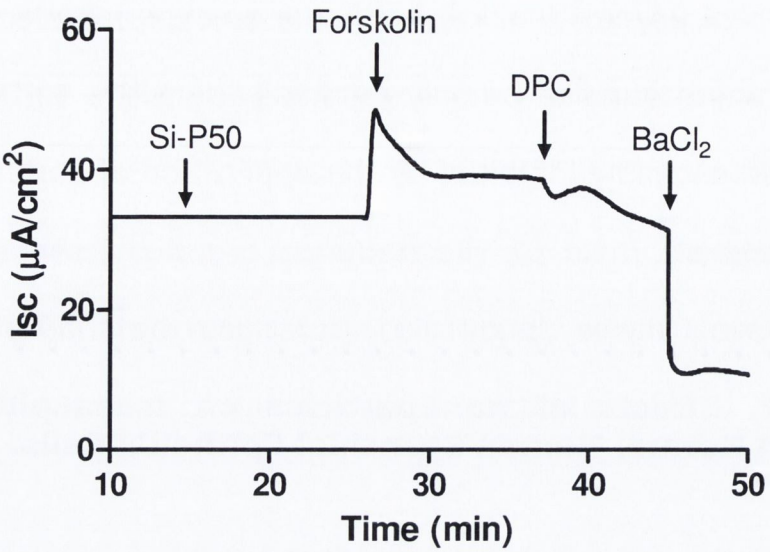

(b) Si-P50 exerted no signficant effect on Isc responses in NHBE cells. Application of Forskolin (10 μM both sides) caused a significant increase in Isc. All currents were inhibited by the application of DPC (1 mM apical) and barium chloride (5 mM basolateral) as shown in **(a-b)**.

1.2.10 SILICA NANOPARTICLES, TEM STUDIES IN THE PRESENCE OF CYTOKINES. Researchers have shown that pro-inflammatory cytokines exert a profound inhibitory effect on transepithelial ion secretion in airway epithelial cells [125]. I wanted to examine if smaller 10-nm silica nanoparticles (**Si-10**) could; (1) affect basal Isc responses in Calu-3 cells and (2) exacerbate the inhibition of transepithelial ion transport across Calu-3 cell monolayers reported in the presence of pro-inflammatory cytokines.

First I investigated the effects of varying concentrations of pro-inflammatory cytokines specifically TNF-α, IL-β and IFN-γ (in combination) on Isc responses in Calu-3 cells. Fig. 18.**a** shows that forskolin-induced Isc in Calu-3 cell monolayers treated overnight with cytokines at concentrations of 50 and 100 ng/ml was significantly inhibited when compared with control (untreated cells) by approximately 64.8 and 47.2 % respectively.

Next, I examined the acute effects of **Si-10** (100 μg/ml apical) on basal Isc responses in Calu-3 cells. As Fig. 18.**b** shows Si-10 exerted no significant effect on basal Isc. Furthermore, I did not observe any significant differences in the response of Calu-3 cell monolayers to forskolin (10 μM apical) upon acute exposure to Si-10 nanoparticles (100 μg/ml apical, Fig. 18.**b**) when compared with control Isc

responses. As expected all Isc currents were sensitive to inhibition by $BaCl_2$ (5 mM basolateral).

Finally, I examined the effects of Si-10 nanoparticles in the presence of cytokines on forskolin-induced Isc responses. No further inhibition of this response was detected when compared to the inhibition observed in the presence of pro-inflammatory cytokines only (100 ng/ml each) (Fig. 18.**c**). Si-10 nanoparticles (100 µg/ml apical) in the presence of cytokine treated cell monolayers showed a significant inhibition of forskolin-induced Isc of 50.5 ± 10.1 % (*$P < 0.05$, n=3) compared to controls (Fig. 18.**c**). However post-tests reveal that this effect was not significantly different ($P > 0.05$, n=3-4) from the inhibition observed on forskolin-induced Isc responses when Calu-3 cell monolayers are treated with cytokines only, 52.8 ± 10.0 % (Fig. 18.**c**).

FIGURE 18. Effect of Si-10 on Isc under pro-inflammatory conditions.

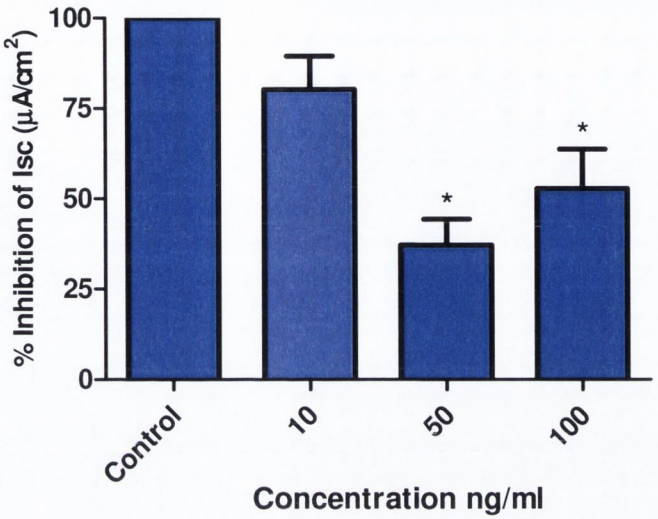

(a) Forskolin-induced Isc was significantly reduced after overnight treatment with cytokines at concentrations of 50 and 100 ng/ml. One-way ANOVA $P < 0.0036$, Tukey-Kramer post-test $*P < 0.05$, n=3-4, treatments vs. control.

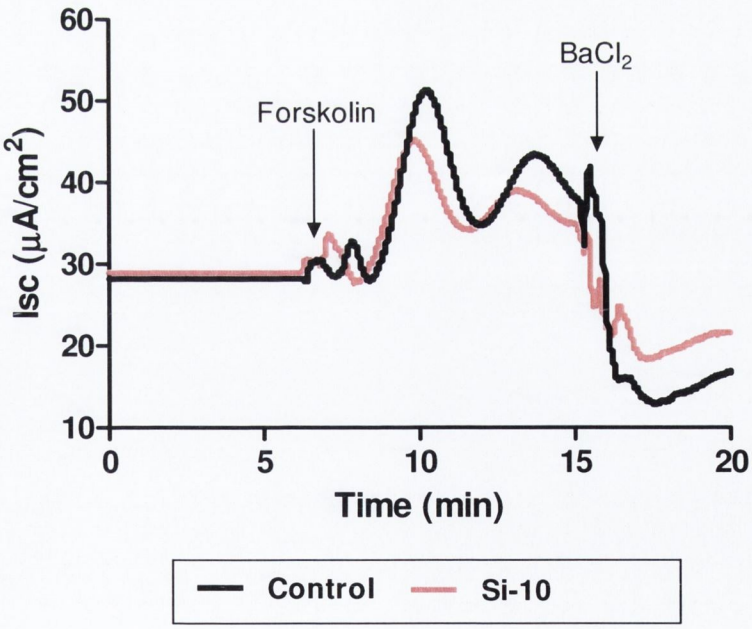

(b) Si-10 (100 μg/ml apical) exerted no significant effect on basal Isc responses in Calu-3 cells. Furthermore, Si-10 showed no effect on forskolin-induced Isc responses in Calu-3 cells compared to controls (unexposed cell monolayers). All Isc currents were significantly reduced by the application of barium chloride (5 mM basolaterally).

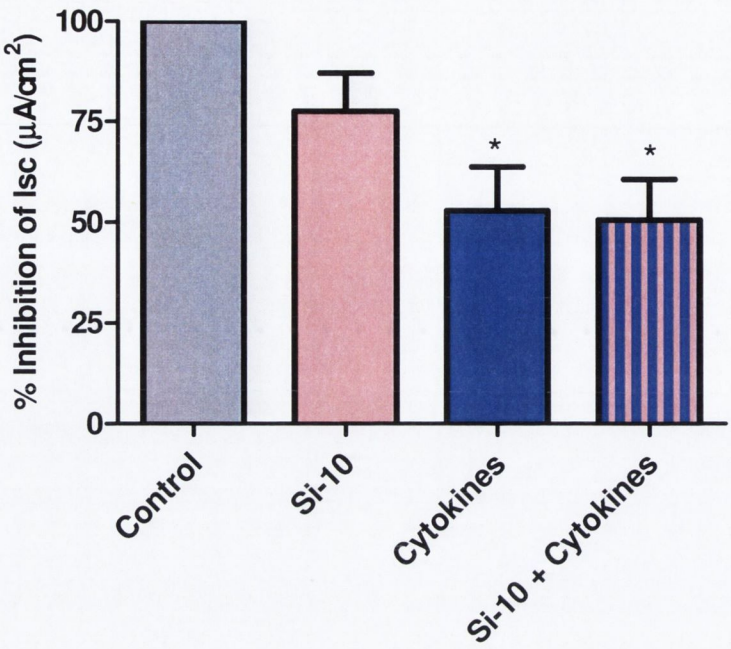

(c) Cytokine-induced decrease in Isc was not significantly modified in the presence of Si-10. One–way ANOVA $P < 0.016$, Tukey-Kramer post-test *$P < 0.05$, n=3-4, cytokines vs. control and Si-10 vs. Si-10 + cytokines; $P > 0.05$ cytokines vs. Si-10 + cytokines.

1.3 TRANSEPITHELIAL MEASUREMENTS: CHRONIC EFFECTS

For the purpose of this investigation I defined chronic exposure of cells to nanoparticles as the "prolonged (hours, days) or repetitive exposure of the lung epithelium/cells to nanoparticles". The aim of these TEM studies was to investigate if chronic exposure of Calu-3 monolayers to N20 and P50 polystyrene NPs could modify Isc responses to carbachol. I decided to use the cholinergic agonist carbachol since it has been proposed that chronic exposure of airway epithelial cells to NPs leads to the accumulation and interaction of NPs with endoplasmic membranes and may in turn lead to the dysregulation of Ca^{2+} homeostasis and second messenger systems affected by various mediators including the cholinergic system [93].

I found that following chronic (overnight) exposure of Calu-3 cell monolayers to high concentrations of **N20** and **P50,** (200 μg/ml), that carbachol-induced Isc was significantly reduced when compared against controls; 46.8 ± 9.2 and 45.5 ± 4.0 %, respectively (Fig. 19.**a** and **b**). This reduction was not due to a loss of cell monolayer permeability, as control and NP-treated Calu-3 cell monolayers exhibited stable transepithelial electrical resistance (TEER) values in the range of 227–334 Ω/cm^2 (Fig. 19.**c**). Permeability values for well-differentiated primary cultured human tracheobronchial cells range between 300 and 650 Ω/cm^2 [126-127].

FIGURE 19. Effect of chronic exposure of N20 and P50 nanoparticles on transepithelial ion fluxes (a-b) and transepithelial electrical resistance (c).

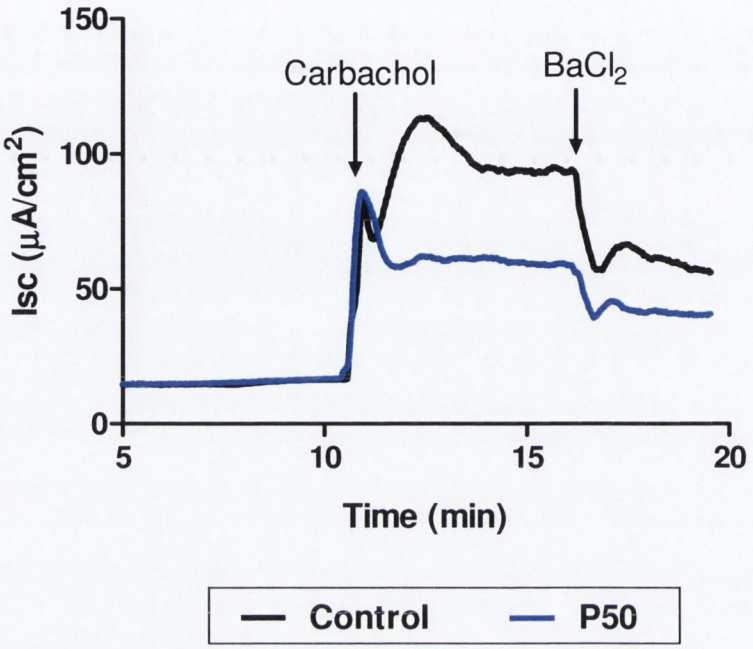

(a) Carbachol (100 μM basolateral) induced Isc was reduced after overnight exposure to P50 (200 μg/ml). All Isc currents were significantly reduced by the application of barium chloride (5 mM basolaterally).

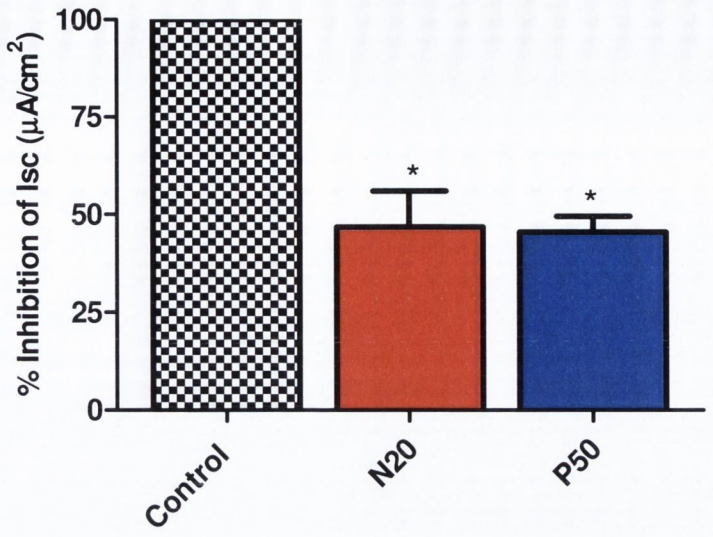

(b) Carbachol-induced Isc was significantly reduced compared to control responses after overnight exposure of Calu-3 cell monolayers to either N20 or P50 nanoparticles (200 µg/ml apical). One-way ANOVA, $P < 0.0003$, Tukey-Kramer post-test * $P < 0.05$, n=3-4, control vs. treatments.

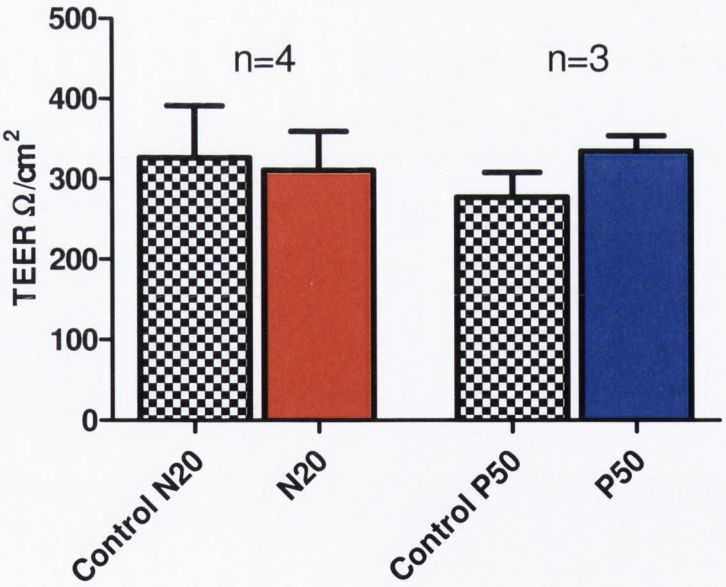

(c) Chronic exposure of Calu-3 cell monolayers to N20 and P50 (200 µg/ml) exerted no significant effect on transepithelial electrical resistance (TEER). One-way ANOVA, $P > 0.05$, control vs. treatments.

1.4 PATCH CLAMP STUDIES

1.4.1 EXCISED, INSIDE-OUT PATCH CLAMP RECORDINGS OF NP-STIMULATED CFTR ACTIVITY. Fig. 20.**a** shows that the addition of **N20** (50 µg/ml) to the bath of the membrane patch activated WT CFTR channels with a P_o value of 0.22 ± 0.031, n=3. **P50** (50 µg/ml) were also capable of activating WT CFTR channels with a P_o value of 0.25 ± 0.033, n=3, (Fig. 20. **b**).

Figures 21.**a** and **b** show the stimulation of WT CFTR channels by 20 nM PKA and 1 mM MgATP. The subsequent addition of either **N20** (50 µg/ml; Fig. 21.**a**) or **P50** (50 µg/ml; Fig. 21.**b**) to the bath further increased channel activity. In other studies, stimulation of the cAMP pathway by 10 nM PKA and 0.2 mM MgATP resulted in the activation of WT CFTR channels with P_o = 0.07 ± 0.05, n=3. Subsequent addition of N20 (50 µg/ml) to the bath further increased CFTR activity to P_o = 0.34 ± 0.09 ($P < 0.05$, paired t test, n=3). P50 (50 µg/ml), were also capable of activating WT CFTR channel gating in the presence of 10 nM PKA and 0.2 mM MgATP. Indeed, the P_o of CFTR channels stimulated by P50 in the presence of 20 nM PKA and 0.2 mM MgATP was significantly increased, (0.37 ± 0.07, $P < 0.0048$, paired t test, n=3). In contrast, **P100** (50 µg/ml), did not affect CFTR channel gating alone (Fig. 22), or in the presence of 10 nM PKA and 0.2 mM MgATP with P_o values similar to control levels (0.093 ± 0.07, $P > 0.05$, paired t test, n=3).

FIGURE 20. Activation of silent CFTR Cl^- channels by N20 and P50 in excised, inside-out BHK membrane patches.

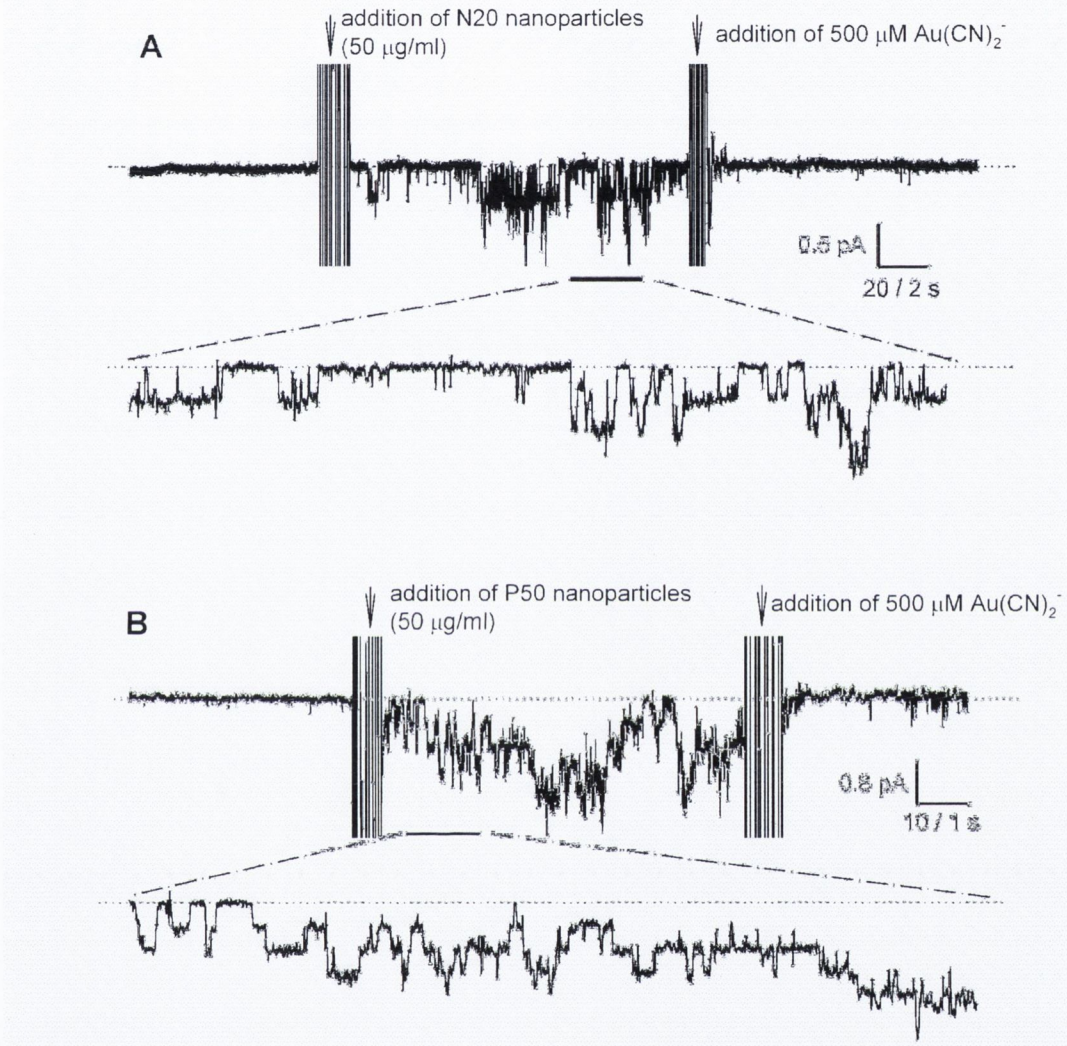

Representative recordings (n=3) of CFTR Cl^- channel opening in membrane patch after the addition of 50 μg/ml of N20 **(a)** or P50 **(b)** to the intracellular bath solution. The straight lines on the left and right indicate the current level when all the channels are closed due to no activation of CFTR Cl^- channels (left, control) or due to the blocking of CFTR by $Au(CN)_2^-$ 500 μM (right, internal control).

FIGURE 21. Effects of N20 and P50 on CFTR Cl^- channels pre-activated by PKA and MgATP in excised inside-out BHK membrane patches.

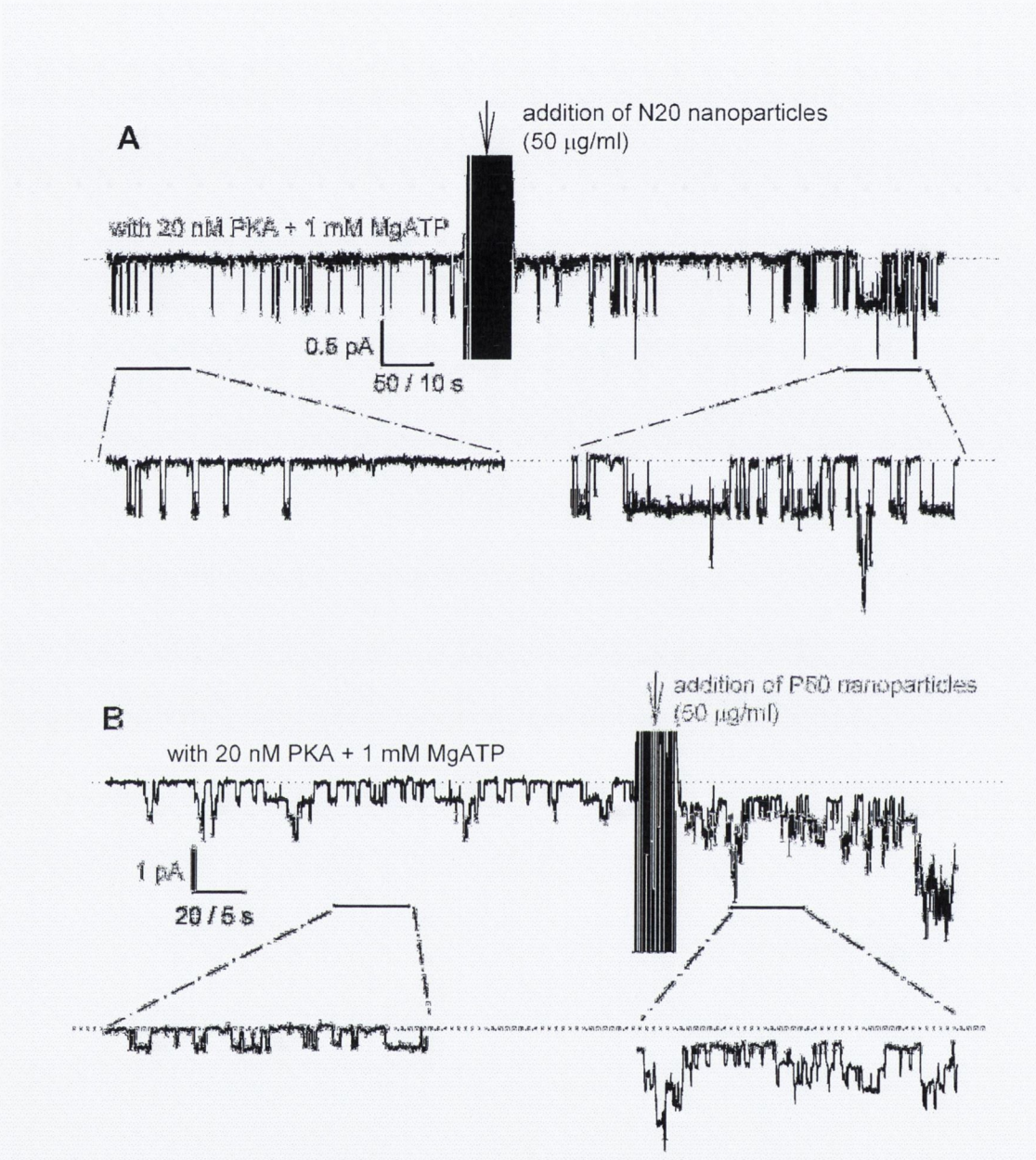

Representative recordings (n=3) of CFTR Cl^- channels opening in membrane patches after the addition of 50 μg/ml of N20 **(a)** or P50 **(b)** to the intracellular bath solution in the presence of 20 nM PKA and 1 mM MgATP.

FIGURE 22. Effect of P100 on silent CFTR Cl^- channels in excised, inside-out BHK membrane patches.

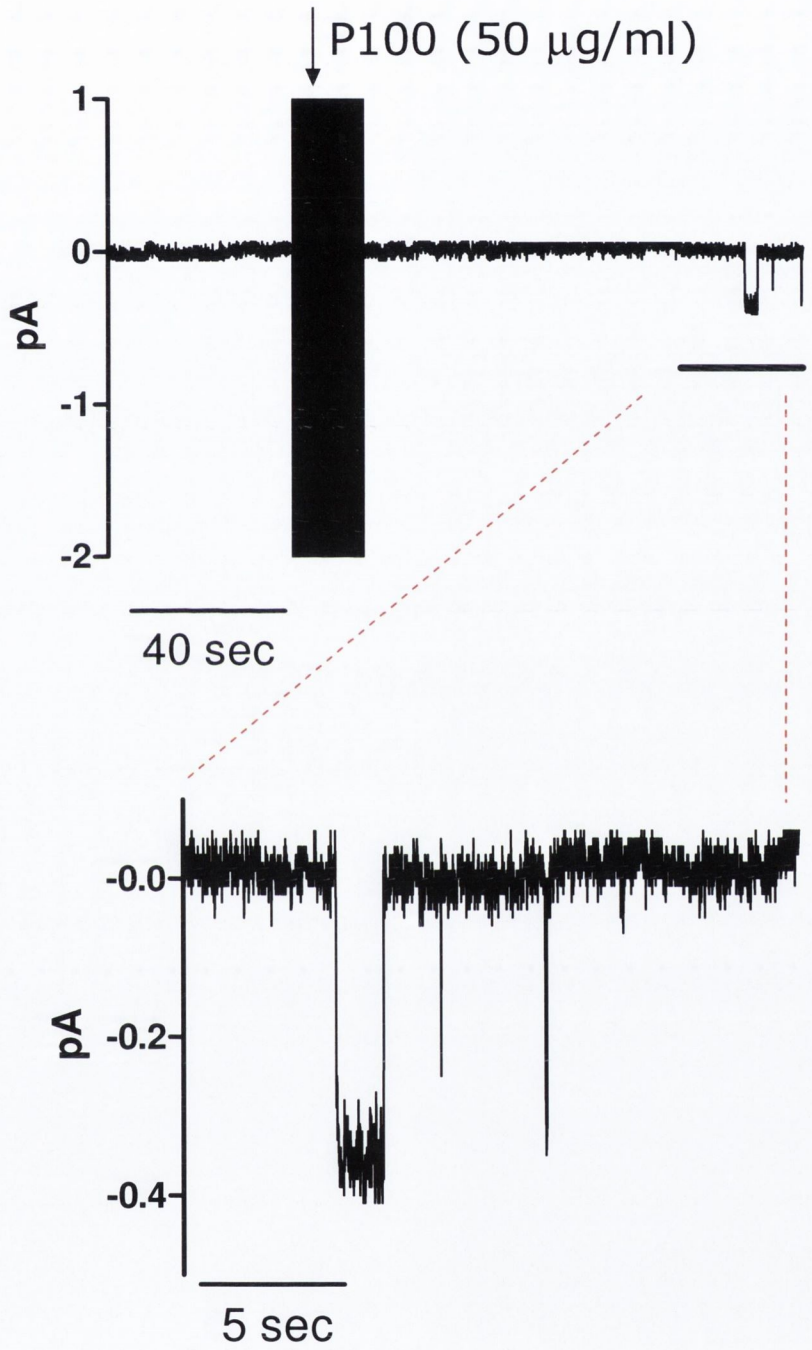

The representative recording (n=3) shows that P100 (100 µg/ml) exerted no significant effect on CFTR Cl^- channel opening in membrane patches after addition to the intracellular bath solution.

1.5 *IN VITRO* TRANSLOCATION ASSAY

Using standard curves of FITC-encapsulated NPs in serum free media (Fig. 23.**a**) the amount of polystyrene nanoparticles translocated by Calu-3 cells was quantified over two time points of 6 and 24 hour. For polystyrene NPs with a size of either 50-nm or 100-nm a significant increase in translocated NPs was observed between the time points of 6 and 24 hour (Fig. 23.**b**). Thus, I detected time-dependent increase in nanoparticle translocation by Calu-3 cells.

At 6hrs there was no significant difference in the translocation of unmodified 50-nm NPs when compared with NPs of the same size but exhibiting a negative charge (**N50**) (1.41 ± 0.26 vs. 0.88 ± 0.15 μg/ml). Furthermore, the translocation of unmodified 100-nm NPs was similar to those of 50-nm or N50 NPs (Fig. 23.**b**). Interestingly, I found that negatively charged 100-nm NPs did not translocate across a polarized Calu-3 cell monolayer at either time point (data not shown).

At 24 hour, unmodified 100-nm NPs were found to be the most highly trafficked nanoparticle with an average translocation amount of; 12.1 ± 0.4 μg/ml (Fig. 23.**b**). Unmodified 50-nm polystyrene NPs were the next most translocated NPs by Calu-3 cells; 6.32 ± 0.53 μg/ml. Finally, N50 NPs were the least translocated at 24 hour; 3.5 ± 0.74 μg/ml. However, when we plot the flux of polystyrene nanoparticles

through polarised Calu-3 cell monolayer's as a function of particle number (which takes account of the vastly different particle numbers at constant particle mass) we find that the trend is reversed with unmodified 50-nm polystyrene NPs being translocated at higher numbers comparable to that of the unmodified 100-nm NPs at 24 hr (Fig. 24.**c**).

To study if the composition of nanoparticle material can affect translocation I investigated the effects of silica nanoparticles. However, 50-nm FITC-labelled silica nanoparticles showed poor fluorescence in SF media. Indeed, standard curves of unmodified and amine modified 50-nm silica nanoparticle showed 3 and 15 times less fluorescent intensity respectively (Fig. 24.**a** and **b**) at the highest concentration used for the standard curve then the FITC-labelled polystyrene nanoparticles used in previous translocation assay. Therefore, studies on translocation of silica nanoparticles in Calu-3 cells could not be completed with reasonable degree of confidence.

FIGURE 23. Translocation of polystyrene nanoparticles through a polarized Calu-3 cell monolayer.

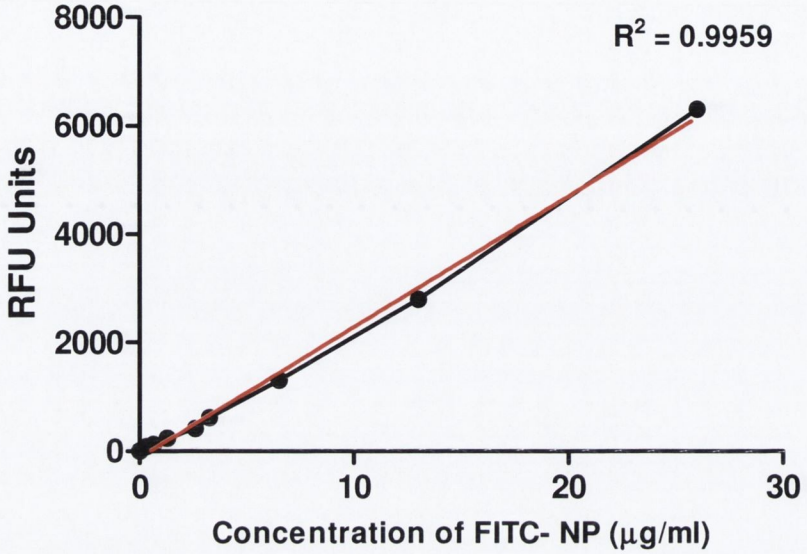

(a) A representative standard curve showing the correlation between the concentration of unmodified 50-nm FITC-encapsulated polystyrene nanoparticle (μg/ml) in SF media and fluorescence intensity (RFU units).

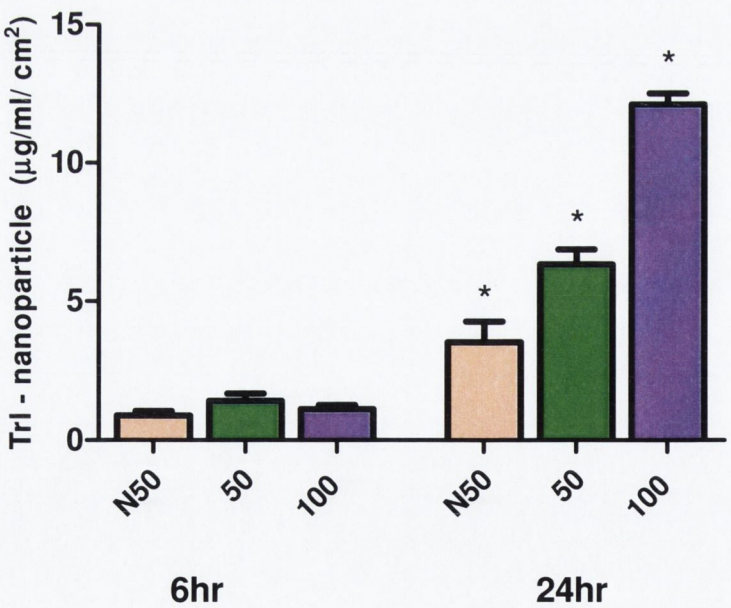

(b) Time-dependent translocation of polystyrene nanoparticles. One-way ANOVA $P < 0.0001$, Tukey-Kramer post test *$P < 0.05$ values at 24 hr vs. 6 hr.

(c) Time-dependent translocation of polystyrene nanoparticles plotted as a function of nanoparticle number.

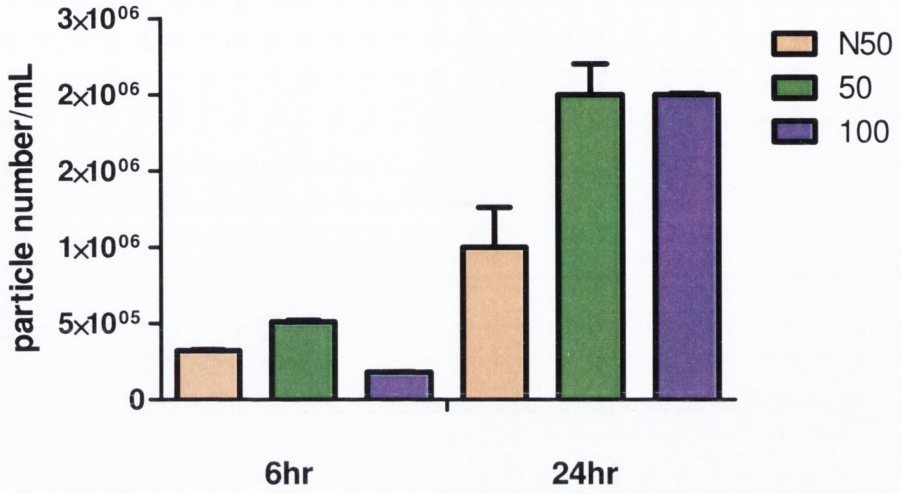

FIGURE 24. Translocation of silica nanoparticles through a polarized Calu-3 cell monolayer.

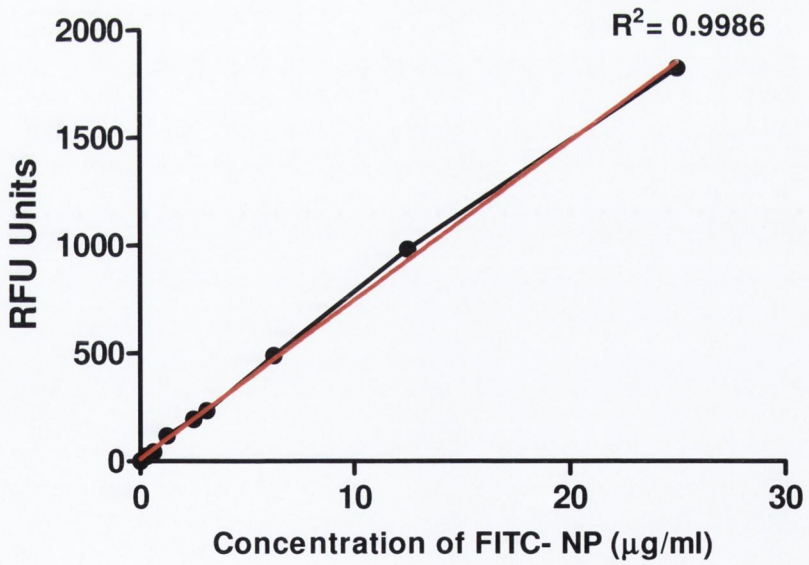

(a) A representative standard curve showing the correlation between the concentration of FITC-encapsulated unmodified 50-nm silica nanoparticle (µg/ml) in SF media and fluorescence intensity (RFU units).

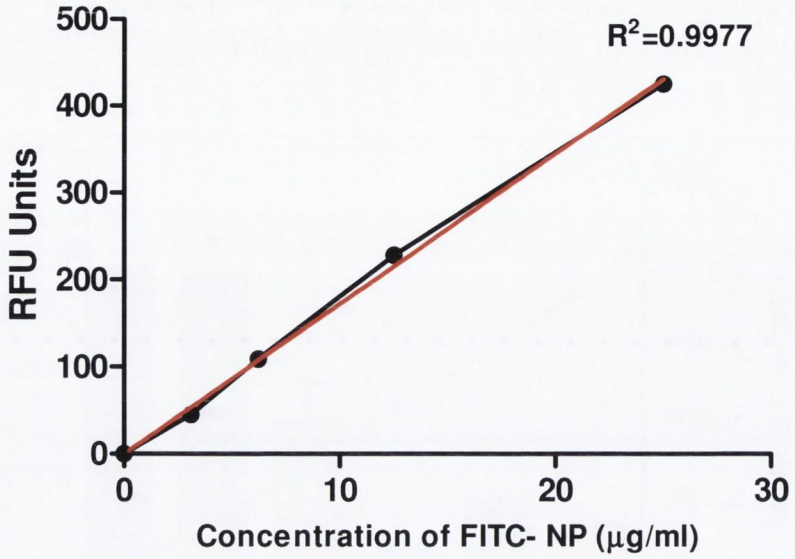

(b) A representative standard curve showing the correlation between the concentration of FITC-encapsulated amine-modified 50-nm silica nanoparticle (µg/ml) in SF media and fluorescence intensity (RFU units).

1.6 MICROSCOPY

1.6.1. CONFOCAL MICOSCOPY. Confocal microscopy of Calu-3 cells upon acute apical exposure to unmodified 50-nm polystyrene NPs (50 µg/ml) revealed that most nanoparticles were found intracellularly and in close contact with cellular membrane. Furthermore, nanoparticles within Calu-3 cells were found to be in agglomerate form.

FIGURE 25. Confocal 3D-imaging of Calu-3 cells exposed apically to polystyrene nanoparticles (unmodified 50-nm, 50 µg/ml).

The attached video shows the merge of planar cross sections of Calu-3 cells starting from the apical aspect until the end at the basolateral aspect of the cell monolayer (1.49 µm/slice). Cell-cell borders are seen as red and polystyrene nanoparticles are seen as green. Nanoparticles can be observed accumulated at cell boundaries or within cells in close proximity to cellular membrane (bar 10µm).

1.7 CYTOTOXICITY

The evaluation of particle-induced cytotoxic effects for silica particles was performed using the LDH and MMT assays. Polystyrene nanoparticles were examined for their cytotoxic effects using only the LDH assay.

1.7.1 LDH ASSAY

1.7.1.1 POLYSTYRENE NANOPARTICLES. A concentration dependent reduction in cell viability after exposure to **P50** but not **N20** polystyrene nanoparticles was observed after 24 hours (Fig. 26.**a** and **b**). After Calu-3 cells were exposed to P50 nanoparticles at a concentration of 200 µg/ml for 24 hours cell viability decreased to 55 ± 3.8 % of controls (Fig. 26.**a**).

FIGURE 26. Effects of polystyrene nanoparticles on cell viability. Values are mean ± SEM from 3 independent experiments.

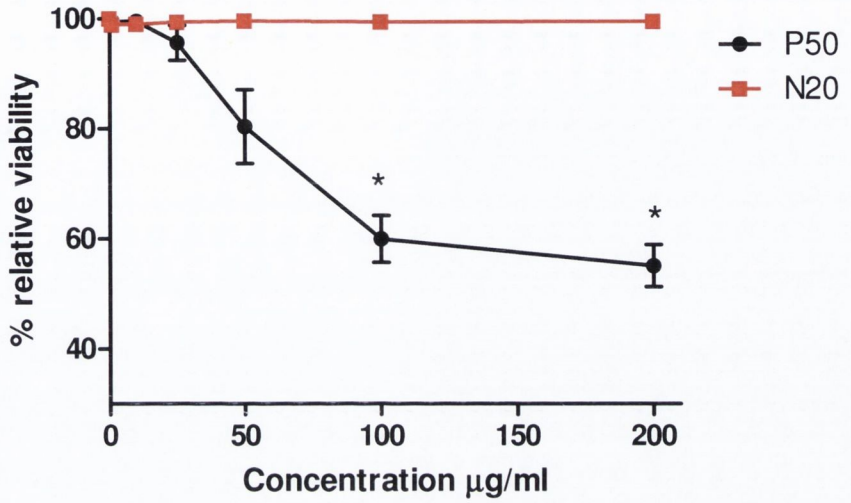

(a) Comparison of N20 and P50 nanoparticles.

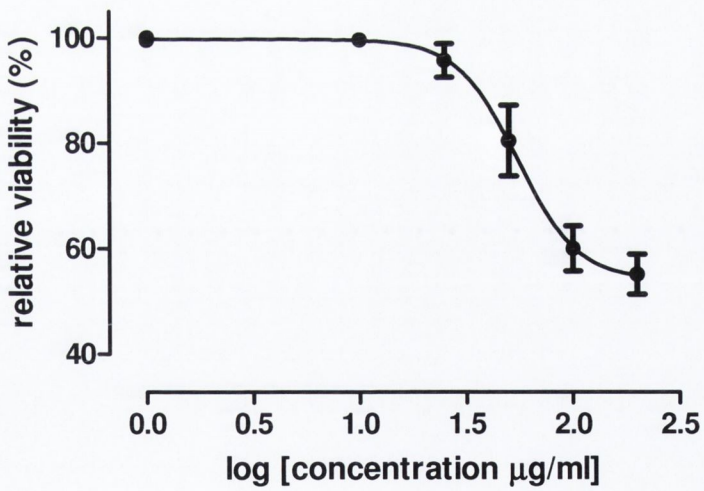

(b) Fitted (nonlinear regression) concentration-response curve to P50.

1.7.1.2 SILICA NANOPARTICLES. A concentration dependent reduction in cell viability after exposure to **Si-10** but not **Si-150** and **Si-500** silica particles was observed after 24 hours (Fig. 27.**a** and **b**). After Calu-3 cells were exposed to Si-10 silica nanoparticles at a concentration of 50 µg/ml for 24 hours cell viability decreased to 46.3 ± 7.1 % of controls (Fig. 27.**a**).

FIGURE 27. Effect of silica particles on cell viability. Values are mean ± SEM from 3 independent experiments.

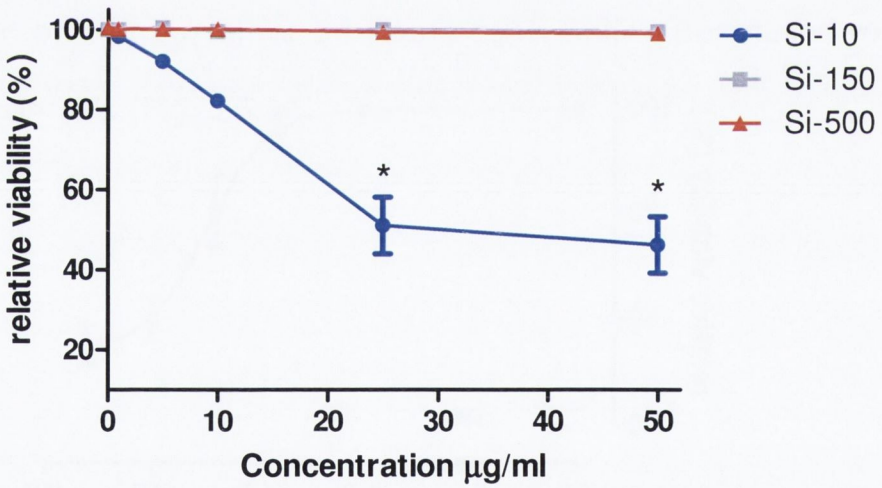

(a) Viability of Calu-3 cells after 24 hour exposure to increasing concentrations of 10, 150 and 500-nm silica particles.

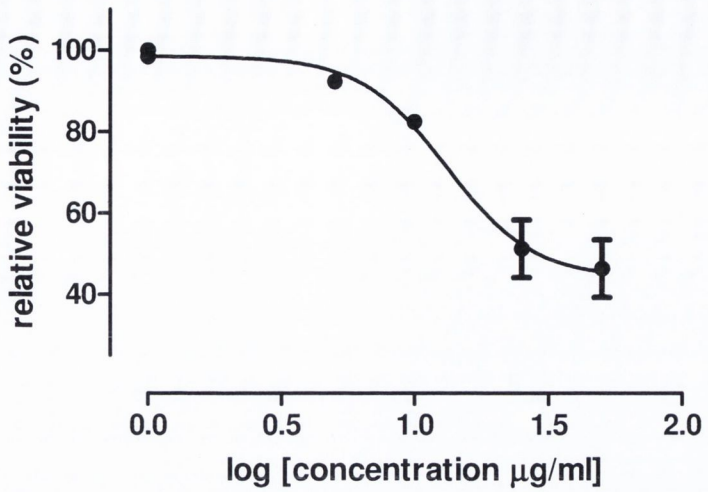

(b) Fitted (nonlinear regression) concentration-response curve to Si-10.

1.7.2 MTT ASSAY

1.7.2.1. SILICA NANOPARTICLES. I used the MTT assay in order to confirm findings that 10-nm silica NPs effect Calu-3 cell viability in a concentration-dependent manner (Fig. 28.**a**). However, the viability curve that we obtained from our MTT assay is considerably different to the one we acquire using the LDH assay. The results of the MTT assay show that when Calu-3 cells were exposed to **Si-10** at a concentration of 50 µg/ml for 24 hours, cell viability decreased to 7.5 ± 0.6 % of controls (Fig. 28.**a**) with the corresponding TC_{50} = 7.6 µg/ml (Fig. 28.**b**).

FIGURE 28. Effect of Si-10 on cell viability. Values are mean ± SEM from 3 independent experiments.

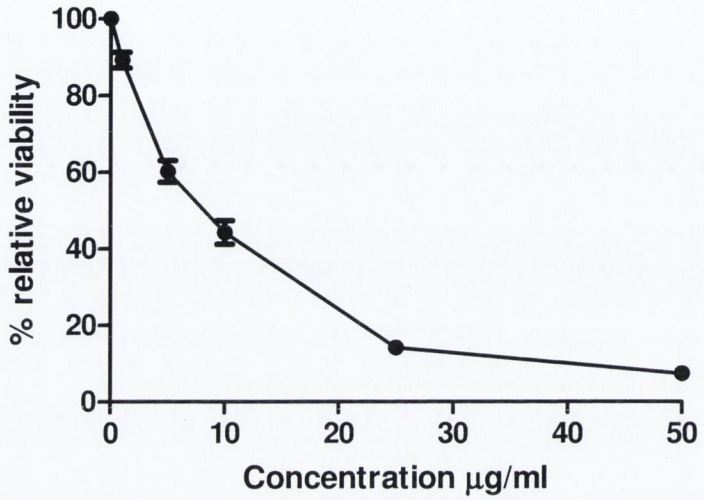

(a) Viability of Calu-3 cells after 24 hour exposure to increasing concentrations of 10-nm silica particles.

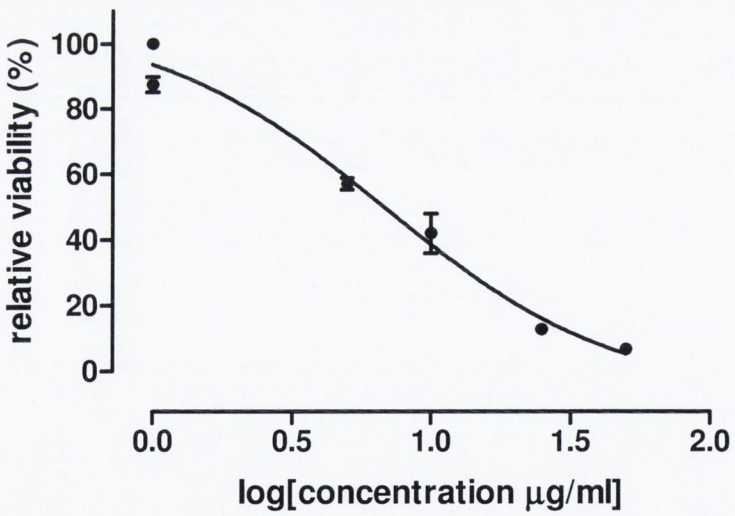

(b) Fitted (nonlinear regression) concentration-response curve to Si-10. TC_{50} = 6.8 µg/ml with a corresponding Hill co-efficient of -1.031 ± 0.94.

2.0 CYTOKINES RELEASE FROM SILICA NP-TREATED CELLS

2.1 FLOW CYTOMETRY AND SILICA NANOPARTICLES. In the absence of silica NPs Calu-3 did not release detectable amounts of IL-1β, IL-10, TNF-α and IL-12p70. The detection limit of BD FACSArray™ (BD Biosciences, Oxford, UK) for these cytokines is shown in Table 11.

TABLE 11. Limit of detection of each cytokine analysed

CYTOKINE	LIMIT OF DETECTION
IL-8	**3.6 pg/ml**
IL-1β	**7.2 pg/ml**
IL-6	**2.5 pg/ml**
IL-10	**3.3 pg/ml**
TNF-α	**3.7 pg/ml**
IL-12p70	**1.9 pg/ml**

The incubation of Calu-3 cells with **Si-10** resulted in a concentration-dependent release of IL-8 (Fig. 29.**a**). **Si-150** and **500** particles did not significantly increase IL-8 release by Calu-3 cells at all concentrations tested (25, 50 and 100 μg/ml) ($P > 0.05$, n=3-4) (Fig. 29.**b** and **c**). Similarly, the levels of IL-6 were significantly increased following 24 hours incubation with Si-10 in a concentration dependent manner (Fig. 30.**a**). Again, Si-150 and 500 particles did not affect IL-6 release by Calu-3 cells at the concentrations tested (25, 50 and 100 μg/ml) ($P > 0.05$, n=3-5) (Fig. 30.**b** and **c**).

FIGURE 29. IL-8 release from Calu-3 cells after exposure to silica particles for 24 hours.

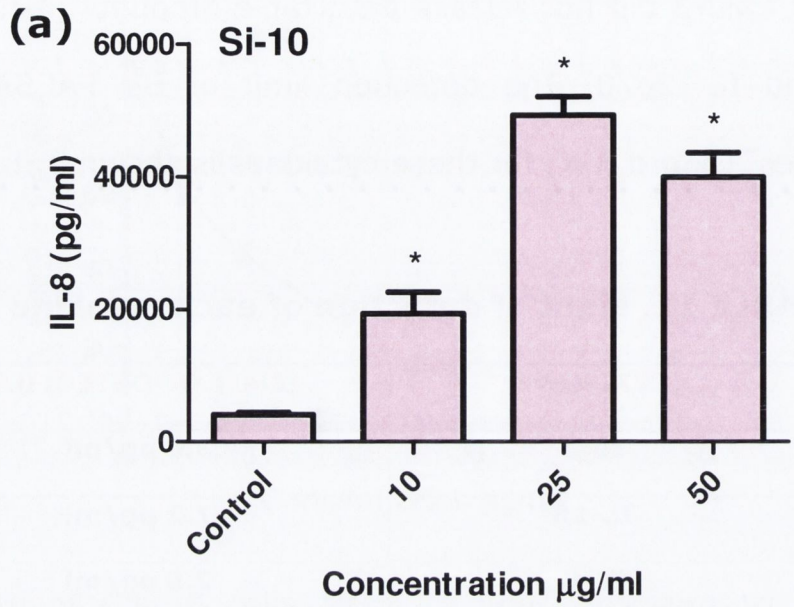

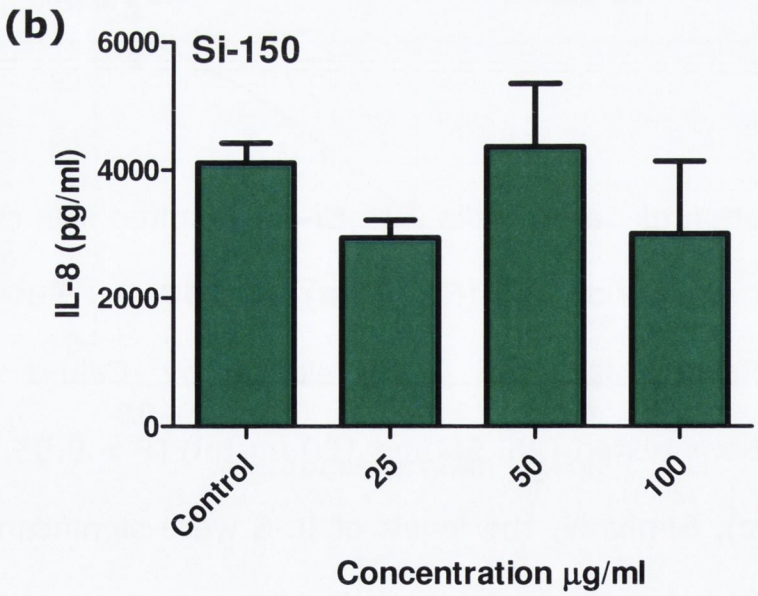

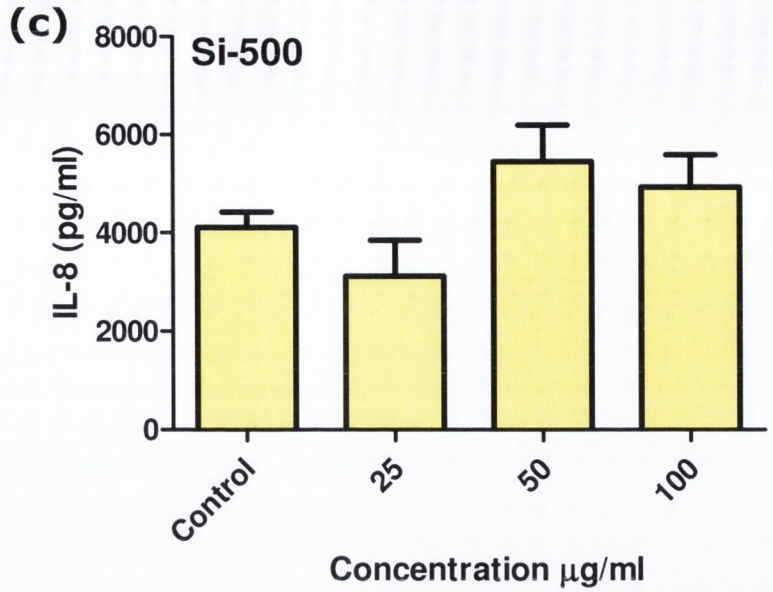

Si-10 induced IL-8 release in a concentration-dependent manner **(a)**. One-way ANOVA, $P < 0.0001$, Tukey-Kramer post test *$P < 0.05$, n=3-4, control vs. treatments. Si-150 and Si-500 exerted no significant effect on the induction of IL-8 release from Calu-3 cells **(b-c)**, one-way ANOVA, $P > 0.05$, n=3-4, control vs. treatments.

FIGURE 30. IL-6 release from Calu-3 cells after exposure to silica particles for 24 hours.

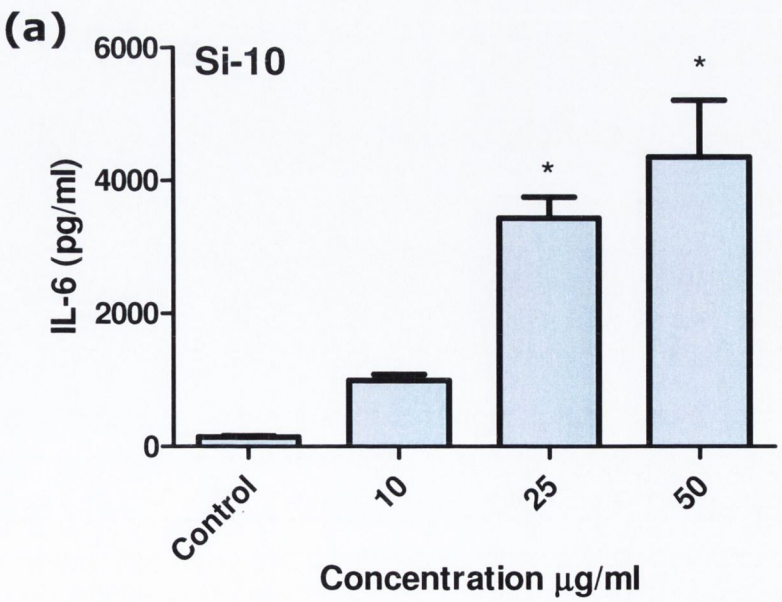

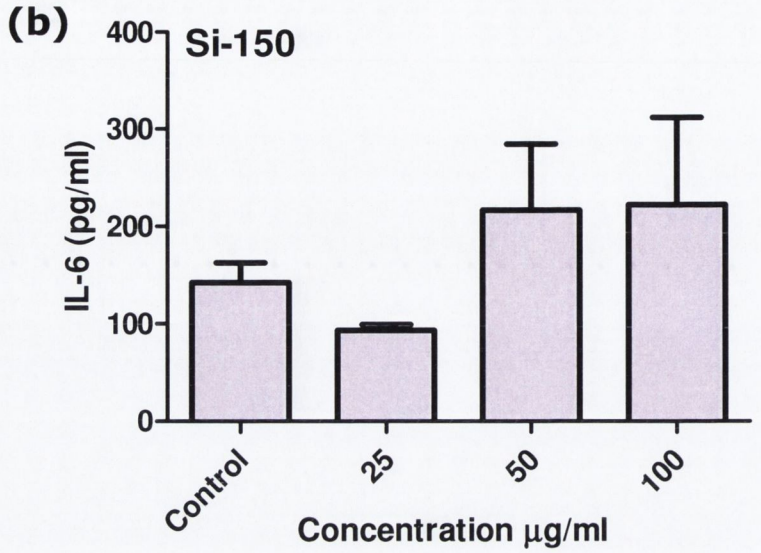

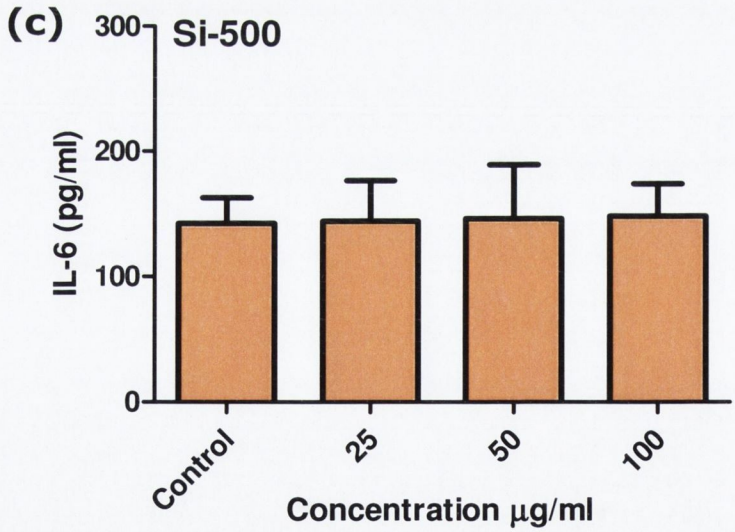

Si-10 induced IL-6 release in a concentration-dependent manner **(a)**. One-way ANOVA, $P < 0.0001$, Tukey-Kramer post test $^*P < 0.05$, n=3-5, control vs. treatments. Si-150 and Si-500 exerted no significant effect on the induction of IL-6 release from Calu-3 cells ($P > 0.05$, n=3-4, control vs. treatments **(b-c)**).

2.1.2 REAL TIME-PCR AND SILICA NANOPARTICLES. The results of our Human Inflammatory Cytokine kit measured by flow cytometry had shown us that Si-10 nanoparticles unlike larger particles (Si-150 and 500) of the same composite material, were capable of up-regulating the release of IL-6 and IL-8 from Calu-3 cells. My next step in assessing the toxicity of silica particles on airways cells was to examine if these particles were capable of up-regulating other inflammatory proteins, specifically the inflammatory mediator MMP-9 at gene level.

The expression of MMP-9 within each sample was normalized against 18S rRNA and expressed relative to control samples. MMP-9 gene expression was significantly up-regulated at 24 hours by **Si-10** nanoparticles in Calu-3 cells in a concentration-dependent manner (Fig. 31.**a**). At a concentration of 25 and 50 μg/ml, Si-10 nanoparticles increased MMP-9 gene expression by a fold increase of 12.5 ± 2.5 and 13.5 ± 0.8 respectively, compared to controls (*$P < 0.05$, n=3) (Fig. 31.**a**). **Si-150** and **500** particles did not affect MMP-9 gene expression in Calu-3 cells at the concentrations tested (25, 50 and 100 μg/ml) ($P > 0.05$, n=3-4) (Fig. 31.**b-c**).

FIGURE 31. Effects of silica particles on MMP-9 gene expression at 24 hours.

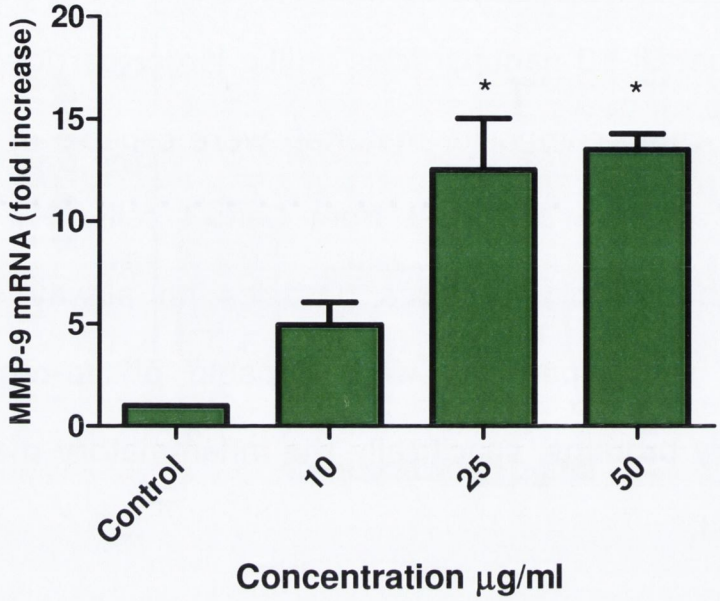

(a) Si-10 induced MMP-9 gene expression in a concentration-dependent manner. One-way ANOVA, $P < 0.0007$, Tukey-Kramer post test *$P < 0.05$, n=3, control vs. treatments.

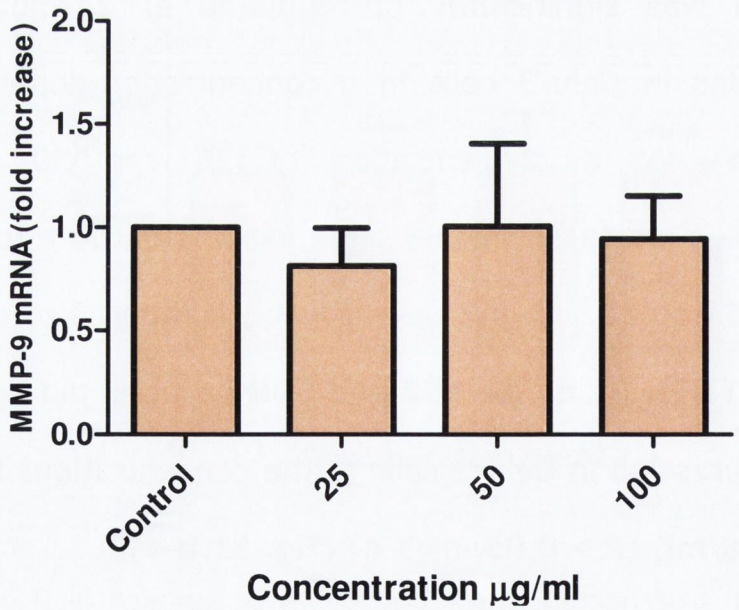

(b) Si-150 exerted no significant effect on the induction of MMP-9 gene expression in Calu-3 cells at 24 hours. One-way ANOVA $P > 0.05$, n=3-4, control vs. treatments.

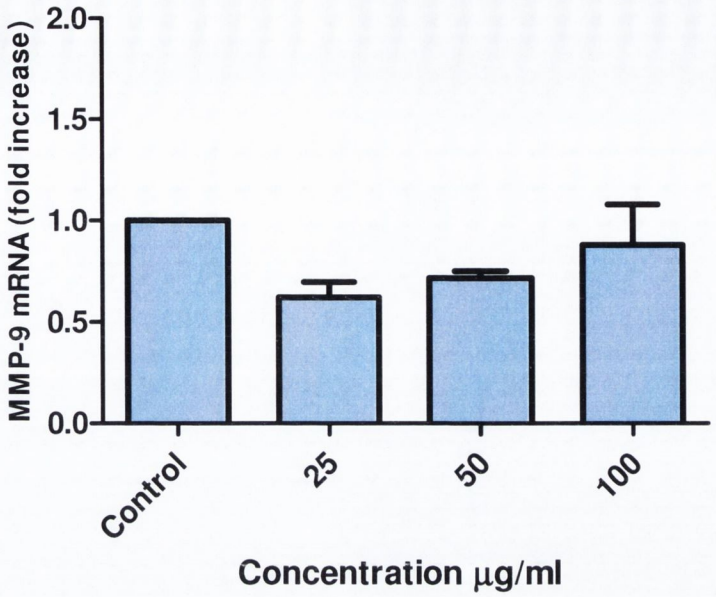

(c) Si-500 exerted no significant effect on the induction of MMP-9 gene expression in Calu-3 cells. One-way ANOVA $P > 0.05$ n=3, control vs. treatments.

DISCUSSION

The major objective of my study was to investigate interactions between nanoparticles and lung epithelium under both acute and chronic conditions. I have selected polystyrene and amorphous silica nanoparticles for these studies for a number of reasons. Polystyrene nanoparticles were chosen as model particles because they are being increasingly characterised for use as nanosensors or in drug nanocarrier investigations [128-129]. Amorphous silica nanoparticles represent a group of nanomaterials which could potentially cause toxic effects similar to crystalline silica [130].

ACUTE EFFECTS OF NANOPARTICLES ON EPITHELIAL ION CHANNELS

I investigated a hypothesis that nanoparticles have the ability to act as modulators of ion channel function in human airway epithelial cells. The main novel findings of this part of my study are; (1) polystyrene NPs, but not silica NPs, within a size range of 20 to 50-nm have the ability to consistently activate transepithelial ion transport in a concentration-dependent manner (2) polystyrene NPs directly activate CFTR Cl^- channels on membrane patches (3) apical membrane Cl^- currents from cell monolayers indicate that CFTR Cl^- channels are the target of polystyrene NPs as shown by the inhibition of Isc by the CFTR blocker, DPC (4) N20 but not P50 activate basolateral K^+ channels (5) polystyrene NPs affect 3 distinct cell

signalling systems concerned with ion channel activation in respiratory cells; cAMP, Ca^{2+} and sGC/cGMP pathways.

The direct activation of CFTR Cl^- channels was detected in excised inside-out membrane patches stimulated by NPs. This experimental set up allowed for the interaction of NPs with the intracellular domains of CFTR Cl^- channels. Structural analysis of the CFTR protein shows that it consists of a 1,480 amino acid backbone which folds into a 3D-structure consisting of 5 regions: 2 membrane-spanning domains, 2 NBDs and a cytoplasmic regulatory domain [131]. Phosphorylation of the RD by cAMP-dependent protein kinase (PKA) is a prerequisite for channel opening [132]. ATP-induced dimerization of NBDs plays also an important role in this process [133]. Studies using NBD mutants demonstrated that most CFTR activators have decreased affinity for activating mutant CFTR Cl^- channels [134]. Therefore putative binding sites on the NBDs of CFTR are proposed to be target(s) for many CFTR activators [135-136].

The fact that the silica NPs tested (Si-10 and Si-P50) did not affect Isc responses by airway cells indicates that the type of nanomaterial used has a profound effect on the cellular response with regard to ion fluxes. Furthermore, although all polystyrene NPs tested were made from the same composite material of polystyrene latex they activated anion fluxes in Calu-3 cell monolayers with different potencies

(N20>P50>P100). Nanoparticle size, surface modification, charge and interactions with the cell membrane and differential uptake can all contribute to this effect and could possibly help to give each nanoparticle tested their own unique "activating fingerprint" with respect to Isc activation. As N20 and P50, but not P100 activated CFTR Cl^- channels both in intact epithelium and in excised membrane preparations it is clear that polystyrene NPs with a **size** between 20 to 50-nm could be taken up rapidly by Calu-3 cells where they elicit their effects on CFTR Cl^- channels. Indeed, our confocal microscopy confirmed the rapid uptake of 50-nm polystyrene latex NPs following acute apical exposure to Calu-3 cell monolayers.

Lundqvist *et al.*, 2007 showed that 50-nm polystyrene NPs with either amine or carboxylate–**surface modifications** in human plasma shared ~ 35–40 % of proteins on their coronas (layer of protein adsorbed onto the particle surface). Further analysis of the protein composition found in the corona showed that ~ 35 % were unique only to NPs of a given surface composition [122]. A study using a novel method of measuring the force of nanoparticle–cell membrane interaction by use of atomic force microscopy, showed that poly ($_{D,L}$–lactide–*co*–gylcolide) (PGLA) nanoparticles functionalised with poly-$_L$-lysine had a five–fold greater force of adhesion with the cell membrane then unmodified PGLA nanoparticles [137].

Membrane fluidity may be affected by NP **charge**. Wang *et al.*, 2008 examined the effects of polystyrene NPs on single-component phospholipid bilayers using fluorescence and calorimetry experiments after mixing together liposomes with either positively or negatively charged NPs of approx 20-nm in size in suspension. The findings of their study showed that there was surface reconstruction where the NPs absorbed onto the bilayer membrane, with negatively charged NPs inducing local gelation in fluid bilayers and positively charged NPs inducing gelled membranes to fluid locally [(138)].

A more recent study by Yang *et al.*, 2010 investigated the interactions between charged NPs (positive, negative, uncharged) and charge-neutral phospholipid membranes by coarse-grained molecular dynamics simulations. Their results were discussed in terms of free energy, entropy and enthalpy where they describe an energy barrier existing between lipids and charged NPs. The main conclusion of their study was that **electrostatic attractions** help to improve the adhesion of charged NPs to phospholipid membranes and that increases in electrostatic energy can result in charged NP being almost fully wrapped by membrane [(139)].

The exposure of human pulmonary epithelial cells (A549 cell line) to fluorescent polystyrene nanospheres (41-nm) without surface charge modifications resulted in particle-induced changes in apical plasma

membrane (APM) surface area measured by design-based stereology. Brandenberger *et al.*, 2009 concluded that this observed enlargement of the APM surface area was dependent on particle surface area dose [140]. Our concentration response curves show that the activation of CFTR Cl^- channels by 20-nm and 50-nm polystyrene NPs by Calu-3 cells occurs in a concentration-dependent manner, thus the number of nanoparticle interactions with the apical membrane may influence conformational changes on the cell membrane that could result in the activation of cell signalling receptors that control ion channels such as CFTR.

The **uptake** of NPs by lung epithelial cells can be energy-dependent or –independent. Indeed, NPs can be taken up transcellularly by energy dependent–endocytosis [93]. Support for energy-dependent transport comes from studies which s how that low temperatures as well as metabolic inhibitors prevent the uptake of magnetic silica-coated NPs by alveolar A549 cells [141]. However, some studies suggest that NPs have the ability to cross cell membranes and enter cells by passive or diffusive movement. For example, the passive uptake of polystyrene NPs has been confirmed in red blood cell culture using microscopic techniques [142]. More recently a study by Yacobi *et al.*, 2009 which investigated the trafficking of fluorescently labelled polystyrene NPs (20 and 100-nm, +/- charges) across primary rat alveolar epithelial cell monolayers (RAECM) concluded

that the NPs tested translocated through cells via the transcellular pathway but suggested that this occurred as a result of the diffusion of polystyrene NP through the lipid bilayer of cell plasma membranes [143]. Once inside an epithelial cell there is also evidence to support a direct interaction between NPs and subcellular structures [93, 144].

My confocal microscopy studies indicate that 50-nm polystyrene latex NPs when taken up by Calu-3 cells are found in close proximity to cellular membrane. This could in turn facilitate interactions between NPs and CFTR Cl^- channels on the apical membrane or with proteins/receptors which modulate ion channel function in respiratory cells. I also observed that 50-nm polystyrene NPs were present intracellularly as aggregates after uptake by Calu-3 cells. Similarly, another study which examined the trafficking of polystyrene NPs across RAECM monolayers by confocal microscopy showed that when RAECM cells were apically exposed to polystyrene NPs for 24 hours, NPs were found intracellularly in agglomerated form and were not present in the nuclei of exposed cells [145].

NPS, CFTR Cl^- CHANNELS AND INTRACELLULAR SIGNALING

My Ussing chamber experiments show that polystyrene NPs upon acute exposure to Calu-3 cells are capable of activating intracellular signalling systems mediated by cAMP, cGMP and Ca^{2+} that control ion channel function.

It is important to realise that most epithelial ion fluxes are cyclic nucleotide driven. As previously stated the secondary messenger molecule cAMP is produced by adenylate cyclase (AC) enzymes from ATP. Two forms of AC exist; soluble adenylyl cyclases (sAC) and transmembrane adenylyl cyclases (tmAC) [146]. Both differ in their regulation and sub-cellular localizations. Forskolin, a flavonoid compound which is extensively used in probing cAMP-dependent ion fluxes activates nearly all isoforms of mammalian tmACs (sAC is insensitive to forskolin) [146]. TmACs show both negative and positive regulation by calcium [147]. The tmAC isoforms AC1 and 8 are recognized to be Ca^{2+}/calmodulin-senstive [147]. The AC3 isoform of tmAcs is insensitive to Ca^{2+}/calmodulin stimulation but can be stimulated by Ca^{2+}/calmodulin in the presence of forskolin. Fully differentiated human airway epithelial cells *in vitro* have been shown to express Ca^{2+}-sensitive tmAC isoforms (1, 3 and 8) [148]. Furthermore, capacitative Ca^{2+} entry (CCE) which is defined as the "entry of Ca^{2+} ions into the cell triggered by the depletion of Ca^{2+} stores" has been shown to activate Ca^{2+}-sensitive adenylate cyclases. Thus, there seems to be a very close association between Ca^{2+}-sensitive adenylate cyclases and CCE channels [147].

Interestingly, we have shown that polystyrene NPs can directly activate CFTR Cl^- channels both in the presence and absence of ATP and PKA in membrane patches. The effectiveness of NPs to activate

CFTR Cl^- channels in Calu-3 cell monolayers was comparable to that of the cAMP elevating agonist forskolin. Furthermore, N20 nanoparticles were able to activate CFTR Cl^- channels in the absence of forskolin. In contrast, pre-stimulation of cells with forskolin significantly decreased N20-induced CFTR stimulation. This is in sharp contrast to known flavonoid CFTR Cl^- channel openers such as genistein and apigenin, which have been shown to have low affinity binding to silent CFTR and high affinity binding for pre-stimulated CFTR [149-150].

The secondary messenger molecule cGMP is produced by cells in response to stimulation with nitric oxide. In mammalian cells, NO is a cell-permeable intracellular messenger molecule which has a short half-life ($t_{1/2}$ = 3 to 8 sec) thus its detection in biological systems has always been challenging [151]. A study carried out by Brovkovych *et al.*, 1999 using an electrochemical porphyrinic sensor reported that NO concentrations were highest at the cell membrane of a single endothelial cell (950 ± 50 nmol/L) and decreased exponentially with increasing distance from the cell [152]. Furthermore, NO concentrations on the cell membrane of generator cells have been recorded in the range of 0.1 - 3 μM [151]. This localisation of NO is logical when we consider that Ca^{2+}-dependent isoforms of NO synthase are located at the cell membrane [153]. Physical agonists such as shear stress have been known to cause the release of NO

from vascular epithelium [154]. Airway epithelial cells exposed to a wide range of nanoparticles *in vitro* including metal oxide NPs such as amorphous silica, ferric oxide, copper (II) oxide and diesel exhaust particles for short periods have been shown to generate reactive oxygen species and these can affect the bioavailability of NO [155-156]. It has been shown that in epithelial cells the effects of NO are mediated by the generation of cGMP [58].

I found that the effects of N20 on CFTR-driven Isc responses in Calu-3 cells were abolished by ODQ, a selective inhibitor of soluble guanylyl cyclase [157] implicating the sGC/cGMP pathway and possibly cGMP-dependent phosphorylation of CFTR Cl^- channels in this action of N20. I also found that the pre-treatment of epithelial cells with an inhibitor of NOS, L-NAME, did not modify the activator effects of N20. As NO synthase is present and active in Calu-3 cells regulating Isc current and anion secretion [58] this data together indicates that sGC- but not NOS-dependent response are targeted by N20.

Next, I investigated the interactions between nanoparticles and epithelial Ca^{2+} levels. I detected synergistic responses between N20 and agonists of $[Ca^{2+}]_i$ release (carbachol and thapsigargin) indicating a possible role for the involvement of $[Ca^{2+}]_i$ in Isc activation by N20 nanoparticles.

Ca^{2+} ions enter cells via calcium channels located on the plasma membrane. Intracellular Ca^{2+} is pumped and stored in the endoplasmic reticulum (ER) by Ca^{2+}-ATPase transmembrane transporters located on the lumen of the ER membrane system at the expense of ATP hydrolysis [158]. Ca^{2+} is a primary regulator of physiological functions in all cells. Nitric oxide produced by cells or released from neighbouring cells is known to be a key messenger molecule controlling Ca^{2+} homeostasis and studies have shown that there is significant cross-talk between Ca^{2+} and NO/cGMP cell signalling systems [159]. Endogenously produced NO works as a sensor for cytoplasmic calcium levels, $[Ca^{2+}]_i$. In addition NO is known to regulate many aspects of Ca^{2+} homeostasis including the release of Ca^{2+} from IP_3 and ryanodine-sensitive Ca^{2+} stores as well as store-operated Ca^{2+} channels and second messenger-operated channels [159-160]. Finally it is well described that increases in $[Ca^{2+}]_i$ in airway epithelial cells are known to activate CFTR and Ca^{2+} activated Cl^- channels [161].

Tang *et al.*, 2008 showed that NPs can affect intracellular Ca^{2+} in mammalian cells. They demonstrated using techniques such as confocal laser scanning and standard whole-cell patch clamp that unmodified cadmium selenium quantum dots elevate cytoplasmic calcium levels in primary cultures of rat hippocampal neurons [162]. The mechanism for this activation is still unknown, however the

group did identify that the increase in $[Ca^{2+}]_i$ involved both extracellular Ca^{2+} influx and internal Ca^{2+} release. In addition, it was found that the extracellular influx of Ca^{2+} could only be partially inhibited by calcium channel antagonist such as verapamil whereas internal Ca^{2+} release was abolished by treatment of cells with clonazepam, a specific inhibitor of mitochondrial sodium–calcium exchangers and with antrolene an antagonist of ryanodine receptors in the ER [163].

Many research groups are interested in the manipulation of magnetic NPs such as magnetic tweezers or ligand-coated magnetic NPs which are capable of mechanical activation of cell receptors, see review [164]. Mechanotransduction is used to describe how cells convert physical force into a biochemical signal. Magnetic particles used to investigate mechanotransduction such as integrin-bound collagen-coated ferric oxide beads have revealed that applied tension on human fibroblasts can cause Ca^{2+} spikes which can modulate cellular functions [165-166]. In one study it was found that the probability of a calcium influx was increased by higher surface bead loading and the degree of cell spreading. Overall cell shape as well as the rigidity of the cell membrane and the cytoskeleton framework specifically related to actin filaments have been proposed to be vital determinants in the regulation of stretch-induced calcium signals [166]. Meyer *et al.*, 2000 using suspended bovine endothelial cells and a magnetic twisting

device demonstrated that when a controlled twisting (shear) stress of 15.6 dyn/cm^{-2} was applied to ligand-coated magnetic microbeads in contact with these cells that cAMP production was increased due to adenylyl cyclase activation [167]. Thus, mechanical stress applied to the cell surface can alter both Ca^{2+} and cAMP signalling.

Interestingly, I found that neither N20 nor silica nanoparticles activated CFTR-driven Isc responses in normal human bronchial epithelial (NHBE) cells as opposed to Calu-3 cells. A number of factors may be responsible for this difference. CFTR Cl^- channels are expressed throughout the human airways from proximal (nose, trachea and bronchi) to distal regions (terminal bronchioles and alveoli) [168]. The expression levels of CFTR in these regions varies with low levels of CFTR expression seen in most native epithelial tissues except for the higher levels of endogenous CFTR found on serous epithelial cells associated with submucosal glands exemplified by Calu-3 [169-170]. Furthermore, it has been shown that the expression of CFTR in NHBE correlates with the presence of mircovilli and cilia; see review on EpiAirway-specific features [171]. Lastly, my own data showed reduced forskolin-induced Isc responses in NHBE when compared to Calu-3 (14.3 ± 1.24 versus 36.3 ± 1.5 μA/cm^2 respectively).

INTERACTIONS OF NPS WITH OTHER ION CHANNEL TARGETS

Polystyrene NPs as well as displaying varying potencies on CFTR–mediated Isc responses, also demonstrated that they can have distinct targets other than CFTR Cl^- channels. Cl^- and HCO_3^- ions are pumped across the basolateral membrane by the NKCC (with a stoichiometry of 1Na:1K:2Cl) and Na^+-HCO_3^- co-transporters respectively and then transported across the apical membrane by Cl^- channels such as CFTR. K^+ ions are recycled across the basolateral membrane by K^+ channels which work to maintain the negative potential difference of the cell interior. The opening of basolateral K^+ channels in epithelial cells is an important process for anion secretion as it causes the cell to become hyperpolarised which in turn increases the electrical gradient for Cl^- ions to exit across the apical surface of the epithelium [172].

Firstly, I have shown that N20 but not P50 nanoparticles activate cAMP-regulated basolateral K^+ channels. The evidence for this comes from experiments which showed that; (1) N20–activated K^+ currents were inhibited by XE991, an inhibitor of cAMP-sensitive basolateral K^+ channels and (2) the effects of N20 NPs on basolateral K^+ currents were abolished by pre–treating cells with the cAMP elevating agonist forskolin. Secondly, the results of our anion substitution experiments also demonstrate that N20 nanoparticles upon acute exposure to Calu-3 cells can affect ion transport involving both Cl^- and HCO_3^- ions.

NKCC is yet another transporter involved in anion fluxes. There are 2 isoforms of the electrically neutral NKCC co-transporter; NKCC1 and 2. The NKCC1 isoform is expressed on the basolateral membrane of secretory epithelia where it acts in concert with other transporters and ion channels such as CFTR, basolateral K^+ channels and Na^+-K^+ pumps to produce transepithelial Cl^- secretion. NKCC is expressed on virtually all mammalian cells where it functions to maintain cell volume [173]. In turn, NKCC1 function appears to be regulated by at least three processes: (1) gene expression (2) protein phosphorylation (3) acute changes in membrane targeting [173]. The major stimuli for NKCC1 activation in epithelial cells is a fall in intracellular [Cl], $[Cl]_i$ in response to secretory stimuli such as elevations in cAMP or $[Ca^{2+}]_i$ which cause Cl^- ions to exit across activated apical Cl^- channels [173]. Experiments using canine trachea epithelial cells show that a depletion of $[Cl]_i$ leads to the phosphorylation and increased activity of basolateral NKCC co-transporters thus preventing cell shrinkage [174].

TRANSDUCTION MECHANISMS INVOLVED IN EFFECTS OF NPS ON EPITHELIAL ION FLUXES: A HOLISTIC HYPOTHESIS

As shown by my imaging experiments polystyrene nanoparticles have the ability to interact with various structures upon apical exposure of epithelial cells. Therefore, the sequential order by which N20 nanoparticles affect intracellular signalling systems to regulate ion

fluxes is difficult to ascertain; however it is likely to involve a significant cross-talk between the pathways as previously discussed.

The experiments using agonists of adenylate (forskolin) and guanylyl (GSNO) cyclases showed that pre-stimulation of either system largely abolishes the effects of NPs. Similarly the inhibition of soluble guanylyl cyclase with ODQ abolished NP-driven Isc responses. There are number of levels where the cAMP and cGMP systems can cross-talk to each other. This includes activation of respective protein kinases (PKA and PKG) involved in channel gating, as well as cGMP-mediated inhibition of cAMP breakdown by the family of phosphodiseterases [175]. I hypothesize that nanoparticle-stimulated increases in cyclic nucleotide levels will increase PK-controlled protein phosphorylation, facilitate the exit of Cl^- through apically located CFTR Cl^- channels (See Fig. 32 for overview) an effect supported by increased bioavailability of Ca^{2+}. The restoration of $[Cl]_i$ levels may result from the phosphorylation and activation of the NKCC co-transporter. It has been shown in Calu-3 cells that elevations in $[Ca^{2+}]_i$ or the direct activation of K^+ channels can stimulate HCO_3^- secretion [176]. The fact that N20 nanoparticles affect intracellular calcium stores in combination with the activation of cAMP-regulated K^+ channels may also help to explain the movement of HCO_3^- through CFTR Cl^- channels. However, the hypothesis is limited by the fact that I did not observe the activation of Ca^{2+}-sensitive K^+ channels. Thus,

more work is needed to clarify the precise sequence of molecular events following the exposure of epithelial cells to nanoparticles.

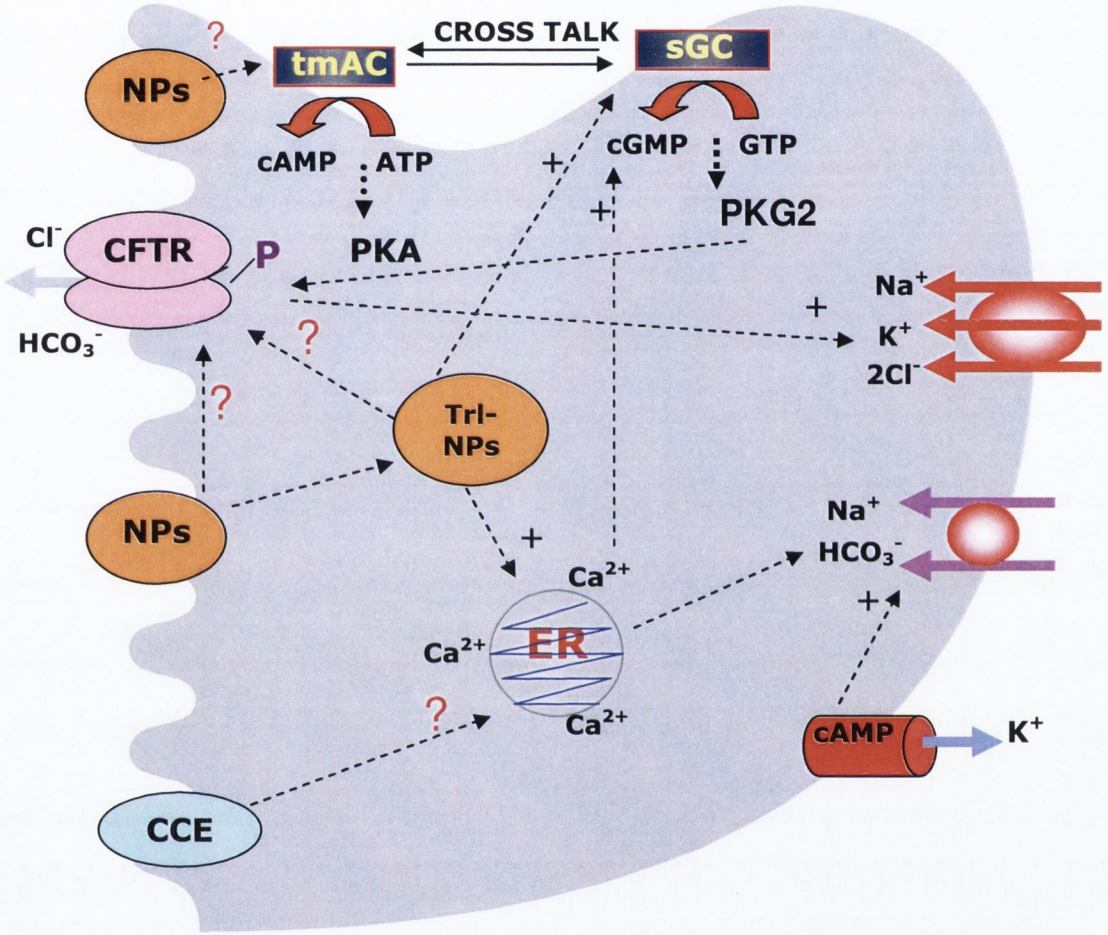

FIGURE 32. Schematic representation of the effect of NPs on the function of ion channels in human airways epithelial cells. In my model polystyrene NPs come in contact with the apical membrane where they induce membrane conformations that may affect CFTR structure and/or tmAC. This intraepithelial uptake of NPs (trl-NP) results in the stimulation of Ca^{2+} and cyclic nucleotide-dependent cell signalling. Calcium signaling may be triggered by capacitative Ca^{2+} entry (CCE) channels leading to the release of free calcium from the endoplasmic reticulum (ER). In turn calcium can activate the Na^{+}-HCO_3^{-} co-transporter on the basolateral membrane. Furthermore, calcium can also regulate the sGC-cGMP system. My studies indicate that cyclic nucleotide levels specifically cAMP and cGMP generated by tmAC and sGC lead to PK-controlled protein phosphorylation of CFTR Cl^{-} channels by either PKA or PKG2.

Increases in cAMP lead to the activation of cAMP-sensitive basolateral K^+ channels this can again positively regulate the Na^+-HCO_3^- co-transporter. The phosphorylation and opening of CFTR Cl^- channels can lead to the activation of the NKCC co-transporter. All these affects lead to the exit of Cl^- and HCO_3^- through apical CFTR Cl^- channels.

EFFECTS OF SILICA NPS IN THE PRESENCE OF CYTOKINES The hypothesis driving these experiments was that acute exposure of Calu-3 lung epithelial cells to nanosilica will be further modified in the presence of pro-inflammatory cytokines that mimic epithelial inflammation.

INF-γ has been shown to differentially regulate CFTR Cl^- channels in mast cells and T-84 epithelial cells. INF-γ treatment in mast cells was found to inhibit antigen–induced Cl^- fluxes. Also in the same study INF-γ was found to down-regulate CFTR Cl^- channel on epithelial cells via the involvement of JAK/STAT pathways [177]. Studies performed with HT-29 colon derived epithelium cells have shown that TNF-α can modulate CFTR Cl^- channel expression at the gene level, more specifically at the post-transcriptional level by decreasing the stability of CFTR mRNA transcripts [178]. Furthermore, it has been shown in epithelial cells that IFN-γ and TNF-α can act synergistically to reduce CFTR gene expression [179]. Finally, the treatment of human cultured bronchial epithelial cells with INF-γ resulted in the down-regulation of CFTR Cl^- channels at the protein level alongside with decreased Na^+ absorption [125].

As expected I found that the exposure of lung epithelial Calu-3 cells to pro-inflammatory cytokines IL-β, TNF-α and IFN-γ (in combination) led to the inhibition of Isc responses to forskolin. However, contrary to my expectations the acute exposure of Calu-3 cells to Si-10 did not lead to the inhibition of Isc or an exaggeration of the effect observed under the influence of cytokines. Furthermore, the lack of acute effects of Si-10 as well as Si-P50 on ion fluxes under normal and pro-inflammatory conditions indicates that lung epithelium could be resistant to the effects of silica nanoparticles over short periods of time.

NANOPARTICLES, ANION SECRETION, CHRONIC EXPOSURE

NANOPARTICLE TRANSLOCATION

We examined the translocation of polystyrene and silica NPs across bronchial epithelial cells using a polarized cell culture model *in vitro.* Polystyrene NPs were found to undergo time-dependent increases in translocation between 6 and 24 hours. Larger polystyrene NPs of 100-nm were found to be trafficked at higher amounts than smaller 50-nm ones. Also charge seemed to be an important factor for translocation, as uncharged NPs translocated in higher amounts then negatively charged NPs. Our translocation assay only measures apical-to-basolateral trafficking of polystyrene NPs. Thus, we cannot rule out the possibility that some nanoparticles might have been recycled across the apical membrane. Due to technical difficulties we

did not observe the translocation of 50-nm nanosilica with either positive or negative charges by Calu-3 cells. In parallel, our confocal microscopy validates the uptake of polystyrene NPs by Calu-3 cells which occurred rapidly within 30 min of exposure.

There are a number of pharmacological reasons why an *in vitro* assay for studying the translocation of NPs across lung epithelial cells could be of interest to pulmonary pharmacologists. As previously stated, NPs can cross the air-blood barrier of the lungs and enter the circulatory system [(180)]. Therefore, our translocation assay allows one to examine which characteristics of NPs are important in determining whether a particular nanoparticle will be translocated by epithelial cells in lung tissue. Also, if NPs are to used as "nanocarriers" of new therapeutic drugs or as gene delivery systems for lung diseases it is necessary to know which characteristics of NPs e.g. size, charge and composition are important factors for endocytosis by the targeted cells. Moreover, the method used in my studies may be useful to measure whether therapeutic nanocarriers can be concentrated within the targeted lung cell or will in fact be translocated into the blood circulatory system where they may elicit toxicity and possible side effects in the patient [(181)].

A study by Yacobi *et al.*, 2008 investigated the translocation of polystyrene NPs across RACEM monolayers. They found that

positively charged polystyrene NPs were trafficked 20-40 times faster then negatively charged nanoparticles of the same size. They also found that trafficking of NPs across RACEM monolayers was reduced at lower temperatures of 4°C compared with 37°C indicating the involvement of active transport in this process [145]. However, the most recent publication from the same research group which again investigated the trafficking of fluorescently labelled polystyrene NPs (20 and 100-nm, +/- charges) across RAECM monolayers found that trafficking rates of polystyrene NPs across RAECM did not change in the presence of inhibitors of endocytosis. They concluded that the NPs tested translocated transcellularly but suggested that this occurred as a result of the diffusion of polystyrene NP through the lipid bilayer of cell plasma membrane [143]. Des Rieux and colleagues exposed co-cultures of Caco-2 and Raji cells to either 200-nm yellow-green polystyrene particles with either carboxyl or amino groups, and found that the transport of both types of particles increased proportionally with the duration of incubation with cells and that particles having cationic sites were transported to a larger extent than those with anionic sites [182]. Yet a study by Patil *et al.*, 2007 showed that negative zeta potentials are favourable for the uptake of cerium oxide nanoparticles by the lung cell line A549 [183].

The results of my study suggest that both size and charge are essential factors in determining whether a particular NP is

translocated across a polarized lung cell monolayer and that there is a preferential translocation by Calu-3 cells for neutral polystyrene NPs. In my study I did not test positively charged NPs. However, there is much evidence to suggest that the net negative surface charge exhibited on the plasma membrane of epithelial cells due to extracellular protein moieties [184] leads to electrostatic repulsion of negatively charged molecules including NPs and that this accounts for the higher rate of uptake and translocation observed for positively charged NPs.

POLYSTYRENE NPS

My results indicate that chronic exposure of Calu-3 cell monolayers to polystyrene NPs can have a deleterious effect on transepithelial ion secretion. Interestingly, Yacobi *et al.*, 2007 investigated the effects of ultrafine ambient particulate suspensions (UAPs), polystyrene NPs, quantum dots and SWCNTs on transmonolayer resistance (R_t, $K\Omega/cm^2$) and equivalent Isc (I_{eq}, $\mu A/cm^2$) by RACEM monolayers [185]. They found that R_t was reduced after apical exposure of RACEM monolayers to UAPs, positively charged quantum dots and SWCNTs at varying concentrations. However, polystyrene NPs with sizes between 20 and 120-nm at a concentration of 176 µg/ml upon apical exposure to RACEM monolayers were found to have no effects on R_t or I_{eq} [185]. Even the apical exposure of RACEM cells to 706 µg/ml of polystyrene

NPs for up to 24 hr was not found to affect R_t and I_{eq} cell barrier properties.

I have shown that the overnight incubation of Calu-3 cells with either P50 or N20 at a high concentration of 200 µg/ml results in a marked reduction (~ 50 %) in Isc responses to carbachol. In addition, LDH data shows that chronic exposure of Calu-3 cells to increasing concentrations of P50 (but not N20) for 24 hr induces cellular cytotoxicity. Thus, the deleterious effects of polystyrene NPS in Calu-3 cells appear to be dependent on NP charge and not size. My results indicate that particle size does not play an important role in the cytotoxicity of polystyrene NPs on Calu-3 cells. In turn, our data shows that surface charge modifications may impact greatly on cell viability. I believe that P50 NPs have increased cytotoxicity due to the presence of an amine group modification on the structure of the NPs and that this is a contributing factor for the increased cytotoxicity of this NP in comparison to N20 NPs.

Similarly, a study by Xia *et al.*, 2007 showed that NP characteristics such as surface modification and charge have a profound effect on toxicity. This study examined the toxicity of polystyrene nanospheres in BEAS-2B human bronchial epithelial cells after 16 hr. Their results showed that positively charged 60-nm NPs (neutral or negatively charged NPs of the same size exhibited no effect) were highly toxic

affecting cell viability as well as causing significant mitochondrial damage and ATP depletion [186].

Interestingly, my data shows that nanoparticle-induced impairment of cell viability correlates with decreased Isc responses to carbachol for P50, but not N20 NPs. Indeed, N20 does not induce cytotoxicity in Calu-3 cells but does negatively affect Ca^{2+}-mediated transepithelial ion transport. The latter effects could be related to nanoparticle uptake and the interaction of N20 with specific proteins or subcellular organelles such as the ER required for Ca^{2+}-mediated anion secretion. There is evidence from studies done with liver cells that negatively charged 20-nm polystyrene NPs following cellular uptake localise in close proximity to membranes of the ER [187].

AMORPHOUS SILICA NPS

The evaluation of SiO_2 particle-induced cytotoxic effects were examined using both LDH and MTT assays. The results showed a clear size-dependent cytotoxic response by Calu-3 cells to small 10-nm SiO_2 NPs in contrast to microparticles of the same composite material with sizes of 150 and 500-nm. Furthermore, the data showed the cytotoxic effects of monodispersed amorphous 10-nm silica NPs in a concentration-dependent manner over a period of 24 hr. We purposely performed two cytotoxic assays to verify the

cytotoxic responses of cells to Si-10. These results confirm that Si-10 is an extremely potent cytotoxic agent for lung epithelial cells.

My data are compatible with the study by Lin *et al.*, 2006 who showed that treatments of human broncho-alveolar A549 cells *in vitro* to either 15-nm or 46-nm SiO_2 NPs for 48 hr at concentrations between 10 and 100 µg/ml decreased cell viability in a concentration-dependent manner, yet the cytotoxicity of these silica NPs were not significantly different from each other. The cell viability of A549 cells exposed to 15-nm SiO_2 NPs decreased to 68.1 % at the highest concentration of 100 µg/ml.[188].

In another study Eom *et al.*, 2009 the effects of fumed and porous silica NPs on Beas-2B human bronchial epithelial cells were investigated. An MTT assay was performed to assess the cytotoxic effects of these silica NPs on Beas-2B cell viability. It was found that after exposure to both types of silica NPs over a 24 hr period that cell viability was reduced to ~ 80 % of controls [189]. In 2009, Napierska and co-workers showed in human endothelial cells (EAHY926) that monodispersed silica NPs caused cytotoxic damage and decreased cell survival again in a concentration-dependent manner. Small SiO_2 NPs of 14, 15 and 16-nm had TC_{50} ranging from 33 to 47 µg/cm^2 of cell culture compared with the microsized SiO_2 NPs of 104 and 335-nm

which had low cytotoxicity with TC_{50} values of 1095 and 1087 μg/cm^2, respectively [190].

My own data reveals that exposure of Calu-3 cells to Si-10 but not Si-150 or Si-500 for 24 hr results in the concentration-dependent release of the two pro-inflammatory cytokines IL-6 and IL-8. Our results indicate that particle size is the main contributing factor for the cytotoxicity of silica particles in Calu-3 cells. Another study comparing the inflammatory and cytotoxic potency of crystalline and amorphous silica particles in A549 cells, found all particles tested caused the release of IL-6 and IL-8, including amorphous silica particles with a mean diameter of 300-nm [191].

Furthermore, Park *et al.*, 2009 used both *in vivo* (mice models) and *in vitro* (RAW 264.7 macrophage cell line) studies to examine the oxidative stress responses and inflammatory processes induced by amorphous silica NPs (12-nm, 50 mg/kg). Post NP-exposure they found that mRNA expressions of many inflammation-related genes such as IL-1, IL-6 and TNF-α were elevated in cultured peritoneal macrophages harvested from treated mice. In turn, treatments of cultured RAW 264.7 cells with 12-nm silica NPs led to the generation of reactive oxygen species and a decreased in intracellular GSH [192].

As already mentioned the uncontrolled release of MMPs in the lungs is linked to tissue destruction and remodelling. I have shown that MMP-9 is up-regulated in response to silica nanoparticles at gene level. This is in keeping with Wan *et al.*, 2008 who investigated the effects of exposing human monocyte cells (U937) to transition metal NPs specifically nano-Co and nano-TiO_2 (20-nm). They found that exposure of monocytes to nano-Co, but not to nano-TiO_2, at a "non-cytotoxicity" concentration (5 μg/ml) led to ROS generation and the up-regulation of MMP-2 and MMP-9 mRNA expression. Their data also demonstrated concentration- and time-related decreases in tissue inhibitors of metalloproteinases-2 in monocytes after exposure to nano-Co. Finally, pre-treatment of these cells for 4 hr with the AP-1 inhibitor curcumin (20 μM) significantly abolished nano-Co-induced pro-MMP-2 and-9 activity [193].

There is much evidence to show that silica-induced diseases activate the pro-inflammatory transcription factors AP-1 and NF-κB [194-195]. Furthermore, in human bronchial airway epithelial cells MAP kinases have been shown to regulate IL-8 promoter activity by NF-κB-dependent and -independent processes [196]. Finally, Singal and Finkelstein, 2005 investigated the effects of 12-nm amorphous silica NPs on mice alveolar epithelial cells (MLE15 cells). By using multiple MAP kinase inhibitors their data indicates that the transcription factor

AP-1 could possibly play a role in amorphous silica induced-inflammatory gene expression [194].

In this study, we established a concentration-response relationship for amorphous silica nanoparticles only (Si-10) on Calu-3 cells with regard to cytotoxicity, cytokine release and MMP-9 gene expression. Taken together, I believe that the inhalation of amorphous silica nanoparticles in an environmental or occupational setting can up-regulate the expression of transcription factors, pro-inflammatory cytokines and inflammation mediators leading to initiation, or more likely, exacerbation of already established inflammatory lung diseases such as those exhibited by infected CF patients resulting in a worsening of airway obstruction and further deterioration of the patients clinical status.

TREATMENT OF CF WITH NANOPARTICLES

Our work points toward the potential value of a nanomedical approach to the treatment of diseases caused by CFTR Cl^- channel dysfunction. Currently available CFTR therapies treat only the symptoms of the disease rather than rectify the functional or genetic defect of the CFTR Cl^- channel. Recent work by Poschet *et al.*, 2007 highlighted how the pharmacological modulation of cGMP levels by phosphodiesterase 5 inhibitors, such as sildenafil, could potentially work as a therapeutic approach for the treatment of CF [197]. They

propose that increasing intracellular cGMP levels with this drug will rectify many CF pathologies such as a reduction in bacterial adhesion to respiratory cells and pro-inflammatory responses [197]. I have found that polystyrene NPs activate CFTR Cl^- channels via the sGC/cGMP pathway in a NO-independent manner. Therefore is seems plausible that a polystyrene NP loaded with an NO releasing agent (interestingly NO production is reduced in the CF lung) could work synergistically to increase cGMP levels and promote transepithelial ion secretion via CFTR Cl^- channel activation leading to disease improvement. Presently, NO releasing nanoparticles are being developed to treat ovarian cancer and to aid in wound healing [198-199]. **It needs to be strongly emphasised that the clinical development of nanoparticles must consider biocompatibility and toxicological aspects that may confound pharmaceutical development.**

Most recently the antibiotic amikacin, which is used in the treatment against *P. aeruginosa,* an opportunistic bacteria which commonly infects and impairs the lung function of CF patients, was encapsulated into a nanoscale liposomal formulation of dipalmitoyl phosphatidylcholine and cholesterol [200]. These amikacin loaded nano–sized liposomes were found to be more effective at penetrating the biofilms of *P. aeruginosa* in infected mucus then micron–sized beads which did not. A phase II clinical trial of nebulized nano-

formulated liposomal amikacin™ has now been completed in Europe [200-201].

Together these studies highlight the great potential of nanoparticle based medicines for the treatment of CF and lung conditions. In addition to CF treatment nanoparticle-based therapies are now being developed to treat lung cancer pathologies. For example, a pulmonary delivery study carried out by Hitzman *et al.*, 2006 using a hamster model *in vivo* and 5-fluorouracil (20 % w/w) lipid-coated NPs showed that these particles were found to be effective at targeting and sustaining efficacious concentrations of the chemotherapeutic drug at tumour sites [202], thus suggesting that a nanoparticle–based delivery system could be used to treat squamous cell carcinoma of the lung [203].

My results also raise the possibility that nano-sized structures such as polystyrene NPs could exert per se therapeutic action in lung disorders such as CF by direct activation of epithelial CFTR Cl^- channels. In addition to CF other pathologies associated with the dysfunction of ion channels could be treated with nano-sized chloride-channel modulators. For example on the apical membrane of ocular epithelia, CFTR Cl^- channels are highly expressed and have a functional role in fluid and ion secretion thus it has been stated that the condition commonly known as dry eye (keratoconjunctivitis sicca)

would benefit from an activator of wild-type CFTR [21]. Yet, we must again highlight that our studies show that while the application of NP-based drug delivery may be beneficial in diseases such as CF, they may exert detrimental effects in other conditions characterised by normal CFTR Cl^- channel function. Thus, our studies show that NPs cannot be considered as a simple neutral vehicle for drug delivery, but depending on condition, may exert beneficial or detrimental effects on their own.

CONCLUSIONS AND FUTURE DIRECTIONS

When I started the research presented in this PhD dissertation focusing on the interaction of NPs with respiratory ion channels I had anticipated that NPs would block (ion channel pore size is ~ 7-8 nm) rather then activate ion channels such as CFTR Cl^- channels and K^+ channels. During the course of my research I encountered unexpected, exciting developments that significantly affected the final directions of my study. This body of work highlights the complex relationship regarding the exposure of airway epithelial cells to NPs and the way the cell communicates this interaction to evoke cellular responses which govern ion channel function as well as physiological processes. I feel that my research to date provides a fascinating proof-of-principle showing that nanoparticles per se modify and regulate ion channel function in lung epithelial cells. This may indicate that nanoparticles could be developed as pharmaceutical agents in

addition to their usefulness as drug carriers. Much more developmental work needs to be done to capitalize on this concept. Here I have listed some useful lines of investigation that in my view should be followed-up.

(1) Our initial excised inside-out patch clamp studies showed that both N20 and P50 NPs can activate WT CFTR Cl^- channels alone and in the presence of ATP and PKA. Research shows that the isoflavone genistein can recover defective CFTR Cl^- channel gating caused by missense mutations that affect the NBDs of CFTR proteins e.g. G551D [85]. Other small molecule potentiators of CFTR Cl^- channels such as 1,4-dihyropyridine felodipine and phenylglycine PG-01 have been shown to be effective on intracellular loop CFTR mutants e.g. E193K [204]. Both G551D- and E193K-CFTR mutant proteins unlike Δ508-CFTR are trafficked to the apical membrane of respiratory cells however the transport capabilities of these Cl^- channels is markedly reduced. From a pharmacological point of view it is important to assess using the patch clamp technique whether polystyrene NPs can activate CFTR-mutants expressed at the cell membrane. Research shows that flavonoid compounds activate weakly phosphorylated CFTR Cl^- channels. Electrophysiological and molecular modelling studies reveal that the NBDs of CFTR Cl^- channels may be the target of these flavonoid compounds [134]. **Therefore, it would be interesting to investigate the effects of polystyrene NPs on**

CFTR Cl^- channels when co-stimulated with flavonoids such as genistein or apigenin to identify how these particles can activate single CFTR Cl^- channels and to locate possible binding sites for NPs.

(2) When investigating the mechanism by which polystyrene NPs activate Isc response in Calu-3 cells we identified that the phosphorylation state of CFTR Cl^- channels plays an important role in this process. We also showed that cAMP-sensitive basolateral K^+ channels are activated by N20. **To further address the cAMP response of Calu-3 cells to N20 we need to (i) measure if there is a rise in cAMP levels after exposure of Calu-3 cells to NPs (ii) verify CFTR Cl^- channels activation by NPs is as a result of phosphorylation.** To achieve this we can pre-treat cells prior to NP exposure in Ussing chambers by using the compound NH-89, which works as a membrane-permeant selective inhibitor of PKA thus blocking the phosphorylation and activation of CFTR Cl^- channels. **We have much evidence from our sGC-cGMP experiments that this is the main pathway leading to the activation of Isc responses by N20 NPs for further affirmation we can also use PKG2 inhibitors (e.g. KT-5823) to identify the specific protein target leading to the phosphorylation of CFTR Cl^- channels.**

It would also be worthwhile to measure intracellular Ca^{2+} levels in cell monolayers exposed to NPs. In my PhD studies I tried to carry out this experiment but some technical issues arose. The main problem with measuring intracellular calcium with this method is that the tetracarboxylate fluorescent indicator used interfered with the fluorescently labelled NPs, N20 and P50. However, there is the possibility that other available calcium-sensitive tetracarboxylate fluorescent dyes or metallochromic dyes could be used if their excitation wavelengths did not interfere with N20 or P50 NPs. Other methods e.g. Ca^{2+}-selective microelectrodes can also be considered used, for review see [205].

(3) Cell monolayers pre-treated with NPs in Ussing chamber studies can be used for subsequent immunocytochemistry using the primary anti-CFTR monoclonal antibody 24-1 (which recognises the C-terminus of CFTR) as well as a secondary antibody. **This would allow us to directly observe an interaction between NPs and CFTR Cl^- channels.**

(4) Again following NP exposure in the Ussing chamber cells can be prepared for atomic force microscopy. **This technique would allow us to examine the topology of the cell monolayer surface and thus the presence of NPs on the cell membrane where they**

could be interacting and thus affecting ion channel function of respiratory cells.

(5) We showed that small silica NPs of 10-nm up-regulated MMP-9 expression at the gene level in respiratory cells over long periods. **The techniques of zymography and ELISA would allow us to examine if MMP-9 protein and enzymatic levels are increased after silica NP exposure.**

(6) Given the data showing strong interactions between nanoparticles and proteins it would be of great interest to study the interactions of crystal CFTR protein and nanoparticles.

(7) Animal models of cystic fibrosis may be used to further pharmaceutical development.

REFERENCES

1. Andersen DH (1938) Cystic Fibrosis of the pancreas and its relation to celiac disease. *Am J Dis Child* **56**:344.
2. Davis PB (2006) Cystic Fibrosis Since 1938. *Am J Respir Crit Care Med* **173**(5):475-482.
3. Di Saint'Agnese PA, Darling RC, Perera GA, & Shea E (1953) Abnormal electrolytes composition of sweat in cystic fibrosis of the pancreas. Clinical significance and relationship to disease. *Pediatrics* **12**:549-563.
4. Davis PB & di Sant'Agnese PA (1984) Diagnosis and treatment of cystic fibrosis. An update. *Chest* **85**(6):802-809.
5. Rowntree RK & Harris A (2003) The Phenotypic Consequences of CFTR Mutations. *Ann Hum Genet* **5**:471-485.
6. Quinton PM (1983) Chloride impermeability in cystic fibrosis. *Nature* **301**(5899):421-422.
7. Kerem B, *et al.* (1989) Identification of the cystic fibrosis gene: genetic analysis. *Science* **245**:1073-1080.
8. Riordan JR, *et al.* (1989) Identification of the cystic fibrosis gene: cloning and characterization of complementary DNA. *Science* **245**:1066-1073.
9. Rommens JM, *et al.* (1989) Identification of the cystic fibrosis gene: chromosome walking and jumping. *Science* **245**:1059-1065.
10. Collins FS (1992) Cystic Fibrosis. *Science* **256**:774-779.

11. Ratjen F & Döring G (2003) Cystic fibrosis. *The Lancet* **361**(9358):681-689.

12. Knowles M, Gatzy J, & Boucher R (1981) Increased bioelectric potential difference across respiratory epithelia in cystic fibrosis. *N Engl J Med* **305**:1489-1495.

13. Gadsby DC, Vergani P, & Csanády L (2006) The ABC protein turned chloride channel whose failure causes cystic fibrosis. *Nature* **440**:477-483.

14. Ikuma M & Welsh MJ (2000) Regulation of CFTR Cl^- channel gating by ATP binding and hydrolysis. *Proc Natl Acad Sci U S A* **97**:8675-8680

15. Vergani P, Lockless SW, Nairn AC, & Gadsby DC (2005) CFTR channel opening by ATP-driven tight dimerization of its nucleotide-binding domains. *Nature* **433**:876-880.

16. Ostedgaard LS, Baldursson O, & Welsh MJ (2001) Regulation of the Cystic Fibrosis Transmembrane Conductance Regulator Cl– Channel by Its R Domain. *J Biol Chem* **276**(11):7689-7692.

17. Csanady L, Chan KW, Nairn AC, & Gadsby DC (2004) Functional Roles of Nonconserved Structural Segments in CFTR's NH2-terminal Nucleotide Binding Domain. *J Gen Physiol* **125**(1):43-55.

18. Tabcharani JA, Chang XB, Riordan JR, & Hanrahan JW (1991) Phosphorylation-regulated Cl- channel in CHO cells stably expressing the cystic fibrosis gene. *Nature* **352**:628-631.

19. Picciotto MR, Cohn JA, Bertuzzi G, Greengard P, & Nairn AC (1992) Phosphorylation of the cystic fibrosis transmembrane conductance regulator. *J Biol Chem* **267**(18):12742-12752.

20. Berger HA, Travis SM, & Welsh MJ (1993) Regulation of the cystic fibrosis transmembrane conductance regulator Cl^- channel by specific protein kinases and protein phosphatases. *J Biol Chem* **268**(3):2037-2047.

21. Verkman AS & Galietta LJV (2009) Chloride channels as drug targets. *Nat Rev Drug Discov* **8**(2):153-171.

22. US Cystic Fibrosis Foundation (*www.genet.sickkids.on.ca/cftr)*.

23. McAuley DF & Elborn JS (2000) Cystic fibrosis: basic science. *Paediatr Respir Rev* **1**(2):93-100.

24. Knowles MR, Friedman KJ, & Silverman LM (1999) In: Yankaskas JR, Knowles MR, (eds). *Cystic Fibrosis in Adults* Philadelphia: Lippincott-Raven p27-44.

25. Du K, Sharma M, & Lukacs GL (2005) The [Delta]F508 cystic fibrosis mutation impairs domain-domain interactions and arrests post-translational folding of CFTR. *Nat Struct Mol Biol* **12**(1):17-25.

26. Farinha CM & Amaral MD (2005) Most F508del-CFTR Is Targeted to Degradation at an Early Folding Checkpoint and Independently of Calnexin. *Mol Cell Biol* **25**:5242-5252.

27. Gregory RJ*, et al.* (1991) Maturation and function of cystic fibrosis transmembrane conductance regulator variants bearing

mutations in putative nucleotide-binding domains 1 and 2. *Mol Cell Biol* **11**(8):3886-3893

28. Sheppard DN & Welsh MJ (1999) Structure and Function of the CFTR Chloride Channel. *Physiol Rev* **79**(1):23-45.
29. Salinas D*, et al.* (2004) Submucosal gland dysfunction as a primary defect in cystic fibrosis. *FASEB J* **3**:431-433.
30. Hummler E*, et al.* (1996) Early death due to defective neonatal lung liquid clearance in [alpha]ENaC-deficient mice. *Nat Genet* **12**(3):325-328.
31. Mall M, Grubb BR, Harkema JR, O'Neal WK, & Boucher RC (2004) Increased airway epithelial Na+ absorption produces cystic fibrosis-like lung disease in mice. *Nat Med* **10**(5):487-493.
32. Chambers LA, Rollins BM, & Tarran R (2007) Liquid movement across the surface epithelium of large airways. *Respir Physiol Neurobiol* **159**(3):256-270.
33. Livraghi A & Randell SH (2007) Cystic Fibrosis and Other Respiratory Diseases of Impaired Mucus Clearance. *Toxicol Pathol* **35**(1):116-129.
34. Matsui H*, et al.* (1998) Evidence for Periciliary Liquid Layer Depletion, Not Abnormal Ion Composition, in the Pathogenesis of Cystic Fibrosis Airways Disease. *Cell* **95**(7):1005-1015.
35. Konstan MW, Hilliard KA, Norvell TM, & Berger M (1994) Bronchoalveolar lavage findings in cystic fibrosis patients with

stable, clinically mild lung disease suggest ongoing infection and inflammation. *Am J Respir Crit Care Med* **150**(2):448-458.

36. Khan TZ*, et al.* (1995) Early pulmonary inflammation in infants with cystic fibrosis. *Am J Respir Crit Care Med* **151**(4):1075-1082.

37. Taggart C*, et al.* (2000) Increased elastase release by CF neutrophils is mediated by tumor necrosis factor-alpha and interleukin-8. *Am J Physiol Lung Cell Mol Physiol* **278**(1):L33-41.

38. Nichols D, Chmiel J, & Berger M (2008) Chronic Inflammation in the Cystic Fibrosis Lung: Alterations in Inter- and Intracellular Signaling. *Clin Rev Allergy Immunol* **34**(2):146-162.

39. Walsh DE*, et al.* (2001) Interleukin-8 Up-regulation by Neutrophil Elastase Is Mediated by MyD88/IRAK/TRAF-6 in Human Bronchial Epithelium. *J Biol Chem* **276**(38):35494-35499.

40. Berger M (1991) Inflammation in the lung in cystic fibrosis. A vicious cycle that does more harm than good. *Clin Rev Allergy* Spring-summer **9**(1-2):119-142.

41. Greenlee KJ, Werb Z, & Kheradmand F (2007) Matrix Metalloproteinases in Lung: Multiple Multifarious and Multifaceted. *Physiol Rev* **87**(1):69-98.

42. Stamenkovic I (2003) Extracellular matrix remodelling: the role of matrix metalloproteinases. *J Pathol* **200**(4):448-464.

43. Sternlicht MD & Werb Z (2001) How matrix metalloproteinases regulate cell behavior. *Annu Rev Cell Dev Biol* **17**:463-516.

44. Sorsa T, *et al.* (1997) Activation of Type IV Procollagenases by Human Tumor-associated Trypsin-2. *J Biol Chem* **272**(34):21067-21074.

45. Faurschou M & Borregaard N (2003) Neutrophil granules and secretory vesicles in inflammation. *Microbes Infect* **5**(14):1317-1327.

46. Kusano K, *et al.* (1998) Regulation of Matrix Metalloproteinases (MMP-2, -3, -9, and -13) by Interleukin-1 and Interleukin-6 in Mouse Calvaria: Association of MMP Induction with Bone Resorption. *Endocrinology* **139**(3):1338-1345.

47. Yao PM, *et al.* (1997) Divergent regulation of 92-kDa gelatinase and TIMP-1 by HBECs in response to IL-1beta and TNF-alpha. *Am J Physiol Lung Cell Mol Physiol* **273**(4):L866-874.

48. Gaggar A, *et al.* (2007) Matrix metalloprotease-9 dysregulation in lower airway secretions of cystic fibrosis patients. *Am J Physiol Lung Cell Mol Physiol* **293**(1):L96-104.

49. Konstan MW & Berger M (1997) Current understanding of the inflammatory process in cystic fibrosis: Onset and etiology. *Pediatr Pulmonol* **24**(2):137-142.

50. Stecenko A, *et al.* (2001) Dysregulated Cytokine Production in Human Cystic Fibrosis Bronchial Epithelial Cells. *Inflammation* **25**(3):145-155.

51. Verhaeghe C, *et al.* (2007) Role of IKK and ERK pathways in intrinsic inflammation of cystic fibrosis airways. *Biochem Pharmcol* **73**(12):1982-1994.

52. Bonfield TL, *et al.* (1995) Inflammatory cytokines in cystic fibrosis lungs. *Am J Respir Crit Care Med* **152**:2111-2118.

53. U.S National Library of Medicine National Institutes of Health (www.ncbi.nlm.nih.gov).

54. Bonfield TL, *et al.* (1995) Normal bronchial epithelial cells constitutively produce the anti-inflammatory cytokine interleukin-10, which is downregulated in cystic fibrosis. *Am J Respir Cell Mol Biol* **13**(3):257-261.

55. Osika E, *et al.* (1999) Distinct sputum cytokine profiles in cystic fibrosis and other chronic inflammatory airway disease. *Eur Respir J* **14**(2):339-346.

56. Moss RB, *et al.* (1996) Reduced IL-10 secretion by CD4+ T lymphocytes expressing mutant cystic fibrosis transmembrane conductance regulator (CFTR). *Clin Exp Immunol* **106**(2):374-388.

57. Watkins DN, Peroni DJ, Basclain KA, Garlepp MJ, & Thompson PJ (1997) Expression and activity of nitric oxide synthases in human airway epithelium. *Am J Respir Cell Mol Biol* **16**(6):629-639.

58. Duszyk M (2001) Regulation of anion secretion by nitric oxide in human airway epithelial cells. *Am J Physiol Lung Cell Mol Physiol* **281**(2):L450-457.

59. Duta V, Duta F, Puttagunta L, Befus A, & Duszyk M (2006) Regulation of Basolateral Cl^- Channels in Airway Epithelial Cells: The Role of Nitric Oxide. *J Membr Biol* **213**(3):165-174.

60. Guo Y, Duvall MD, Crow JP, & Matalon S (1998) Nitric oxide inhibits Na^+ absorption across cultured alveolar type II monolayers. *Am J Physiol Lung Cell Mol Physiol* **274**(3):L369-377.

61. Nagaki M, Shimura MN, Irokawa T, Sasaki T, & Shirato K (1995) Nitric oxide regulation of glycoconjugate secretion from feline and human airways in vitro. *Respir Physiol* **102**(1):89-95.

62. Song J, *et al.* (2007) Nitric oxide induces MUC5AC mucin in respiratory epithelial cells through PKC and ERK dependent pathways. *Respir Res* **8**(1):28.

63. Foerster J, Harteneck C, Malkewitz J, Schultz G, & Koesling D (1996) A Functional Heme-Binding Site of Soluble Guanylyl Cyclase Requires Intact N-Termini of alpha 1 and beta 1 Subunits. *Eur J Biochem* **240(**2):380-386.

64. Zabel U, Weeger M, La M, & Schmidt HH (1998) Human soluble guanylate cyclase: functional expression and revised isoenzyme family. *Biochem J* **355**(1):51-57.

65. Hofmann F, Feil R, Kleppisch T, & Schlossmann J (2006) Function of cGMP-Dependent Protein Kinases as Revealed by Gene Deletion. *Physiol Rev* **86**(1):1-23.

66. Beavo JA (1995) Cyclic nucleotide phosphodiesterases: functional implications of multiple isoforms. *Physiol Rev* **75**(4):725-748.

67. Widdicombe JH (2000) Yet Another Role for the Cystic Fibrosis Transmembrane Conductance Regulator. *Am J Respir Cell Mol Biol* **22**(1):11-14.

68. Grasemann H, Michler E, Wallot M, & Ratjen F (1997) Decreased concentration of exhaled nitric oxide (NO) in patients with cystic fibrosis. *Pediatr Pulmonol* **24**(3):173-177.

69. Steagall WK, Elmer HL, Brady KG, & Kelley TJ (2000) Cystic Fibrosis Transmembrane Conductance Regulator-Dependent Regulation of Epithelial Inducible Nitric Oxide Synthase Expression. *Am J Respir Cell Mol Biol* **22**(1):45-50.

70. Kelley TJ & Drumm ML (1998) Inducible nitric oxide synthase expression is reduced in cystic fibrosis murine and human airway epithelial cells. *J Clin Invest* **102**(6):1200-1207.

71. Mhanna MJ, *et al.* (2001) Nitric Oxide Deficiency Contributes to Impairment of Airway Relaxation in Cystic Fibrosis Mice. *Am J Respir Cell Mol Biol* **24**(5):621-626.

72. Kamosinska B, Radomski A, Man SFP, Radomski MW, & Duszyk M (2000) Role of Inducible Nitric-Oxide Synthase in Regulation

of Whole-Cell Current in Lung Epithelial Cells. *J PET* **295**(2):500-505.

73. Grasemann H, *et al.* (2006) Decreased systemic bioavailability of L-arginine in patients with cystic fibrosis. *Respir Res* **7**(1):87.

74. Grasemann H, Schwiertz R, Matthiesen S, Racke K, & Ratjen F (2005) Increased Arginase Activity in Cystic Fibrosis Airways. *Am J Respir Crit Care Med* **172**(12):1523-1528.

75. Murray JF (1979) The ketchup-bottle method. *N Engl J Med* **300**(20):1155-1157.

76. Fuchs HJ, *et al.* (1994) Effect of aerosolized recombinat human DNase on exacerbations of respiratory symptoms and on pulmonary function in patients with cystic fibrosis. *N Engl J Med* **331**:637-642.

77. Ramsey BW, *et al.* (1999) Intermittent administration of inhaled tobramycin in patients with cystic fibrosis. Cystic Fibrosis Inhaled Tobramycin Study Group. *N Engl J Med* **340**(1):23-30.

78. Hodson ME, Roberts CM, Butland RJ, Smith MJ, & Batten JC (1987) Oral ciprofloxacin compared with conventional intravenous treatment for *Pseudmonas aeruginosa* infection in adults with cystic fibrosis. *Lancet* **1**:235-237.

79. Ferrin M, Zuckerman JB, Meagher A, & Blumberg EA (2002) Successful treatment of methicillin-resistant *Staphylococcus*

aureus pulmonary infection with linezolid in a patient with cystic fibrosis. *Paediatr pulmonol* **33**:221-223.

80. Konstan MW, Byard JP, Hoppel CL, & Davis PB (1999) Effect of high-dose ibuprofen in patients with cystic fibrosis: trends and physicans attitudes. *Chest* **124**:689-693.

81. Auphan N, DiDonato JA, Rosette C, Helmberg A, & Karin M (1995) Immunosuppression by glucocorticoids: inhibition of NF-kappa B activity through induction of I kappa B synthesis. *Science* **270**:286-290.

82. Yin MJ, Yamamoto Y, & Gaynor RB (1998) The anti-inflammatory agents aspirin and salicylate inhibit the activity of I(kappa)B kinase-beta. *Nature* **386**:77-80.

83. Illek B & Fischer H (1998) Flavonoids stimulate Cl conductance of human airway epithelium in vitro and in vivo. *Am J Physiol Lung Cell Mol Physiol* **275**(5):L902-910.

84. Caci E, *et al.* (2003) CFTR activation in human bronchial epithelial cells by novel benzoflavone and benzimidazolone compounds. *Am J Physiol Lung Cell Mol Physiol* **285**(1):L180-188.

85. Illek B, *et al.* (1999) Defective function of the cystic fibrosis-causing missense mutation G551D is recovered by genistein. *Am J Physiol Cell Physiol* **277**(4):C833-839.

86. Otake Y, Hsieh F, & Walle T (2002) Glucuronidation versus Oxidation of the Flavonoid Galangin by Human Liver

Microsomes and Hepatocytes. *Drug Metab Dispos* **30**(5):576-581.

87. Fischer H & Illek B (2008) Activation of the CFTR Cl- channel by trimethoxyflavone in vitro and in vivo. *Cell Physiol Biochem* **22**:685-692.

88. The Cystic Fibrosis Association of Ireland (www.cfireland.ie).

89. Devaney J, *et al.* (2003) Cystic fibrosis mutation frequencies in an Irish population. *Clin Genet* **63**(2):121-125.

90. Pollock RM (2005) Pollock Report. www.cfireland.ie.

91. Medina C, Santos-Martinez MJ, Radomski A, Corrigan OI, & Radomski MW (2007) Nanoparticles: pharmacological and toxicological significance. *Br J Pharmacol* **150**(5):552-558.

92. Borm P, *et al.* (2006) The potential risks of nanomaterials: a review carried out for ECETOC. *Part Fibre Toxicol* **3**(1):11.

93. Muhlfeld C, *et al.* (2008) Interactions of nanoparticles with pulmonary structures and cellular responses. *Am J Physiol Lung Cell Mol Physiol* **294**(5):L817-829.

94. Donaldson K, *et al.* (2005) Combustion-derived nanoparticles: A review of their toxicology following inhalation exposure. *Part Fibre Toxicol* **2**(1):10.

95. The Royal Society and the Royal Academy of Engineering (R 2004) Nanoscience and nanotechnologies: opportunities and uncertainties.

96. United States Nanotechnology Initiative (http://www.nano.gov).

97. Reiser KW & Last JA (1979) Silicosis and fibrogenesis: fact and artifact. *Toxicology* **13**:51-72.

98. Merget R, *et al.* (2002) Health hazards due to the inhalation of amorphous silica. *Arch Toxicol* **75**(11-12):625-634.

99. Peters A & Pope Iii CA (2002) Cardiopulmonary mortality and air pollution. *The Lancet* **360**(9341):1184-1185.

100. Dockery DW, *et al.* (1989) Effects of inhalable particles on respiratory health of children. *Am Rev Respir Dis* **139**(3):587-594.

101. Goss CH, Newsom SA, Schildcrout JS, Sheppard L, & Kaufman JD (2004) Effect of Ambient Air Pollution on Pulmonary Exacerbations and Lung Function in Cystic Fibrosis. *Am J Respir Crit Care Med* **169**(7):816-821.

102. Qu F, *et al.* (2009) Ozone stress down-regulates the expression of cystic fibrosis transmembrane conductance regulator in human bronchial epithelial cells. *Chemico-Biological Interactions* **179**(2-3):219-226.

103. Mills NL, *et al.* (2009) Adverse cardiovascular effects of air pollution. *Nat Clin Pract Cardiovasc Med* **6**(1):36-44.

104. Ghio AJ, Kim C, & Devlin RB (2000) Concentrated Ambient Air Particles Induce Mild Pulmonary Inflammation in Healthy Human Volunteers. *Am J Respir Crit Care Med* **162**(3):981-988.

105. Salvi S, *et al.* (1999) Acute Inflammatory Responses in the Airways and Peripheral Blood After Short-Term Exposure to Diesel Exhaust in Healthy Human Volunteers. *Am J Respir Crit Care Med* **159**(3):702-709.

106. Ram Suresh, *et al.* (2009) Assessment of association of exposure to polycyclic aromatic hydrocarbons with bronchial asthma and oxidative stress in children: A case control study. *Indian J Occup Environ Med* **13**(1):33-37.

107. Araujo JA, *et al.* (2008) Ambient Particulate Pollutants in the Ultrafine Range Promote Early Atherosclerosis and Systemic Oxidative Stress. *Circ Res* **102**(5):589-596.

108. Card JW, Zeldin DC, Bonner JC, & Nestmann ER (2008) Pulmonary applications and toxicity of engineered nanoparticles. *Am J Physiol Lung Cell Mol Physiol* **295**(3):L400-411.

109. The Project on Emerging Nanotecnologies (http://www.nanotechproject.org/inventories/consumer/).

110. Chen H-W, *et al.* (2006) Titanium dioxide nanoparticles induce emphysema-like lung injury in mice. *FASEB J* **20**(13):2393-2395.

111. Gao F, Lu Q, & Komarneni S (2006) Fast synthesis of cerium oxide nanoparticles and nanorods. *J Nanosci Nanotechnol* **6**(12):3812-3819.

112. Park E-J, Choi J, Park Y-K, & Park K (2008) Oxidative stress induced by cerium oxide nanoparticles in cultured BEAS-2B cells. *Toxicology* **245**(1-2):90-100.

113. Liu Z, Tabakman S, Welsher K, & Dai H (2009) Carbon Nanotubes in Biology and Medicine: In vitro and in vivo Detection, Imaging and Drug Delivery. *Nano Res* **2**(2):85-120.

114. Shvedova AA*, et al.* (2008) Sequential Exposure to Carbon Nanotubes and Bacteria Enhances Pulmonary Inflammation and Infectivity. *Am J Respir Cell Mol Biol* **38**(5):579-590.

115. Lam C-W, James JT, McCluskey R, & Hunter RL (2004) Pulmonary Toxicity of Single-Wall Carbon Nanotubes in Mice 7 and 90 Days After Intratracheal Instillation. *Toxicol Sci* **77**(1):126-134.

116. Oberdörster G*, et al.* (2004) Translocation of Inhaled Ultrafine Particles to the Brain. *Inhal Toxicol* **16**(6-7):437-445.

117. Kleinman MT*, et al.* (2008) Inhaled ultrafine particulate matter affects CNS inflammatory processes and may act via MAP kinase signaling pathways. *Toxicol Lett* 178(2):127-130.

118. Radomski A*, et al.* (2005) Nanoparticle-induced platelet aggregation and vascular thrombosis. *Br J Pharmacol* **146**(6):882-893.

119. Yamawaki H & Iwai N (2006) Mechanisms Underlying Nano-Sized Air-Pollution-Mediated Progression of Atherosclerosis Carbon Black Causes Cytotoxic Injury/Inflammation and

Inhibits Cell Growth in Vascular Endothelial Cells. *Cir J* **70**(1):129-140.

120. Azarmi S, Roa WH, & Löbenberg R (2008) Targeted delivery of nanoparticles for the treatment of lung diseases. *Adv Drug Deliv Rev* **60**(8):863-875.
121. Smola M, Vandamme T, & Sokolowski A (2008) Nanocarriers as pulmonary drug delivery systems to treat and to diagnose respiratory and non respiratory diseases. *Int J Nanomedicine* **3**(1):1-19.
122. Lundqvist M, *et al.* (2008) Nanoparticle size and surface properties determine the protein corona with possible implications for biological impacts. *Proc Natl Acad Sci U S A.* **105**(38):14265-14270.
123. Duszyk M, MacVinish L, & Cuthbert AW (2001) Phenanthrolines--a new class of CFTR chloride channel openers. *Br J Pharmacol* **134**(4):853-864.
124. Linsdell P & Gong X (2002) Multiple inhibitory effects of $Au(CN)_2^-$ ions on cystic fibrosis transmembrane conductance regulator Cl^- channel currents. *J Physiol* **540**:29-38.
125. Galietta LJV, *et al.* (2000) Modification of transepithelial ion transport in human cultured bronchial epithelial cells by interferon-gamma. *Am J Physiol Lung Cell Mol Physiol* **278**(6):L1186-1194.

126. Lehr C (2002) Culture Models of Biological Barriers – in vitro test systems for drug adsorption and delivery.

127. Sachs LA, Finkbeiner WE, & Widdicombe JH (2009) Effects of media on differentiation of cultured human tracheal epithelium. *In Vitro Cell Dev Biol Anim* **39**:56-62.

128. Borisov SM, *et al.* (2009) Precipitation as a simple and versatile method for preparation of optical nanochemosensors. *Talanta* **79**(5):1322-1330.

129. Tsapis N, Bennett D, Jackson B, Weitz DA, & Edwards DA (2002) Trojan particles: Large porous carriers of nanoparticles for drug delivery. *Proc Natl Acad Sci U S A* **99**(19):12001-12005.

130. Kaewamatawong T, *et al.* (2006) Acute and Subacute Pulmonary Toxicity of Low Dose of Ultrafine Colloidal Silica Particles in Mice after Intratracheal Instillation. *Toxicol Pathol* **34**(7):958-965.

131. Gadsby DC, Vergani P, & Csanády L (2006) The ABC protein turned chloride channel whose failure causes cystic fibrosis. *Nature* **440**:477-483.

132. Ostedgaard LS, Baldursson O, & Welsh MJ (2001) Regulation of the Cystic Fibrosis Transmembrane Conductance Regulator Cl^- Channel by its R Domain. *J Biol Chem* **276**:7689-7692.

133. Vergani P, Lockless SW, Nairn AC, & Gadsby DC (2005) CFTR channel opening by ATP-driven tight dimerization of its nucleotide-binding domains. *Nature* **433**:876-880.

134. Moran O, Galietta LJ, & Zegarra-Moran O (2005) Binding site of activators of the cystic fibrosis transmembrane conductance regulator in the nucleotide binding domains. *Cell Mol Life Sci* **62**:446-460.

135. Cai Z & Sheppard DN (2002) Phloxine B Interacts with the Cystic Fibrosis Transmembrane Conductance Regulator at Multiple Sites to Modulate Channel Activity. *J Biol Chem* **277**:19546-19553.

136. Ai T*, et al.* (2004) Capsaicin Potentiates Wild-Type and Mutant Cystic Fibrosis Transmembrane Conductance Regulator Chloride-Channel Currents. *Mol Pharmacol* **65**:1415-1426.

137. Vasir JK & Labhasetwar V (2008) Quantification of the force of nanoparticle-cell membrane interactions and its influence on intracellular trafficking of nanoparticles. *Biomaterials* **29**(31):4244-4252.

138. Wang B, Zhang L, Bae SC, & Granick S (2008) Nanoparticle-induced surface reconstruction of phospholipid membranes. *Proc Natl Acad Sci U S A* **105**:18171-18175.

139. Li Yang & Gu Ning (2010) Thermodynamics of Charged Nanoparticle Adsorption on Charge-Neutral Membranes: A Simulation Study. *J Phys Chem B* **114**(8):2749-2754.

140. Brandenberger C, Rothen-Rutishauser B, Blank F, Gehr P, & Muhlfeld C (2009) Particles induce apical plasma membrane enlargement in epithelial lung cell line depending on particle surface area dose. *Respir Res* **10**(1):22.

141. Kim JS*, et al.* (2006) Cellular uptake of magnetic nanoparticle is mediated through energy dependent endocytosis in A549 cells. *J vet Sci* **7**:321-326.

142. Rothen-Rutishauser BM, SchÜrch S, Haenni B, Kapp N, & Gehr P (2006) Interaction of fine particles and nanoparticles with red blood cells visualized with advanced microscopic techniques. *Environ Sci Technol* **40**:4253-4259.

143. Yacobi NR*, et al.* (2009) Mechanisms of alveolar epithelial translocation of a defined population of nanoparticles. *Am J Respir Cell Mol Biol* **45**(5):604-614.

144. Stearns RC, Paulauskis JD, & Godleski JJ (2001) Endocytosis of Ultrafine Particles by A549 Cells. *Am J Respir Cell Mol Biol* **24**:108-115.

145. Yacobi NR*, et al.* (2008) Polystyrene nanoparticle trafficking across alveolar epithelium. *Nanomedicine* **4**:139-145.

146. Kamenetsky M*, et al.* (2006) Molecular Details of cAMP Generation in Mammalian Cells: A Tale of Two Systems. *J Mol Biol* **362**(4):623-639.

147. Cooper D (2003) Molecular and cellular requirements for the regulation of adenylate cyclases by calcium. *Biochem Soc Trans* **31**(Pt 5):912-915.

148. Nlend M-C, *et al.* (2007) Calcium-mediated, purinergic stimulation and polarized localization of calcium-sensitive adenylyl cyclase isoforms in human airway epithelia. *FEBS Lett* **581**(17):3241-3246.

149. Illek B & Fischer H (1998) Flavonoids stimulate Cl^- conductance of human airway epithelium in vitro and in vivo. *Am J Physiol* **227**:L902-910.

150. Illek B, *et al.* (2000) Structural determinants for activation and block of CFTR-mediated chloride currents by apigenin. *Am J Physiol Cell Physiol* **279**:C1838-1846.

151. Malinski T & Huk I (2001) Measurement of nitric oxide in single cells and tissue using a porphyrinic microsensor. *Curr Protoc Neurosci* Chapter 7, Unit 7.14.

152. Brovkovych V, Stolarczyk E, Oman J, Tomboulian P, & Malinski T (1999) Direct electrochemical measurement of nitric oxide in vascular endothelium. *J Pharm Biomed Anal* **19**(1-2):135-143.

153. Pollock JS, *et al.* (1991) Purification and characterization of particulate endothelium-derived relaxing factor synthase from cultured and native bovine aortic endothelial cells. *Proc Natl Acad Sci U S A* **88**(23):10480-10484.

154. Kanai AJ, *et al.* (1995) Shear Stress Induces ATP-Independent Transient Nitric Oxide Release From Vascular Endothelial Cells, Measured Directly With a Porphyrinic Microsensor. *Circ Res* **77**(2):284-293.

155. Fahmy B & Cormier SA (2009) Copper oxide nanoparticles induce oxidative stress and cytotoxicity in airway epithelial cells. *Toxicol in Vitro* **23**(7):1365-1371.

156. Auger F, Gendron M-C, Chamot C, Marano F, & Dazy A-C (2006) Responses of well-differentiated nasal epithelial cells exposed to particles: Role of the epithelium in airway inflammation. *Toxicol Appl Pharmacol* **215**(3):285-294.

157. Moro MA, *et al.* (1996) cGMP mediates the vascular and platelet actions of nitric oxide: confirmation using an inhibitor of the soluble guanylyl cyclase. *Proc Natl Acad Sci U S A* **93**(4):1480-1485.

158. Asahi M, McKenna E, Kurzydlowski K, Tada M, & MacLennan DH (2000) Physical Interactions between Phospholamban and Sarco(endo)plasmic Reticulum Ca^{2+}-ATPases Are Dissociated by Elevated Ca^{2+}, but Not by Phospholamban Phosphorylation, Vanadate, or Thapsigargin, and Are Enhanced by ATP. *J Biol Chem* **275**(20):15034-15038.

159. Clementi E (1998) Role of Nitric Oxide and Its Intracellular Signalling Pathways in the Control of Ca^{2+} Homeostasis. *Biochem Pharmacol* **55**(6):713-718.

160. Zabel U, *et al.* (2002) Calcium-dependent membrane association sensitizes soluble guanylyl cyclase to nitric oxide. *Nat Cell Biol* **4**(4):307-311.

161. Moon S, Singh M, Krouse ME, & Wine JJ (1997) Calcium-stimulated Cl^- secretion in Calu-3 human airway cells requires CFTR. *Am J Physiol Lung Cell Mol Physiol* **273**(6):L1208-1219.

162. Tang M, *et al.* (2008) Unmodified CdSe quantum dots induce elevation of cytoplasmic calcium levels and impairment of functional properties of sodium channels in rat primary cultured hippocampal neurons. *Environ Health Perspect* **116**(7):915-922.

163. Tang M, *et al.* (2008) Mechanisms of unmodified CdSe quantum dot-induced elevation of cytoplasmic calcium levels in primary cultures of rat hippocampal neurons. *Biomaterials* **29**(33):4383-4391.

164. Sniadecki NJ (2010) Minireview: A Tiny Touch: Activation of Cell Signaling Pathways with Magnetic Nanoparticles. *Endocrinology* **151**(2):451-457.

165. Glogauer M, Ferrier J, & McCulloch CA (1995) Magnetic fields applied to collagen-coated ferric oxide beads induce stretch-activated Ca^{2+} flux in fibroblasts. *Am J Physiol Cell Physiol* **269**(5):C1093-1104.

166. Wu Z, Wong K, Glogauer M, Ellen R, & McCulloch C (1999) Regulation of Stretch-Activated Intracellular Calcium Transients

by Actin Filaments. *Biochem Biophys Res Commun* **261**(2):419-425.

167. Meyer CJ, *et al.* (2000) Mechanical control of cyclic AMP signalling and gene transcription through integrins. *Nat Cell Biol* **2**(9):666-668.
168. Engelhardt JF, Zepeda M, Cohn JA, Yankaskas JR, & Wilson JM (1994) Expression of the cystic fibrosis gene in adult human lung. *J Clin Invest* **93**(2):737-740.
169. Trapnell BC, *et al.* (1991) Expression of the cystic fibrosis transmembrane conductance regulator gene in the respiratory tract of normal individuals and individuals with cystic fibrosis. *Proc Natl Acad Sci U S A* **88**(15):6565-6569.
170. Engelhardt JF, *et al.* (1992) Submucosal glands are the predominant site of CFTR expression in the human bronchus. *Nat Genet* **2**(3):240-248.
171. MatTek Corporation (The EpiAirway™ Tissue Model) http://www.mattek.com/pages/products/epiairway.
172. Cowley EA & Linsdell P (2002) Characterization of basolateral K+ channels underlying anion secretion in the human airway cell line Calu-3. *J Physiol* **538**(3):747-757.
173. Matthews JB (2002) Molecular Regulation of Na^+-K^+-$2Cl^-$ Cotransporter (NKCC1) and Epithelial Chloride Secretion. *W J Surg* **26**(7):826-830.

174. Haas M, McBrayer D, & Lytle C (1995) Cl-dependent Phosphorylation of the Na-K-Cl Cotransport Protein of Dog Tracheal Epithelial Cells. *J Biol Chem* **270**(48):28955-28961.

175. Zaccolo M & Movsesian MA (2007) cAMP and cGMP Signaling Cross-Talk: Role of Phosphodiesterases and Implications for Cardiac Pathophysiology. *Circ Res* **100**(11):1569-1578.

176. Krouse ME, Talbott JF, Lee MM, Joo NS, & Wine JJ (2004) Acid and base secretion in the Calu-3 model of human serous cells. *Am J Physiol Lung Cell Mol Physiol* **287**(6):L1274-1283.

177. Kulka M, Dery R, Nahirney D, Duszyk M, & Befus AD (2005) Differential Regulation of Cystic Fibrosis Transmembrane Conductance Regulator by Interferon γ in Mast Cells and Epithelial Cells. *J Pharmacol Exp Ther* **315**(2):563-570.

178. Nakamura H, *et al.* (1992) Tumor necrosis factor modulation of expression of the cystic fibrosis transmembrane conductance regulator gene. *FEBS Lett* **314**(3):366-370.

179. Besancon F, *et al.* (1994) Interferon-gamma downregulates CFTR gene expression in epithelial cells. *Am J Physiol Cell Physiol* **267**(5):C1398-1404.

180. Donaldson K. AR, Tran L., Stone V., Duffin R., Forrest G. and Alexander A (2006) Carbon Nanotubes: A Review of Their Properties in Relation to Pulmonary Toxicology and Workplace Safety. *Toxicol Sci* **92**(1):5–22.

181. Azarmi S, Roa WH, & Löbenberg R (2008) Targeted delivery of nanoparticles for the treatment of lung diseases. *Adv Drug Deliv Rev* **60**(8):863-875.

182. Rieux Ad, *et al.* (2005) Transport of nanoparticles across an in vitro model of the human intestinal follicle associated epithelium. *Eur J Pharm Sci* **25**(4-5):455-465.

183. Patil S, Sandberg A, Heckert E, Self W, & Seal S (2007) Protein adsorption and cellular uptake of cerium oxide nanoparticles as a function of zeta potential. *Biomaterials* **28**(31):4600-4607.

184. Rojanasakul Y, *et al.* (1992) The Transport Barrier of Epithelia: A Comparative Study on Membrane Permeability and Charge Selectivity in the Rabbit. *Pharm Res* **9**(8):1029-1034.

185. Yacobi NR, *et al.* (2007) Nanoparticle effects on rat alveolar epithelial cell monolayer barrier properties. *Toxicol in Vitro* **21**(8):1373-1381.

186. Xia T, Kovochich M, Liong M, Zink JI, & Nel AE (2007) Cationic Polystyrene Nanosphere Toxicity Depends on Cell-Specific Endocytic and Mitochondrial Injury Pathways. *ACS Nano* **2**(1):85-96.

187. Fröhlich E, *et al.* (2010) Size-dependent effects of nanoparticles on the activity of cytochrome P450 isoenzymes. *Toxicol Appl Pharmacol* **242**(3):326-332.

188. Lin W, Huang Y-w, Zhou X-D, & Ma Y (2006) In vitro toxicity of silica nanoparticles in human lung cancer cells. *Toxicol Appl Pharmacol* **217**(3):252-259.

189. Eom H-J & Choi J (2009) Oxidative stress of silica nanoparticles in human bronchial epithelial cell, Beas-2B. *Toxicol in Vitro* **23**(7):1326-1332.

190. Napierska D, *et al.* (2009) Size-Dependent Cytotoxicity of Monodisperse Silica Nanoparticles in Human Endothelial Cells. *Small* **5**(7):846-853.

191. Hefland RB, *et al.* (2001) Silica-induced cytokine release from A549 cells: importance of surface area versus size. *Hum Exp Toxicol* **20**(1):46-55.

192. Park E-J & Park K (2009) Oxidative stress and pro-inflammatory responses induced by silica nanoparticles in vivo and in vitro. *Toxicol Lett* **184**(1):18-25.

193. Wan R, *et al.* (2008) Matrix metalloproteinase-2 and -9 are induced differently by metal nanoparticles in human monocytes: The role of oxidative stress and protein tyrosine kinase activation. *Toxicol Appl Pharmacol* **233**(2):276-285.

194. Singal M & Finkelstein JN (2005) Amorphous silica particles promote inflammatory gene expression through the redox sensitive transcription factor, AP-1, in alveolar epithelial cells. *Exp Lung Res* **31**(6):581-597.

195. Chen F & Shi X (2002) NF-κB, a pivotal transcription factor in silica-induced diseases. *Mol Cell Biochem* **234-235**(1):169-176.

196. Li J, *et al.* (2002) Regulation of human airway epithelial cell IL-8 expression by MAP kinases. *Am J Physiol Lung Cell Mol Physiol* **283**(4):L690-699.

197. Poschet JF, *et al.* (2007) Pharmacological modulation of cGMP levels by phosphodiesterase 5 inhibitors as a therapeutic strategy for treatment of respiratory pathology in cystic fibrosis. *Am J Physiol Lung Cell Mol Physiol* **293**(3):L712-719.

198. Stevens E, *et al.* (2010) Nitric oxide-releasing silica nanoparticle inhibition of ovarian cancer cell growth. *Mol Pharm* **7**(3):775-785.

199. Weller RB (2009) Nitric Oxide-Containing Nanoparticles as an Antimicrobial Agent and Enhancer of Wound Healing. *J Invest Dermatol* **129**(10):2335-2337.

200. Buxton DB (2009) Nanomedicine for the management of lung and blood diseases. *Nanomedicine* **4**:331-339.

201. Transave Inhalation therapeutics (http://www.transaveinc.com).

202. Hitzman CJ, Wattenberg LW, & Wiedmann TS (2006) Pharmacokinetics of 5-fluorouracil in the hamster following inhalation delivery of lipid-coated nanoparticles. *J Pharm Sci* **95**:1196-1211.

203. Yang W, Peters JI, & Williams RO 3rd (2008) Inhaled nanoparticles--a current review. *Int J Pharm* **356**:239-247.

204. Caputo A, *et al.* (2009) Mutation-Specific Potency and Efficacy of Cystic Fibrosis Transmembrane Conductance Regulator Chloride Channel Potentiators. *J Pharm Exp Ther* **330**(3):783-791.

205. Borle AB (1990) An overview of techniques for the measurement of calcium distribution, calcium fluxes, and cytosolic free calcium in mammalian cells. *Environ Health Perspect* **84**:45-56